

Multi-Stage Hybrid Federated Learning over Large-Scale Wireless Fog Networks

Seyyedali Hosseinalipour, Sheikh Shams Azam, Christopher G. Brinton,
Nicolo Michelusi, Vaneet Aggarwal, David J. Love, and Huaiyu Dai

Abstract

One of the popular methods for distributed machine learning (ML) is federated learning, in which devices train local models based on their datasets, which are in turn aggregated periodically by a server. In large-scale fog networks, the “star” learning topology of federated learning poses several challenges in terms of resource utilization. We develop multi-stage hybrid model training (MH-MT), a novel learning methodology for distributed ML in these scenarios. Leveraging the hierarchical structure of fog systems, MH-MT combines multi-stage parameter relaying with distributed consensus formation among devices in a hybrid learning paradigm across network layers. We theoretically derive the convergence bound of MH-MT with respect to the network topology, ML model, and algorithm parameters such as the rounds of consensus employed in different clusters of devices. We obtain a set of policies for the number of consensus rounds at different clusters to guarantee either a finite optimality gap or convergence to the global optimum. Subsequently, we develop an adaptive distributed control algorithm for MH-MT to tune the number of consensus rounds at each cluster of local devices over time to meet convergence criteria. Our numerical experiments validate the performance of MH-MT in terms of convergence speed and resource utilization.

Index Terms

Fog learning, federated learning, D2D communications, cooperative learning, machine learning, ad-hoc networks, distributed learning, wireless networks, fog computing, edge intelligence.

I. INTRODUCTION

The number of Internet-connected devices continues to rise dramatically. It is currently estimated that the Internet of Things (IoT) will reach 31 billion devices in 2020 and 75 billion by

S. Hosseinalipour, S. Azam, C. Brinton, N. Michelusi, V. Aggarwal, and D. Love are with Purdue University. e-mail: {hosseina, azam1, cgb, michelus, vaneet, djlove}@purdue.edu. H. Dai is with NC State University. email: {hdai@ncsu.edu}

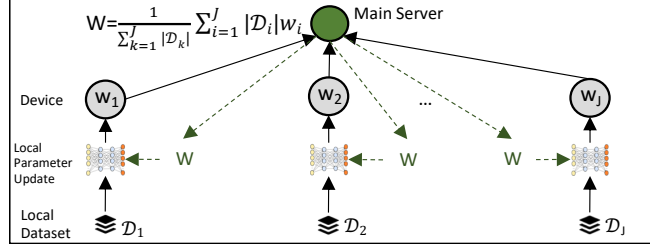


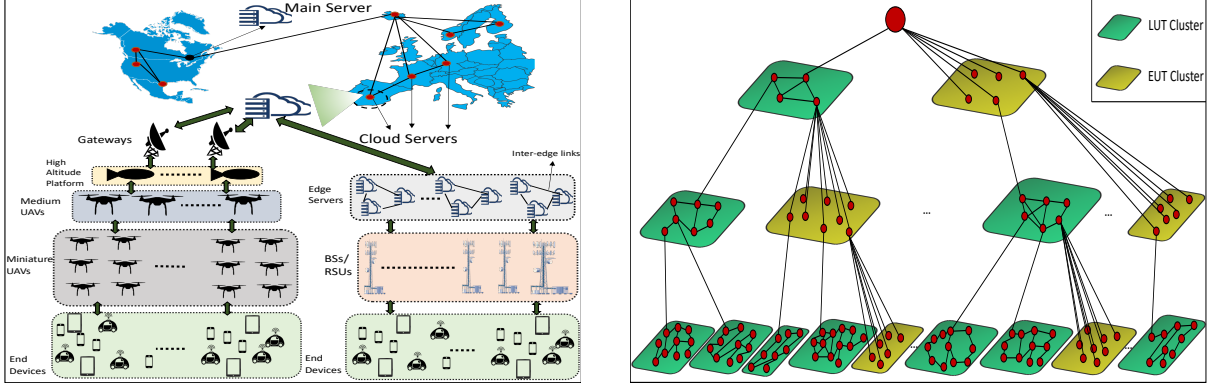
Fig. 1: Architecture of conventional federated learning. User devices perform local model updates based on their own datasets, and send their learned parameters to the main server. The main server aggregates the received parameters into a new global model and sends it back to the devices for the next round of local updates.

2025 [1]. These numbers, combined with increasing computational capabilities, is motivating the fog computing paradigm, which seeks to leverage these distributed resources along with cloud networks to satisfy emerging processor-intensive tasks at scale [2].

Machine learning (ML) tasks in particular have attracted significant attention in fog computing. When provided with sufficient data for model training, ML has produced automated solutions to problems ranging from natural language processing to object detection/tracking [3], [4]. Traditionally, model training has been carried out at a central node (i.e., a server). In many contemporary applications of ML, however, the relevant data is generated at the end user devices themselves. As these devices generate larger volumes of data, transferring it to a central server for model training has several drawbacks: (1) it can require significant energy consumption for battery limited devices, (2) the “round-trip-times” between data generation and model training can constitute prohibitive delays, and (3) in privacy-sensitive applications, end users may not be willing to transmit their raw data in the first place.

Federated learning has emerged recently as a technique for spreading model training across devices while keeping user datasets local [5], [6]. The conventional architecture of federated learning is depicted in Fig. 1. The learning network is comprised of a main server connected to multiple worker devices. Each round of model training consists of two steps performed sequentially: (i) *local updating*, where each worker device updates the current global model on its local dataset, typically using gradient descent methods, to arrive at an updated local model, and (ii) *global aggregation*, where the main server gathers the local parameters of the devices periodically and computes a new global model. The new global model is then synchronized across the worker devices, which begin the next round of training [5], [6].

In federated learning, only device-to-server (in step (i)) and server-to-device (in step (ii)) communications are presumed. This “star” learning topology poses problems in fog computing systems, which are characterized by heterogeneity in computation and communication capabili-



(a): A schematic of model transfer stages for a large-scale ML task in a fog network. The main server aggregates the parameters of multiple cloud servers. The parameters of the end devices are carried through base stations (BSs), road side units (RSUs), unmanned aerial vehicles (UAVs), high altitude platforms, edge clouds, and cloud servers before reaching the main server.

(b): Partitioning the network layers into multiple LUT/EUT clusters for FogL. The parents of LUT clusters obtain the consensus of their children by sampling the model parameter of one node, while the parents of EUT clusters receive all the parameters of their children nodes. Each LUT cluster possesses a time varying network topology.

Fig. 2: Architecture of (a) the multi-layer network structure of fog computing systems and (b) the partitioning of nodes into hierarchical clusters for FogL.

ties across devices, and are thus prone to straggler node problems [2], [7]. We will next describe fog learning (FogL), an architecture that we consider in this paper which migrates to a more distributed learning topology via device-to-device (D2D) communications.

A. Fog Learning (FogL)

A fog computing system is a continuum of communication and computation resources between edge devices and cloud servers, generally stretching over a large geographical region. We recently introduced FogL [8] as an architecture that will leverage this structure to handle ML tasks. A sample network architecture of FogL is depicted in Fig. 2a, which shows multiple layers between user devices and the cloud, including base stations (BSs) and edge servers. Compared with federated learning, FogL has two key characteristics: (1) It includes *parameter aggregations at each layer of the hierarchy*, instead of just at the cloud server. (2) In addition to inter-layer communications, it includes *intra-layer communications via D2D*. D2D communications is being enabled today in 5G and IoT [9], and there is a well-developed body of literature on D2D communication protocols for ad-hoc and sensor networks including vehicular ad-hoc networks (VANET), mobile ad-hoc networks (MANET), and flying ad-hoc networks (FANET) deployments [10]–[13]. FogL can also consider direct server-to-server communications [14].

In this paper, we will leverage these characteristics of FogL to improve the resource utilization in training ML models. Specifically, we consider partitioning the network layers into different clusters, as depicted in Fig. 2b, where all nodes in a cluster are connected to the same node

in the next layer up. There are two types of clusters: (i) limited uplink transmission (LUT) clusters, where D2D communications are enabled, and (ii) extensive uplink transmission (EUT) clusters, where all nodes only communicate with their upper layer. Based on this, we develop a methodology called *multi-stage hybrid model training* (MH-MT) that considers both intra-cluster average consensus formation and inter-cluster aggregations for distributing ML in fog computing systems. In doing so, we incorporate the time-varying network topology as a dimension of federated learning, and show how it impacts model convergence.

B. Related Work

Federated learning has received significant research attention. The relevant existing literature can be categorized into three aspects: works on studying/improving (i) network communication demands, (ii) device computation requirements, and (iii) privacy/security guarantees. In the first category, research has considered the effects of limited and imperfect communication capabilities in wireless networks – such as channel fading, packet loss, and limited bandwidth – on the operation of federated learning [15]–[18]. Additionally, communication techniques such as quantization [19] and sparsification of model updates (i.e., when only a fraction of the model parameters are shared during model training) [20] have been studied to facilitate transfers between the server and worker devices under limited communication capabilities. Recently, [21] analyzed the convergence bounds in the presence of edge network resource constraint, and developed an algorithm that adapts the frequency of global aggregations to minimize model loss. Focusing on the case of FogL, our work generalizes the communication strategy of federated learning to include both distributed average consensus formation via D2D and multi-layer aggregations.

In the second category, research has considered the computation aspects of implementing federated learning in wireless networks [7], [16], [21]–[23]. Part of this literature has focused on federated learning in the presence of straggler nodes, i.e., when a node has significantly lower computation capabilities than others and cannot train as quickly [7], [16], [22]. Another emphasis in this direction has been reducing the computation requirements of devices in the network, through coding techniques to offload processing tasks from the devices to the server [23], intelligent D2D offloading between devices [7], and judicious selection of device training participation [24]. More general techniques for mitigating compute limitations, e.g., through model compression, have also been applied to distributed ML environments [25]. In our

work, we study the computation requirements of devices in FogL in terms of the number of required training rounds.

Recent works have also studied privacy and security in federated learning [26], [27]. Even though source data is never transmitted over the network in federated learning, it can be possible to extract sensitive information from transmitted model parameters. These works have thus studied adapting security techniques such as differential privacy [26] and homomorphic encryption [27] to federated learning. Our focus is instead on the communication and computation aspects.

Beyond federated learning, there is a well developed literature on other distributed ML techniques (e.g., [28]–[30]). Our proposed framework for FogL inherits its local updating rule and global aggregation rule from federated learning, i.e., local gradient descent at the devices and weighted averaging to obtain the global model. We choose this due to specific characteristics that make it better suited for fog: keeping the user data local, handling non-iid datasets across devices, and handling imbalances between sizes of local datasets [5]. These capabilities have made federated learning the most widely acknowledged distributed learning framework for future wireless systems [31], [32]. However, the multi-stage architecture of FogL could also be studied in the context of other distributed ML techniques, e.g., ADMM [28].

Finally, there exist a literature on distributed average consensus algorithms for different applications in multi-agent systems [33], [34], sensor networks [35], [36], and solving optimization problems [37]–[39]. The FogL scenario we consider is unique given its multi-layer network structure and focus on ML model training, where the goal is to propagate an expectation of the nodes' parameters through the hierarchy to train an ML model. The results we obtain have thus not yet appeared in either consensus-related or ML-related literature.

C. Summary of Contributions

Compared to the related work, our contributions can be summarized as follows:

- We formalize multi-stage hybrid model training (MH-MT), a novel methodology for distributed ML in fog networks. Different from federated learning, MH-MT incorporates (i) distributed average consensus formation within node clusters, and (ii) model aggregations between layers of the network hierarchy, to improve resource utilization in large-scale wireless networks.
- We analytically characterize the convergence bound of MH-MT. We show how this bound is dependent on characteristics of the ML model, the network topology, and the learning

algorithm, including the number of model parameters, the communication graph structure, and the number of consensus rounds at different network layers.

- Assuming a constant gradient descent step size, we obtain a condition with respect to these characteristics under which a constant optimality gap can be achieved asymptotically. Further, we demonstrate that under limited finely-tuned consensus rounds, MH-ML will converge to the optimal ML model with a linear decrease in loss distance at each global aggregation round.
- We obtain analytical relationships for tuning the number of consensus rounds in different clusters and the number of global iterations to meet these convergence characteristics. We use these relationships to develop distributed control algorithms that each cluster can employ individually to adapt the number of consensus rounds it uses over time.
- Our experimental results verify that MH-MT can improve network resource utilization significantly with negligible impact on model training convergence.

II. SYSTEM MODEL AND PROBLEM FORMULATION

In this section, we formulate the novel FogL network architecture (Sec. II-A) and its associated machine learning problem (Sec. II-B) for FogL. Then, we formalize our proposed hybrid learning paradigm via intra- and inter-cluster communications (Sec. II-C) and parameter sharing (Sec. II-D).

A. Network Architecture and Graph Model

We consider the network architecture of FogL as depicted on the left in Fig. 3. As discussed in Sec. I-A, there are both inter-layer and intra-layer communications. The inter-layer communications are captured via a tree graph, with the main server at the root and edge devices as the leaves. Each layer is partitioned into multiple clusters, with each device in a cluster sharing the same parent node in the next layer up. In general, each node may have a parent node located multiple layers above (e.g., an edge device can be directly connected to edge server) and multiple clusters can share the same parent node (e.g., multiple groups of cellular devices share the same BS). Except at the bottom layer, each node in the hierarchy is the parent for a subset of the nodes in the next layer down, and is responsible for gathering the parameters of its children nodes.

To aid our analysis, from the FogL network representation on the left in Fig. 3, we construct the *FogL augmented network graph* shown on the right, where several virtual nodes and clusters

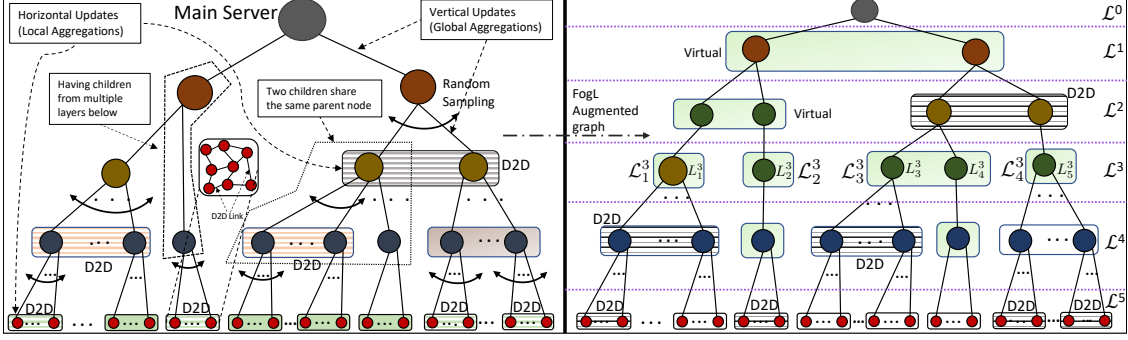


Fig. 3: Left: Network representation of FogL for an example network. The root of the tree corresponds to the main server, the leaves of the tree correspond to the edge devices, and the nodes in-between correspond to intermediate fog nodes. The nodes belonging to the same layer that have the same parent node form clusters. In D2D-enabled clusters, the nodes form a certain topology over which the devices communicate with their neighbors for distributed model consensus formation. Right: The corresponding FogL augmented graph for analysis. Virtual nodes and clusters are highlighted in green.

have been added. Virtual nodes are added in such a way that each node has a single parent node in its immediate upper layer. Also, when multiple clusters share the same parent node, a layer is added to the FogL augmented graph that consists of multiple intermediate virtual nodes forming a virtual cluster such that there is a one-to-one mapping between the clusters and parent nodes. If they already do not form a cluster, the nodes in the highest layer before the main server will form a virtual cluster to preserve this desired one-to-one mapping. A node without any neighbors in its layer is also assumed to form a virtual cluster. Throughout, we do not distinguish between virtual and non-virtual nodes, clusters, and layers unless specified.

The FogL augmented graph has the following characteristics: (i) each parent node is associated with a single cluster, (ii) the length of the paths between the root and each leaf node is the same, and (iii) the layer below the root always consists of exactly one cluster. Formally, the network consists of $|\mathcal{L}| + 1$ layers, where the root is located at \mathcal{L}^0 and $\mathcal{L} = \{\mathcal{L}^1, \mathcal{L}^2, \dots, \mathcal{L}^{|\mathcal{L}|}\}$ denotes the set of subsequent layers. The end devices are contained in layer $\mathcal{L}^{|\mathcal{L}|}$. Each layer \mathcal{L}^j , $0 \leq j \leq |\mathcal{L}|$, consists of $|\mathcal{L}^j|$ clusters denoted by $\mathcal{L}_1^j, \mathcal{L}_2^j, \dots, \mathcal{L}_{|\mathcal{L}^j|}^j$. For convenience, we will sometimes use \mathcal{C} to denote an arbitrary cluster (i.e., any \mathcal{L}_i^j). We let $\mathcal{N}_j = \{L_1^j, L_2^j, \dots, L_{N_j}^j\}$ denote the set of nodes located in layer \mathcal{L}^j , where $N_j \triangleq \sum_{i=1}^{|\mathcal{L}^j|} |\mathcal{L}_i^j|$ is the total number of nodes in the layer. For convenience, we will sometimes use n to denote an arbitrary node (i.e., any L_i^j). For each node n located in layers $\mathcal{L}^{|\mathcal{L}|-1}, \dots, \mathcal{L}^0$, we let $\mathcal{Q}(n)$ denote the set of its children nodes, which in the augmented graph forms a cluster at the layer below for which n is the parent.

B. Machine Learning Model

Each edge device n is associated with a dataset \mathcal{D}_n that it has generated, where $\mathcal{D}_n \cap \mathcal{D}_{n'} = \emptyset$, $n \neq n'$. Each element $d_i \in \mathcal{D}_n$ of the dataset, called a training sample, is represented via a feature

vector \mathbf{x}_i and a label y_i for the ML task of interest. For example, in image classification, \mathbf{x}_i may be the RGB colors of all pixels in the image, and y_i may be the identity of the person in the image. The goal of the ML task is to learn the parameters $\mathbf{w} \in \mathbb{R}^M$ of a particular M -dimensional model (e.g., an SVM or a neural network) that are expected to maximize the accuracy in mapping from \mathbf{x}_i to y_i across any sample in the network. The model is associated with a loss $\tilde{f}(\mathbf{w}, \mathbf{x}_i, y_i)$ that quantifies the error of parameter realization \mathbf{w} on sample d_i , which for brevity we refer to as $\tilde{f}_i(\mathbf{w})$. We refer the reader to Table 1 in [21] for a list of loss functions for common ML models.

The global loss of the ML model across the entire network dataset is formulated as

$$F(\mathbf{w}) = \frac{1}{D} \sum_{n \in \mathcal{N}_{|\mathcal{L}|}} |\mathcal{D}_n| f_n(\mathbf{w}), \quad D = \sum_{n \in \mathcal{N}_{|\mathcal{L}|}} |\mathcal{D}_n|, \quad (1)$$

where f_n is the local loss over datapoints at node n , i.e., $f_n(\mathbf{w}) = \frac{1}{|\mathcal{D}_n|} \sum_{d_i \in \mathcal{D}_n} \tilde{f}_i(\mathbf{w})$. The goal of the model training is to identify the optimal $\mathbf{w}^* \in \mathbb{R}^M$ that minimize the global loss:

$$\mathbf{w}^* = \arg \min_{\mathbf{w}} F(\mathbf{w}). \quad (2)$$

To achieve this in a distributed manner, training is conducted through consecutive global iterations. At the start of global iteration $k \in \mathbb{N}$, the main server possesses a parameter vector $\mathbf{w}^{(k-1)} \in \mathbb{R}^M$, which will propagate through the hierarchy to the edge devices. Each edge device n overrides its current local model parameter vector $\mathbf{w}_n^{(k-1)}$ with this global model, as

$$\mathbf{w}_n^{(k-1)} = \mathbf{w}^{(k-1)}, \quad (3)$$

and then performs a local update using gradient descent with step size β on its local dataset as

$$\mathbf{w}_n^{(k)} = \mathbf{w}_n^{(k-1)} - \beta \left(\nabla f_n(\mathbf{w}_n^{(k-1)}) \right), \quad n \in \mathcal{N}_{|\mathcal{L}|}. \quad (4)$$

The main server is then interested in obtaining the global model used for initiating the next global iteration, which is defined as a weighted average of the edge devices' parameters:

$$\mathbf{w}^{(k)} = \frac{\sum_{n \in \mathcal{N}_{|\mathcal{L}|}} |\mathcal{D}_n| \mathbf{w}_n^{(k)}}{D}. \quad (5)$$

Similar to the literature on federated learning, parameter D is assumed to be known at the server. As we will see, our method does not require knowledge of the size of each users' dataset at the

server, which eliminates communication overhead. On the downlink from the server to the edge devices, we assume that the (common) global parameter \mathbf{w}^k can be readily shared through the hierarchy to reach to the end devices, e.g., through a broadcasting protocol. These devices will then conduct (3) and (4) locally. The challenge, then, is computing (5) at the main server. In federated learning, the devices will directly upload (4) to the server for this. This is prohibitive in a large-scale fog computing system, however. For one, it may require *high energy consumption*: uplink transmissions from battery-limited devices to nodes at a higher layer typically correspond to long physical distances, and can deplete individual device batteries. Also, it may induce *high network traffic and long latencies*: a neural network with even hundreds of parameters, which would be small by today's standards [25], would require transmission of billions of parameters in the upper layers during each iteration over a network with millions of nodes. Additionally, it may *overload current cellular and vehicular architectures*: these communication infrastructures are not designed to handle large jumps in the number of active users [40], which would be the case with simultaneous uplink transmissions at the bottom-most layer. These issues require a novel approach to parameter aggregations, which we develop in this paper.

C. Hybrid Learning through Intra- and Inter-Layer Communications

The main server in FogL is only interested in the weighted average (5) of the local parameters. Consequently, we advocate local aggregations at each network layer. To achieve this, during a global update, each cluster in Fig. 3 follows one of two mechanisms:

- 1) *Distributed aggregation*: The children nodes engage in distributed consensus formation of their local model parameters, facilitated by D2D communications. Subsequently, the parent node samples parameters of one of the children and scales it by the number of children to calculate an approximate sum of the children nodes' parameters.
- 2) *Instant aggregation*: Each node instead uploads its local model to the parent node. The parent computes the aggregation directly as a sum of the children nodes' parameters.

The communication requirement of the instant aggregation is significantly higher than the distributed aggregation: even though the distributed aggregation may require multiple consensus rounds, it generally occurs over much shorter distances. We refer to mechanisms 1 and 2 as limited uplink transmission (LUT) and extensive uplink transmission (EUT), respectively. Not all clusters can operate in LUT mode, since not all are D2D enabled, due to e.g., sparse connections between devices or privacy restrictions. Still, we can expect significant advantages in terms of

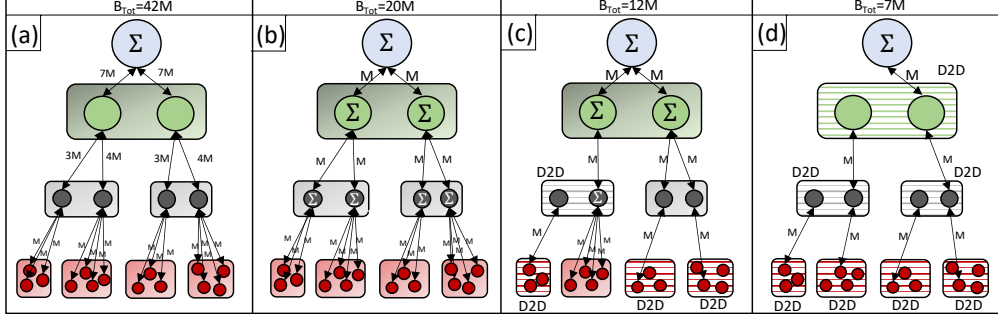


Fig. 4: Example of the network traffic reduction provided by multi-layer aggregations in FogL, where each edge device trains a model with parameter length M . The sum of the length of parameters transferred among the layers is depicted at the top of each graph. (a): Network consisting of all EUT clusters, where the parent nodes upload all received parameters from their children. (b): Network consisting of all EUT clusters, where the parent nodes sum all received parameters and upload to the next layer. (c): Network with a portion of clusters in LUT mode, where each parent node only samples the parameters of one device after consensus formation. (d): Network consisting of all LUT clusters.

the volume of parameters uploaded through the fog system with a combination of EUT and LUT clusters, as depicted in Fig. 4. At the bottom layers of the hierarchy where communication is mostly over the air, D2D can also be implemented as out-band D2D [41], which has the additional advantage of not occupying licensed spectrum bands that may otherwise be used.

A cluster may switch between EUT and LUT over time. For instance, the connectivity between a fleet of miniature UAVs will vary as they travel, necessitating EUT when D2D is not feasible. To model this dynamic, for each cluster \mathcal{C} , we define $\mathbb{1}_{\{\mathcal{C}\}}^{(k)}$ to capture the operating mode of the cluster at global aggregation k , which is 1 if the cluster operates in LUT mode, and 0 otherwise.

In each LUT cluster, a node will only communicate with its neighboring devices, which may not include the whole cluster. Further, each node's neighborhood may evolve over time. For example, when the communications are conducted over the air as in Fig. 2a, the neighbors in one aggregation interval are identified based on the distances among the nodes and their transmit powers. We will explicitly consider such evolutions in cluster topology in our distributed consensus model in Sec. III. Though individual nodes may move between clusters, we assume that the total number of nodes inside each cluster does not evolve over time.

In the simple case where there is only one layer below the server, i.e., $|\mathcal{L}| = 1$, which is comprised of a single EUT cluster, our FogL architecture reduces to federated learning. If instead the bottom layer is an LUT cluster, FogL can be reduced to fully distributed learning or serverless federated learning, e.g., [42], [43]. As discussed in Sec. I-C, one of the main contributions of our work is developing and analyzing this generalized multi-layer hybrid learning paradigm for FogL.

D. Parameter Sharing vs. Gradient Sharing

Note that the parameter update in (5) can be written as:

$$\mathbf{w}^{(k)} = \frac{\sum_{n \in \mathcal{N}_{|\mathcal{L}|}} |D_n| \left(\mathbf{w}_n^{(k-1)} - \beta \left(\nabla f_n(\mathbf{w}_n^{(k-1)}) \right) \right)}{D} = \mathbf{w}^{(k-1)} - \beta \frac{\sum_{n \in \mathcal{N}_{|\mathcal{L}|}} |D_n| \nabla f_n(\mathbf{w}_n^{(k-1)})}{D}. \quad (6)$$

This asserts that the global parameters can also be obtained via the gradients of the devices, implying that the devices can either share their gradients or their parameters during training. This equivalence arises from the one-step update in (4), which is a common assumption in federated learning [15], [16], [44]. However, recent work [7], [21] has advocated conducting multiple rounds of local updates between global aggregations to reduce communication costs; in this case, the parameters are required for each aggregation. In this paper, we focus on the more general case of parameter sharing, though we will consider one theoretical result based on gradient sharing.

In LUT clusters, devices must leverage D2D communications to obtain an approximate value of the sum of their parameters. A basic approach would be to implement a message passing algorithm where nodes exchange parameters with their neighbors until each node in the cluster has all parameters stored locally. Each node can then readily calculate the aggregated value, and one of them can be sampled by the parent node. Collecting a table of parameters at each node may not be feasible, however, given how large these vectors can be for contemporary ML models, as discussed in Sec. II-B. Instead, we desire a technique that (i) does not require any node to store a table of all model parameters in the cluster, (ii) can be implemented in a distributed manner via D2D, and (iii) is generalizable across different network layers. In the next section, we leverage distributed average consensus methods to develop and analyze this technique.

III. MULTI-STAGE HYBRID MODEL TRAINING FOR FOG LEARNING

In this section, we develop our algorithm for hybrid model training in FogL (Sec. III-A&III-B). Then, we conduct a detailed performance analysis of our method (Sec. III-C). Finally, based on this analysis, we develop algorithms for adapting the number of consensus rounds in each cluster over time to account for resource constraints at devices (Sec. III-D).

A. Distributed Average Consensus within Clusters

Referring to Fig. 3, during each round k of training, the LUT clusters engage in D2D communications, where each node desires estimating the average value of the parameters inside

its cluster. For each cluster \mathcal{C} that is LUT during the k th global aggregation (i.e., for which $\mathbb{1}_{\{\mathcal{C}\}}^{(k)} = 1$), we let $G_{\mathcal{C}}^{(k)} = (\mathcal{C}, \mathcal{E}_{\mathcal{C}}^{(k)})$ denote its communication graph during k . In this graph, \mathcal{C} is the set of nodes belonging to the cluster, and there is an edge $(m, n) \in \mathcal{E}_{\mathcal{C}}^{(k)}$ between nodes $m, n \in \mathcal{C}$ if they can communicate via D2D during k . We assume that $G_{\mathcal{C}}^{(k)}$ is undirected, connected, and static for the duration of one round k , though it may change between rounds.

We consider the general family of linear distributed consensus algorithms [45], where during the D2D communications, the nodes inside LUT cluster \mathcal{C} conduct $\theta_{\mathcal{C}}^{(k)} \in \mathbb{N}$ rounds of consensus. Formally, each node $n \in \mathcal{C}$ engages in the following iterative update for $t = 0, \dots, \theta_{\mathcal{C}}^{(k)} - 1$:

$$\mathbf{z}_n^{(t+1)} = v_{n,n}^{(k)} \mathbf{z}_n^{(t)} + \sum_{m \in \zeta^{(k)}(n)} v_{n,m}^{(k)} \mathbf{z}_m^{(t)}, \quad (7)$$

where $\mathbf{z}_n^{(0)} = \mathbf{w}_n^{(k)}$ corresponds to node n 's initial consensus parameter vector, and $\mathbf{z}_n^{(\theta_{\mathcal{C}}^{(k)})}$ denotes the parameter after the consensus process. $\zeta^{(k)}(n)$ denotes the set of neighbors of node n at global iteration k , and $v_{n,p}^{(k)}$, $p \in \{n\} \cup \zeta^{(k)}(n)$ are the consensus weights associated with node n . We assume that each node has knowledge of these weights at each global iteration. For instance, one common choice for these weights [45] gives $\mathbf{z}_n^{(t+1)} = \mathbf{z}_n^{(t)} + d_{\mathcal{C}}^{(k)} \sum_{m \in \zeta^{(k)}(n)} (\mathbf{z}_m^{(t)} - \mathbf{z}_n^{(t)})$, $0 < d_{\mathcal{C}}^{(k)} < 1/D_{\mathcal{C}}^{(k)}$, where $D_{\mathcal{C}}^{(k)}$ is the maximum degree of the nodes in $G_{\mathcal{C}}^{(k)}$. With this implementation, the nodes inside LUT cluster \mathcal{C} only need to have the knowledge of the parameter $d_{\mathcal{C}}^{(k)}$ to perform D2D communications, which can be broadcasted by the respective parent node. Note that due to time constraints (i.e., depending on the required time between global aggregations), the number of consensus rounds cannot be arbitrary large, and thus the nodes inside a cluster often do not have a perfect estimate of the average value of their parameters. In Sec. III-C, we will analyze the effect of the number of consensus rounds for general choices of $v_{n,p}^{(k)}$, $p \in \{n\} \cup \zeta^{(k)}(n)$, $\forall n$.

B. Consensus Propagation through the Hierarchy

We now explain the procedure for propagating the consensus update (7) through the network:

1) *Nodes' parameters in the bottom-most layer:* Given $\mathbf{w}^{(k-1)}$, the edge devices in layer $\mathcal{L}^{|\mathcal{L}|}$ first perform the local update described in (4). Since the nodes' parameters go through multiple stages of aggregations (see Fig. 4), even if the server knows the number of data points of each device, it still cannot recover the individual parameters from the aggregated ones to calculate (5) directly. To overcome this, each edge device $n \in \mathcal{N}_{|\mathcal{L}|}$ shares $\tilde{\mathbf{w}}_n^{(k)} = |D_n| \mathbf{w}_n^{(k)}$ with its neighbors during the consensus process for global iteration k , i.e., its parameters weighted by its number

$$\widehat{\mathbf{w}}_{n'}^{(k)} = \frac{\sum_{j \in \mathcal{Q}(n)} |D_j| \mathbf{w}_j^{(k-1)}}{|\mathcal{Q}(n)|} - \frac{\sum_{j \in \mathcal{Q}(n)} \beta |D_j| \nabla f_j(\mathbf{w}_j^{(k-1)})}{|\mathcal{Q}(n)|} + \mathbb{1}_{\{\mathcal{Q}(n)\}}^{(k)} \mathbf{c}_{n'}^{(k)}, \quad n' \in \mathcal{Q}(n) \quad (9)$$

$$\widehat{\mathbf{w}}_{n'}^{(k)} = \frac{\sum_{i \in \mathcal{Q}(n)} \sum_{j \in \mathcal{Q}(i)} |D_j| \mathbf{w}_j^{(k-1)}}{|\mathcal{Q}(n)|} - \frac{\sum_{i \in \mathcal{Q}(n)} \sum_{j \in \mathcal{Q}(i)} \beta |D_j| \nabla f_j(\mathbf{w}_j^{(k-1)})}{|\mathcal{Q}(n)|} + \frac{\sum_{i \in \mathcal{Q}(n)} \mathbb{1}_{\{\mathcal{Q}(i)\}}^{(k)} |\mathcal{Q}(i)| \mathbf{c}_{i'}^{(k)}}{|\mathcal{Q}(n)|} + \mathbb{1}_{\{\mathcal{Q}(n)\}}^{(k)} \mathbf{c}_{n'}^{(k)} \quad (10)$$

of datapoints.¹ Using this technique, the number of datapoints of the nodes is preserved during multi-layer aggregations. Specifically, each node $n \in \mathcal{N}_{|\mathcal{L}|}$ belonging to cluster $\mathcal{C} \in \mathcal{L}^{|\mathcal{L}|}$ engages in the local iterations described by (7), where $\mathbf{z}_n^{(0)} = \widetilde{\mathbf{w}}_n^{(k)}$. Finally, the node stores $\widehat{\mathbf{w}}_n^{(k)} = \mathbf{z}_n^{(\theta_c^{(k)})}$.

2) *Nodes' parameters in the middle layers:* Once the consensus is finished in layer $\mathcal{L}^{|\mathcal{L}|}$, in layer $\mathcal{L}^{|\mathcal{L}|-1}$, each parent node $n \in \mathcal{N}_{|\mathcal{L}|-1}$ of a cluster that operated in LUT mode selects a cluster head n' among its children $\mathcal{Q}(n)$ in layer $\mathcal{L}^{|\mathcal{L}|}$ based on a selection/sampling distribution. This child n' uploads its final parameter vector $\widehat{\mathbf{w}}_{n'}^{(k)}$ to the parent node. The resulting sampled/gathered parameter vector by the parent node is given by (9), where the first two terms correspond to the true average of the parameters of the nodes inside cluster $\mathcal{Q}(n)$, and $\mathbf{c}_{n'}^{(k)} \in \mathbb{R}^M$ is the error arising from the consensus. This error is only applicable to the LUT clusters, and is concerned with the deviation from the true cluster average (which would be obtained in an EUT cluster). The parent node $n \in \mathcal{N}_{|\mathcal{L}|-1}$ then computes its own parameter $\mathbf{w}_n^{(k)}$ by scaling the received vector by the number of its children, and stores the corresponding vector:

$$\mathbf{w}_n^{(k)} = |\mathcal{Q}(n)| \widehat{\mathbf{w}}_{n'}^{(k)}, \quad n \in \mathcal{N}_{|\mathcal{L}|-1}, \quad n' \in \mathcal{Q}(n), \quad \mathbb{1}_{\{\mathcal{Q}(n)\}}^{(k)} = 1. \quad (8)$$

At the same time, in layer $\mathcal{L}^{|\mathcal{L}|-1}$, each parent node n of a cluster that operated in EUT mode receives all the parameters of its children and computes $\mathbf{w}_n^{(k)} = \sum_{i \in \mathcal{Q}(n)} \widetilde{\mathbf{w}}_i^{(k)}$. The LUT clusters in layer $\mathcal{L}^{|\mathcal{L}|-1}$ then engage in distributed consensus formation.

This procedure continues up the hierarchy at each layer \mathcal{L}^j , $j = |\mathcal{L}| - 2, \dots, 1$. The difference between the parameter sharing in the middle layers versus the bottom-most layer is that the nodes no longer share weighted versions of their parameters. More precisely, for an LUT cluster \mathcal{C} located in one of the middle layers, each node $n \in \mathcal{C}$ performs the local iterations described by (7) with $\mathbf{z}_n^{(0)} = \mathbf{w}_n^{(k)}$. At the end of its consensus process, each of these nodes stores $\widehat{\mathbf{w}}_n^{(k)} = \mathbf{z}_n^{(\theta_c^{(k)})}$, and passes it up if sampled by its parent. Also, each node n inside an EUT cluster \mathcal{C} located in one of the middle layers directly shares \mathbf{w}_n^k with its parent node.

¹Nodes inside EUT clusters of layer $\mathcal{L}^{|\mathcal{L}|}$ also share the weighted version of their parameter with their parents.

As we move up the layers, the errors in the consensus vectors accumulate. For example, (10) gives the expression for the final consensus parameter vector of a node $n' \in \mathcal{Q}(n)$ inside an LUT cluster at layer $\mathcal{L}^{|\mathcal{L}|-1}$, which will be sampled by a parent node $n \in \mathcal{N}_{|\mathcal{L}|-2}$ located in the upper layer. In this expression, i' denotes the sampled node chosen by parent node i .

3) *Main server*: If the cluster in layer \mathcal{L}^1 operates in LUT mode, the parameter received by the main server is $\mathbf{w}_{L_1^0}^{(k)} = |\mathcal{L}_1^1| \widehat{\mathbf{w}}_m^{(k)}$, where $m \in \mathcal{L}_1^1$ denotes the node sampled by the main server with parameter $\widehat{\mathbf{w}}_m^{(k)}$ obtained after performing consensus². Otherwise, the main server sums all the received parameters $\mathbf{w}_{L_1^0}^{(k)} = \sum_{m \in \mathcal{L}_1^1} \mathbf{w}_m^{(k)}$. The main server then computes the global parameter vector as:

$$\mathbf{w}^{(k)} = \frac{\mathbf{w}_{L_1^0}^{(k)}}{D}. \quad (11)$$

The value of $\mathbf{w}^{(k)}$ is then broadcast down the hierarchy to start the next global aggregation round $k + 1$, beginning with local updates at the devices.

The methodology we develop throughout this section – multi-stage hybrid model training (MH-MT) – is summarized in Algorithm 1. The lines beginning with ****** and **##** are enhancements for tuning the consensus rounds over time at different clusters, which we present in Sec. III-D.

C. Theoretical Analysis of MH-MT

We first introduce a few common assumptions and additional definitions used in our analysis.

Assumption 1. *The global ML loss function (1) has the following properties [15], [44], [46]–[48]: (i) μ -strong convexity, i.e., $F(\mathbf{y}) \geq F(\mathbf{x}) + (\mathbf{y} - \mathbf{x})^\top \nabla F(\mathbf{x}) + \frac{\mu}{2} \|\mathbf{y} - \mathbf{x}\|^2$ for some $\mu > 0 \forall \mathbf{x}, \mathbf{y}$, and (ii) η -smoothness, i.e., $\|\nabla F(\mathbf{x}) - \nabla F(\mathbf{y})\| \leq \eta \|\mathbf{x} - \mathbf{y}\|$ for some $\eta > \mu \forall \mathbf{x}, \mathbf{y}$.*

We will also find it useful to write the consensus algorithm in matrix form. Letting $\mathbf{W}_C^{(k)} \in \mathbb{R}^{|\mathcal{C}| \times M}$ denote the matrix of model parameters across all nodes in an LUT cluster \mathcal{C} prior to consensus in round k , the evolution of the nodes' parameters described by (7) can be written as:

$$\left[\widehat{\mathbf{W}}_C^{(k)} \right]_m = \left(\mathbf{V}_C^{(k)} \right)^{\theta_C^{(k)}} \left[\mathbf{W}_C^{(k)} \right]_m, \quad (12)$$

where $\left[\mathbf{W}_C^{(k)} \right]_m$ is the m th column of $\mathbf{W}_C^{(k)}$, $m = 1, \dots, M$, corresponding to the m th parameter across nodes in the cluster, and $\widehat{\mathbf{W}}_C^{(k)}$ denotes the matrix of node parameters after the consensus.

²Since \mathcal{L}^1 consists of one cluster, $|\mathcal{L}_1^1|$ represents the total number of nodes in that layer.

Algorithm 1: Multi-stage hybrid model training in fog networks (MH-MT)

input : $\mathcal{L} = \mathcal{L}^1, \dots, \mathcal{L}^{|\mathcal{L}|}$, number of global aggregations K , default number of consensus rounds $\theta_{\mathcal{L}_i^j}^{(k)} \forall i, j, k$.

output: Final global model $\mathbf{w}^{(K)}$.

- 1 **Initial operations at main server:** Initialize the global parameter $\mathbf{w}^{(0)}$ and synchronize the edge devices with it.
- 2 **** Initial operations at main server:** If asymptotic convergence to optimal is desired: (i) server randomly sets $\|\nabla F(\mathbf{w}^0)\|$, and broadcasts it; (ii) Server sets δ either arbitrarily or according to (21) to guarantee a certain accuracy, and broadcasts it. Otherwise, the server sets consensus tuning parameters $\{\sigma_j\}_{j=1}^{|\mathcal{L}|}$ as described in Sec. III-D and broadcasts them.
- 3 **for** $k = 1$ **to** K **do**
- 4 **for** $l = |\mathcal{L}|$ **down to** $l = 0$ **do**
- 5 **if** $l = |\mathcal{L}|$ **then**
- 6 Given $\mathbf{w}^{(k-1)}$, each node n in the layer performs local update (4) to obtain $\mathbf{w}_n^{(k)}$, and uses it to obtain $\widetilde{\mathbf{w}}_n^{(k)} = |\mathcal{D}_n| \mathbf{w}_n^{(k)}$, which shared by the node either through consensus with neighbors or transmission to the parent node in the upper layer.
- 7 ** Each cluster operating in LUT mode runs Algorithm 2 to obtain the number of consensus rounds.
- 8 ## Each cluster operating in LUT mode runs Algorithm 3 to obtain the number of consensus rounds.
- 9 Nodes inside LUT clusters update their parameters via distributed average consensus described in (7).
- 10 **else if** $1 \leq l \leq |\mathcal{L}| - 1$ **then**
- 11 Parent nodes of EUT clusters sum the received parameters of their children nodes to obtain their parameters.
- 12 Each node n that is the parent node of an LUT cluster $\mathcal{Q}(n)$ samples a child $n' \in \mathcal{Q}(n)$, and uses its parameter to obtain its own parameter $\mathbf{w}_n^{(k)}$ as $\mathbf{w}_n^{(k)} = |\mathcal{Q}(n)| \widetilde{\mathbf{w}}_{n'}^{(k)}$.
- 13 ** Each cluster operating in LUT mode runs Algorithm 2 to obtain the number of consensus rounds.
- 14 ## Each cluster operating in LUT mode runs Algorithm 3 to obtain the number of consensus rounds.
- 15 Nodes inside LUT clusters update their parameters via distributed average consensus described in (7).
- 16 **else if** $l = 0$ **then**
- 17 Depending on the operating mode of the cluster in layer \mathcal{L}^1 , the main server obtains its parameter $\mathbf{w}_{\mathcal{L}^0}^{(k)}$ by either sampling or summing all the received parameters, and computes $\mathbf{w}^{(k)}$ for the next global iteration using (11).
- 18 The main server synchronizes the edge devices with $\mathbf{w}^{(k)}$.
- 19 ** If asymptotic convergence to optimal is desired, the main server approximates the gradient of the loss function used for the next iteration as described in Sec. III-D and broadcasts it.

$\mathbf{V}_C^{(k)} \in \mathbb{R}^{|\mathcal{C}| \times |\mathcal{C}|}$ denotes the consensus matrix applied to each parameter's vector to realize (7).

Assumption 2. The consensus matrices $\mathbf{V}_C^{(k)}$ for each LUT cluster \mathcal{C} during global aggregation k have the following properties [45], [49]: (i) $\left(\mathbf{V}_C^{(k)}\right)_{m,n} = 0$ if $(m, n) \notin \mathcal{E}_C$, (ii) $\mathbf{V}_C^{(k)} \mathbf{1} = \mathbf{1}$, (iii) $\mathbf{V}_C^{(k)} = \mathbf{V}_C^{(k)\top}$, and (iv) $\rho\left(\mathbf{V}_C^{(k)} - \frac{\mathbf{1}\mathbf{1}^\top}{|\mathcal{C}|}\right) \leq \lambda_C^{(k)} < 1$, where $\mathbf{1}$ is the vector of 1s and $\rho(\mathbf{A})$ is the spectral radius of matrix \mathbf{A} .

In Assumption 2, $\lambda_C^{(k)}$ can be interpreted as an upper bound on the spectral radius. We also define the divergence of parameters within a cluster:

Definition 1. The divergence of parameters in cluster \mathcal{C} during iteration k , denoted by $\Upsilon_C^{(k)}$, is defined as an upper bound on the difference of belonging nodes parameters as follows:

$$\begin{cases} \|\mathbf{w}_q^{(k)} - \mathbf{w}_{q'}^{(k)}\|_2 \leq \Upsilon_C^{(k)}, & \forall q, q' \in \mathcal{C}, \text{ if } \mathcal{C} \in \mathcal{L}^j, 1 \leq j \leq |\mathcal{L}| - 1, \\ \|\widetilde{\mathbf{w}}_q^{(k)} - \widetilde{\mathbf{w}}_{q'}^{(k)}\|_2 \leq \Upsilon_C^{(k)}, & \forall q, q' \in \mathcal{C}, \text{ if } \mathcal{C} \in \mathcal{L}^{|\mathcal{L}|}. \end{cases} \quad (13)$$

This quantity has some similarity to the divergence of gradients in ML literature (e.g., see Definition 1 of [21]). We will see next in Theorem 1 how it impacts the convergence bound, and

$$\begin{aligned}
F(\mathbf{w}^{(k)}) - F(\mathbf{w}^*) &\leq \frac{\eta \Phi M^2}{2D^2} \sum_{t=0}^{k-1} \left(\frac{\eta - \mu}{\eta} \right)^t \left[\right. \\
&\sum_{a_1 \in \mathcal{L}_1^1} \sum_{a_2 \in \mathcal{Q}(a_1)} \sum_{a_3 \in \mathcal{Q}(a_2)} \cdots \sum_{a_{|\mathcal{L}|-1} \in \mathcal{Q}(a_{|\mathcal{L}|-2})} \mathbb{I}_{\{\mathcal{Q}(a_{|\mathcal{L}|-1})\}}^{(k-t)} |\mathcal{Q}(a_{|\mathcal{L}|-1})|^4 \left(\lambda_{\mathcal{Q}(a_{|\mathcal{L}|-1})}^{(k-t)} \right)^{2\theta_{\mathcal{Q}(a_{|\mathcal{L}|-1})}^{(k-t)}} \left(\Upsilon_{\mathcal{Q}(a_{|\mathcal{L}|-1})}^{(k-t)} \right)^2 \\
&+ \sum_{a_1 \in \mathcal{L}_1^1} \sum_{a_2 \in \mathcal{Q}(a_1)} \cdots \sum_{a_{|\mathcal{L}|-2} \in \mathcal{Q}(a_{|\mathcal{L}|-3})} \mathbb{I}_{\{\mathcal{Q}(a_{|\mathcal{L}|-2})\}}^{(k-t)} |\mathcal{Q}(a_{|\mathcal{L}|-2})|^4 \left(\lambda_{\mathcal{Q}(a_{|\mathcal{L}|-2})}^{(k-t)} \right)^{2\theta_{\mathcal{Q}(a_{|\mathcal{L}|-2})}^{(k-t)}} \left(\Upsilon_{\mathcal{Q}(a_{|\mathcal{L}|-2})}^{(k-t)} \right)^2 + \cdots \\
&+ \sum_{a_1 \in \mathcal{L}_1^1} \mathbb{I}_{\{\mathcal{Q}(a_1)\}}^{(k-t)} |\mathcal{Q}(a_1)|^4 \left(\lambda_{\mathcal{Q}(a_1)}^{(k-t)} \right)^{2\theta_{\mathcal{Q}(a_1)}^{(k-t)}} \left(\Upsilon_{\mathcal{Q}(a_1)}^{(k-t)} \right)^2 + \mathbb{I}_{\{\mathcal{L}_1^1\}}^{(k-t)} |\mathcal{L}_1^1|^4 \left(\lambda_{\mathcal{L}_1^1}^{(k-t)} \right)^{2\theta_{\mathcal{L}_1^1}^{(k-t)}} \left(\Upsilon_{\mathcal{L}_1^1}^{(k-t)} \right)^2 \left. \right] \\
&+ \underbrace{\left(\left(\frac{\eta - \mu}{\eta} \right)^k \left(F(\mathbf{w}^{(0)}) - F(\mathbf{w}^*) \right) \right)}_{(a)}
\end{aligned} \tag{14}$$

in the subsequent propositions how it dictates the consensus rounds required for optimality guarantees. Then, in Sec. III-D, we will develop control algorithms that approximate the divergence in distributed manner at every cluster of the network, and use it to control the convergence rate.

1) *General convergence bound:* The following theorem establishes the convergence bound of Algorithm 1, and is one of the main contributions of this paper:

Theorem 1. *With a learning rate $\beta = 1/\eta$, after k global iterations of any realization of MH-MT, an upper bound on $F(\mathbf{w}^{(k)}) - F(\mathbf{w}^*)$ is given in (14), where $\Phi = N_{|\mathcal{L}|-1} + N_{|\mathcal{L}|-2} + \cdots + N_1 + 1$ is the total number of nodes in the network besides the bottom layer.*

Proof. See Appendix A. ■

The bound in (14) quantifies how the convergence is dependent on several learning and system parameters. In particular, we see a dependence on (i) the characteristics of the loss function (i.e., η, μ), (ii) the number of nodes and clusters at each network layer (through the $|\mathcal{Q}|$ terms), (iii) the characteristics of the communication graph among the nodes inside the clusters, captured via the spectral radius bounds (i.e., λ), (iv) the number of consensus rounds performed at each cluster (i.e., the θ), (v) the dimension of the ML model (i.e., M), and (vi) the divergence among the node parameters at each cluster (i.e., Υ). Given a fixed set of parameters at iteration $k-1$, we can see that increasing the number of consensus rounds at each cluster in iteration k results in a smaller bound, and thus a better expected learning accuracy, as we would expect.

The term (a) in (14) corresponds to the case where there is no consensus error in the system, i.e., when all LUT clusters have $\theta_c^{(k)} \rightarrow \infty$ or when the network consists of all EUT clusters. Since $\frac{\eta - \mu}{\eta} < 1$, the overall rate of convergence of MH-MT is at best linear with rate $1 - \mu/\eta$.

Achieving this would incur prohibitively long delays, however, which motivates us to further consider the effects of the number of consensus rounds. Also, note that the terms $\left(\frac{\eta-\mu}{\eta}\right)^t$ inside the summation have a dampening effect: at global iteration k , the errors from global iteration $t < k$ are multiplied by $\left(\frac{\eta-\mu}{\eta}\right)^{k-t}$, meaning the initial errors for $t \ll k$ are dampened by very small coefficients, while the final errors have a more pronounced effect on the bound. At first glance, this seems to suggest that at higher global iteration indices, more consensus rounds are needed to reduce the errors. However, we can expect the parameters of the end devices to become more similar to one another with increasing global iteration count, which in turn would decrease the divergence within clusters over time. Further, the connectivity of the clusters will change at different layers of the hierarchy, causing the spectral radius to vary. This motivates us to consider adapting the consensus rounds over time (i.e., global iterations) and space (i.e., network layers).

2) *Asymptotic bounds on optimality:* We now connect the number of consensus rounds performed at different network clusters with the asymptotic optimality behavior of MH-MT.

Proposition 1. *For any realization of MH-MT, when the number of consensus rounds at different clusters of different layers of the network satisfies*

$$\begin{cases} \theta_{\mathcal{L}_i^j}^{(k)} \geq \left\lceil \frac{\log(\sigma_j) - 2 \log\left(|\mathcal{L}_i^j|^2 \Upsilon_{\mathcal{L}_i^j}^{(k)}\right)}{2 \log\left(\lambda_{\mathcal{L}_i^j}^{(k)}\right)} \right\rceil, & \text{if } \sigma_j \leq |\mathcal{L}_i^j|^4 \left(\Upsilon_{\mathcal{L}_i^j}^{(k)}\right)^2, \forall k, i, j, \\ \theta_{\mathcal{L}_i^j}^{(k)} \geq 0, & \text{otherwise} \end{cases} \quad (15)$$

for a given set of non-negative constants $\sigma_1, \dots, \sigma_{|\mathcal{L}|}$, then we have the following asymptotic upper bound on the achieved distance from the optimal:

$$\lim_{k \rightarrow \infty} F(\mathbf{w}^{(k)}) - F(\mathbf{w}^*) \leq \frac{\eta^2 \Phi M^2}{2\mu D^2} \sum_{j=0}^{|\mathcal{L}|-1} \sigma_{j+1} N_j. \quad (16)$$

Proof. See Appendix B. ■

Proposition 1 gives a guideline for designing the number of consensus rounds at different network clusters over time to achieve a desired (finite) upper bound on the achieved distance from optimality. By imposing an extra condition on the tuning of the variables $\sigma_1, \dots, \sigma_{|\mathcal{L}|}$ through time we can guarantee a linear convergence to the optimal solution:

Proposition 2. Suppose that the number of consensus iterations employed at different clusters of different network layers satisfies

$$\begin{cases} \theta_{\mathcal{L}_i^j}^{(k)} \geq \left\lceil \frac{\log(\sigma_j^{(k)}) - 2 \log\left(|\mathcal{L}_i^j|^2 \Upsilon_{\mathcal{L}_i^j}^{(k)}\right)}{2 \log\left(\lambda_{\mathcal{L}_i^j}^{(k)}\right)} \right\rceil, & \text{if } \sigma_j^{(k)} \leq |\mathcal{L}_i^j|^4 \left(\Upsilon_{\mathcal{L}_i^j}^{(k)}\right)^2, \forall k, i, j, \\ \theta_{\mathcal{L}_i^j}^{(k)} \geq 0, & \text{otherwise,} \end{cases} \quad (17)$$

where the non-negative constants $\sigma_1^{(k)}, \dots, \sigma_{|\mathcal{L}|}^{(k)}$ are chosen to satisfy

$$\sum_{j=0}^{|\mathcal{L}|-1} \sigma_{j+1}^{(k)} N_j \leq \frac{D^2 \mu (\mu - \delta \eta)}{\eta^4 \Phi M^2} \|\nabla F(\mathbf{w}^{(k-1)})\|^2 \quad (18)$$

for $0 < \delta \leq \mu/\eta$. Then, we have

$$\frac{F(\mathbf{w}^{(k+1)}) - F(\mathbf{w}^*)}{F(\mathbf{w}^{(k)}) - F(\mathbf{w}^*)} \leq (1 - \delta), \quad (19)$$

which implies a linear convergence of MH-MT and that $\lim_{k \rightarrow \infty} F(\mathbf{w}^{(k)}) - F(\mathbf{w}^*) = 0$.

Proof. See Appendix C. ■

Proposition 2 asserts that under this stricter tuning of the number of consensus rounds at different layers, convergence to the optimal solution can be guaranteed with a rate that is upper bounded by $1 - \mu/\eta$, i.e., properties of the ML loss function. On the other hand, Proposition 2's condition boosts the required $\theta_{\mathcal{L}_i^j}^{(k)}$ over time, since the norm of the gradient in (18) decreases over time, in turn lowering the values of $\{\sigma_j^k\}_{j=1}^{|\mathcal{L}|}$. In Proposition 1, the consensus rounds will become tapered over time, since σ_j is fixed over k and the divergence of the parameters is expected to decrease over global iterations. Our experiments in Sec. IV verify these effects. Proposition 2's result also assumes knowledge of the global loss gradient $\|\nabla F(\mathbf{w}^{(k-1)})\|$, which is not known at the beginning of global iteration k ; in Sec. III-D, we will develop an approximation technique for implementing this result in practice.

3) *Relationship between global iterations and consensus rounds:* The following two corollaries to Propositions 1&2 investigate the impact of the number of global iterations on the required consensus rounds, and vice versa. First, we obtain the number of consensus rounds required at different clusters to reach a desired accuracy in a desired global iteration:

Corollary 1. Let $\epsilon \in [(1 - \mu/\eta)^\kappa (F(\mathbf{w}^{(0)}) - F(\mathbf{w}^*)), F(\mathbf{w}^{(0)}) - F(\mathbf{w}^*)]$. To guarantee that MH-MT obtains a solution to within ϵ of the optimal by global iteration κ , i.e., $F(\mathbf{w}^{(\kappa)}) - F(\mathbf{w}^*) \leq \epsilon$, a sufficient number of consensus rounds is given by either of the following conditions:

1) $\theta_{\mathcal{L}_i^j}^{(k)}$ are given by (15), where the values of $\sigma_1, \dots, \sigma_{|\mathcal{L}|}$ satisfy the following inequality:

$$\sum_{j=0}^{|\mathcal{L}|-1} \sigma_{j+1} N_j \leq \frac{\epsilon - (1 - \mu/\eta)^\kappa (F(\mathbf{w}^{(0)}) - F(\mathbf{w}^*))}{(1 - (1 - \mu/\eta)^\kappa) \frac{\eta^2 \Phi M^2}{2\mu D^2}}. \quad (20)$$

2) $\theta_{\mathcal{L}_i^j}^{(k)}$ are given by (17), where the values of $\sigma_1^{(k)}, \dots, \sigma_{|\mathcal{L}|}^{(k)}$ satisfy (18) with δ given by:

$$\delta \geq 1 - \sqrt[\kappa]{\frac{\epsilon}{F(\mathbf{w}^{(0)}) - F(\mathbf{w}^*)}}. \quad (21)$$

Proof. See Appendix D. ■

Second, we obtain the number of global iterations required to reach a desired accuracy for a predetermined policy of determining the consensus rounds in different clusters:

Corollary 2. With ϵ as in Corollary 1, either of the following two conditions give a sufficient number of global iterations κ to achieve $F(\mathbf{w}^{(\kappa)}) - F(\mathbf{w}^*) \leq \epsilon$:

1) If the $\theta_{\mathcal{L}_i^j}^{(k)}$ satisfy (15) given $\sigma_1, \dots, \sigma_{|\mathcal{L}|}$, and $\epsilon \geq \frac{\eta^2 \Phi M^2}{2\mu D^2} \sum_{j=0}^{|\mathcal{L}|-1} \sigma_{j+1} N_j$, we can have:

$$\kappa \geq \left\lceil \frac{\log \left(\epsilon - \frac{\eta^2 \Phi M^2}{2\mu D^2} \sum_{j=0}^{|\mathcal{L}|-1} \sigma_{j+1} N_j \right) - \log \left(F(\mathbf{w}^{(0)}) - F(\mathbf{w}^*) - \frac{\eta^2 \Phi M^2}{2\mu D^2} \sum_{j=0}^{|\mathcal{L}|-1} \sigma_{j+1} N_j \right)}{\log(1 - \mu/\eta)} \right\rceil \quad (22)$$

2) If the number of consensus rounds at different network layers satisfies (17) and (18) given $\sigma_1^{(k)}, \dots, \sigma_{|\mathcal{L}|}^{(k)}$ and δ , we can have:

$$\kappa \geq \left\lceil \frac{\log(\epsilon) - \log(F(\mathbf{w}^{(0)}) - F(\mathbf{w}^*))}{\log(1 - \delta)} \right\rceil. \quad (23)$$

Proof. See Appendix E. ■

4) *Varying gradient step size:* The gradient update (4) is based on a constant step size β . If we design a time-varying step size β_k that is decreasing in each global iteration k , we can sharpen the convergence result in Proposition 1, if we assume that devices share gradients instead of parameters (see Sec. II-D). In particular, we can guarantee that MH-MT will converge to the optimal solution, rather than to a solution with a finite optimality gap:

Proposition 3. *Suppose that instead of sharing parameters, the nodes share gradients using the same procedure described in Algorithm 1, and that each parent node samples one of its children uniformly at random. Also, assume that edge devices use a step size $\beta_k = \frac{\alpha}{k+\lambda}$, where $\lambda > 1$ and $\alpha > 1/\mu$ at global iteration k , with $\beta_0 \leq 1/\eta$. If the number of consensus rounds are performed according to (15) with constants $\sigma_1, \dots, \sigma_{|\mathcal{L}|}$, we have:*

$$\mathbb{E}[F(\mathbf{w}^{(k)}) - F(\mathbf{w}^*)] \leq \frac{\Gamma}{k + \lambda}, \quad (24)$$

where

$$\Gamma = \max \left\{ \lambda(F(\mathbf{w}^{(0)}) - F(\mathbf{w}^*)), \frac{\eta\alpha^2\Phi M^2 \sum_{j=0}^{|\mathcal{L}|-1} \sigma_{j+1} N_j}{2D^2(\alpha\mu - 1)} \right\}. \quad (25)$$

Consequently, under such conditions MH-MT converges to the optimal solution:

$$\lim_{k \rightarrow \infty} \mathbb{E}[F(\mathbf{w}^{(k)}) - F(\mathbf{w}^*)] = 0. \quad (26)$$

Proof. See Appendix F. ■

The bound (24) implies a rate of convergence of $O(1/k)$, which is slower than the linear convergence obtained in Proposition 2, but also allows tapering of the consensus rounds.

5) *Cluster sampling:* In a fog network with millions of nodes, it may be desirable to reduce upstream communication demand even further than what is provided by LUT clusters in Fig. 3. One possibility is to implement a cluster sampling technique where only a portion of the clusters in the bottom-most layer are engaged in model training at each global iteration. We develop this method in Appendix G, and extend Theorem 1 to this case.

D. Control Algorithms for Distributed Consensus Tuning

With all else constant, fewer rounds of consensus results in lower power consumption and network load among the devices in LUT clusters. Here, we develop control algorithms for MH-MT that tune the number of consensus rounds through time and space (network layers).

1) *Adaptive consensus for strongly convex and smooth loss functions:* We are interested in realizing the two consensus tuning policies that we obtained in Propositions 1 and 2, which we refer to as Policies A and B, respectively. Policy A will provide a finite optimality gap, with tapering consensus through time, while Policy B will provide linear convergence to the optimal, with of boosting the number of consensus rounds though time. We are interested in realizing

these policies in a distributed manner, where the number of consensus rounds inside different clusters are tuned by the corresponding parent nodes in real-time. It is assumed that parent node of cluster \mathcal{C} has an estimate about the topology of the cluster, and thus the upper-bound of the spectral radius of its children cluster graph $\lambda_{\mathcal{C}}^k$ at each global iteration.

According to (15) and (17), for both policies, tuning of the consensus rounds for cluster \mathcal{C} requires the knowledge of the divergence of parameters $\Upsilon_{\mathcal{C}}^{(k)}$. Also, Policy A requires a set of fixed consensus control parameters σ_j for clusters located in layer \mathcal{L}^j , while Policy B requires the global gradient of the broadcasted weight $\|\nabla F(\mathbf{w}^{(k-1)})\|$ and the real-time consensus control parameters $\sigma_j^{(k)}$. In the following, we first derive the divergence of parameters in a distributed manner. Then, we focus on realizing the other specific parameters for each policy.

Given (13), at cluster \mathcal{C} , the divergence of the devices parameters can be approximated as³

$$\Upsilon_{\mathcal{C}}^{(k)} \approx \max_{q, q' \in \mathcal{C}} \{ \|\mathbf{w}_q^{(k)}\| - \|\mathbf{w}_{q'}^{(k)}\| \} = \underbrace{\max_{q \in \mathcal{C}} \|\mathbf{w}_q^{(k)}\|}_{(a)} - \underbrace{\min_{q' \in \mathcal{C}} \|\mathbf{w}_{q'}^{(k)}\|}_{(b)}, \quad \mathcal{C} \in \mathcal{L}^j, 1 \leq j \leq |\mathcal{L}| - 1. \quad (27)$$

To obtain (a) and (b) in a distributed manner, at any given LUT cluster, each node $n \in \mathcal{C}$ first computes scalar value $\|\mathbf{w}_n^{(k)}\|$.⁴ Nodes then share their values with their neighbors iteratively. In each iteration, each node saves two scalars: the (i) maximum and (ii) minimum values among the received values and its current value. It is easy to verify that for any given communication graph $\mathcal{G}_{\mathcal{C}}^{(k)}$ among the cluster nodes, once the number of iterations has exceeded the diameter of $\mathcal{G}_{\mathcal{C}}^{(k)}$, the saved values at each node will correspond to (a) and (b) for cluster \mathcal{C} in (27). The parent node can then sample the value of one of its children to compute (27).

For Policy A, since the values of $\{\sigma_j\}_{j=1}^{|\mathcal{L}|}$ are fixed through time, one option is for the server to tune them once at the beginning of training and distribute them among the nodes at different layers. If satisfaction of a given accuracy ϵ at a certain iteration κ is desired, we use the result of Corollary 1 and obtain the consensus control parameters as the solution of the following max-min optimization problem: $\arg \max_{\{\sigma_j\}_{j=1}^{|\mathcal{L}|}} \min \{N_{j-1}\sigma_j\}$ subject to (20). The solution is given by

$$\sigma_j^* = \frac{\epsilon - (1 - \mu/\eta)^\kappa (F(\mathbf{w}^{(0)}) - F(\mathbf{w}^*))}{(1 - (1 - \mu/\eta)^\kappa) \frac{\eta^2 \Phi M^2}{2\mu D^2} N_{j-1} |\mathcal{L}|}, \quad 1 \leq j \leq |\mathcal{L}|, \quad (28)$$

³Here, for practical purposes, we use the lower bound of divergence $|\|\mathbf{a}\| - \|\mathbf{b}\|| \leq \|\mathbf{a} - \mathbf{b}\|$. The upper bound alternative $\|\mathbf{a} - \mathbf{b}\| \leq \|\mathbf{a}\| + \|\mathbf{b}\|$ can be arbitrarily large even when $\mathbf{a} = \mathbf{b}$.

⁴For $\mathcal{C} \in \mathcal{L}^{|\mathcal{L}|}$, as in (13), we have $\Upsilon_{\mathcal{C}}^{(k)} \approx \max_{q \in \mathcal{C}} \|\tilde{\mathbf{w}}_q^{(k)}\| - \min_{q' \in \mathcal{C}} \|\tilde{\mathbf{w}}_{q'}^{(k)}\|$.

which can be broadcasted at the beginning of training among the nodes. The reason behind the choice of the aforementioned max-min problem is two-fold. First, according to (15), for a given set of divergence of parameters $\Upsilon_{\mathcal{C}}^{(k)}$ across \mathcal{C} , fewer numbers of consensus at each layer \mathcal{L}^j is associated with larger values of σ_j , so larger values of consensus control parameters are desired at every layer of the network. Second, this choice of objective function results in smaller values of consensus tuning parameters as we move down the hierarchy (from the main server to the edge devices) and the number of nodes increases. This leads to lower errors in the bottom layers, which is desired in practice given the discussion in Sec. III-B that the errors from the bottom layers are propagated and amplified as we move up the hierarchy.

For Policy B, to obtain $\|\nabla F(\mathbf{w}^{(k-1)})\|$, we use (4) to approximate $\nabla F(\mathbf{w}^{(k-2)})$ as $\nabla F(\mathbf{w}^{(k-2)}) \approx (\mathbf{w}^{(k-2)} - \mathbf{w}^{(k-1)}) / \beta$. This is an approximation due to the error introduced in the consensus process. Using this, the main server estimates $\|\nabla F(\mathbf{w}^{(k-1)})\|$ via $\|\widetilde{\nabla F(\mathbf{w}^{(k-1)})}\| = \frac{1}{\omega} \|\nabla F(\mathbf{w}^{(k-2)})\|$, where $\omega > 1$ based on the intuition that the norm of the gradient should be decreasing over k , and broadcasts it along with $\mathbf{w}^{(k-1)}$. The choice of ω can be viewed as a tradeoff between the number of global aggregations k and the number of consensus rounds $\theta_{\mathcal{C}}^{(k)}$ per aggregation: as ω increases, we tolerate less consensus error in (18), requiring more $\theta_{\mathcal{C}}^{(k)}$ and less k . Then, the cluster heads can obtain the $\sigma_j^{(k)}$ for all \mathcal{L}^j and k according to the following max-min problem: $\arg \max_{\{\sigma_j^{(k)}\}_{j=1}^{|\mathcal{L}|}} \min \{N_{j-1}\sigma_j^{(k)}\}$ subject to (18) for a given δ . The solution is:

$$\sigma_j^{(k)*} = \frac{D^2 \mu (\mu - \delta \eta)}{\eta^4 \Phi M^2 N_{j-1} |\mathcal{L}|} \|\widetilde{\nabla F(\mathbf{w}^{(k-1)})}\|^2, \quad 1 \leq j \leq |\mathcal{L}|, \quad \forall k. \quad (29)$$

The parameter δ can be tuned by the main server at the beginning of training to guarantee a desired linear convergence, or it can be tuned by (21) to satisfy a desired accuracy at a certain global iteration. In both cases, the server broadcasts this parameter among the nodes at the beginning of training. With δ and $\|\widetilde{\nabla F(\mathbf{w}^{(k-1)})}\|$ in hand along with the ML model characteristics (D, μ, η, M) and networked related parameters $(\Phi, |\mathcal{L}|, N_{j-1})$ that can be once broadcasted by the server, all the parent nodes of the clusters can calculate (29) at each global iteration, which then can be used in (17) to tune the number of consensus rounds for the children nodes.

A summary of this procedure for tuning the consensus rounds at a cluster is given in Algorithm 2. In the full MH-MT method described in Algorithm 1, this is (optionally) called for each cluster, referred to lines marked via **.

Algorithm 2: Adaptive consensus tuning at each cluster \mathcal{C} .

- input :** Global aggregation count k , tuning parameter $\omega > 1$, cluster index $\mathcal{C} = \mathcal{L}_i^j$.
output: Number of consensus rounds $\theta_{\mathcal{C}}^{(k)}$ for the cluster.
- 1 Nodes inside the cluster \mathcal{C} iteratively compute (a) and (b) of (27).
 - 2 Parent node of cluster samples one child and computes (27).
 - 3 **if** *asymptotic convergence to optimal desired* **then**
 - 4 Parent node uses (29) with stored $\|\nabla F(\mathbf{w}^{(k-1)})\|$ and δ received from the server to compute $\sigma_j^{(k)}$.
 - 5 Parent node uses (17) to compute the number of consensus rounds $\theta_{\mathcal{L}_i^j}^{(k)}$.
 - 6 **else**
 - 7 Parent node uses the received consensus tuning parameter $\sigma_j^{(k)}$ from the server in (15) to compute the $\theta_{\mathcal{L}_i^j}^{(k)}$.
 - 8 Parent node broadcasts $\theta_{\mathcal{L}_i^j}^{(k)}$ among its children.
-

Algorithm 3: Adaptive consensus tuning at each cluster \mathcal{C} for non-convex loss functions.

- input :** Tolerable error of aggregations ψ , global aggregation count k , cluster index $\mathcal{C} = \mathcal{L}_i^j$.
output: Number of consensus rounds $\theta_{\mathcal{C}}^{(k)}$ for the cluster.
- 1 Nodes inside the cluster iteratively compute (a) and (b) of (27).
 - 2 Parent node of cluster samples one child and computes (27).
 - 3 Parent node of the cluster computes the required rounds of consensus as follows:
- $$\begin{cases} \theta_{\mathcal{L}_i^j}^{(k)} \geq \frac{\log(\sigma_j) - 2 \log(|\mathcal{L}_i^j|^2 \Upsilon_{\mathcal{L}_i^j}^{(k)})}{2 \log(\lambda_{\mathcal{L}_i^j}^{(k)})}, & \text{if } \sigma_j \leq |\mathcal{L}_i^j|^4 \left(\Upsilon_{\mathcal{L}_i^j}^{(k)} \right)^2, \\ \theta_{\mathcal{L}_i^j}^{(k)} \geq 0, & \text{otherwise} \end{cases}, \quad \text{where } \sigma_j = \frac{\psi}{\frac{\Phi M^2}{D^2} N_{j-1} |\mathcal{L}|}. \quad (30)$$
- 4 Parent node broadcasts $\theta_{\mathcal{L}_i^j}^{(k)}$ among its children.
-

2) *Adaptive consensus for non-convex loss functions:* Several contemporary ML models, such as neural networks, possess non-convex loss functions for which Assumption 1 does not apply. Tractable convergence bounds for distributed ML in these settings, to our knowledge, have yet to be discovered. We can, however, develop a heuristic approach to tune the consensus rounds of MH-MT in these settings, if we specify a maximum tolerable error of aggregations ψ at each global iteration. The resulting procedure is given in Algorithm 3, which would be called once for each cluster in Algorithm 1 in place of Algorithm 2 (see the lines marked ##). To execute this, prior to the start of training, each parent node should receive ψ and the number of nodes in its layer. Using Algorithm 3, we can show that the 2-norm of aggregation errors is always bounded by parameter ψ (see Appendix H).

IV. EXPERIMENTAL EVALUATION

We conducted several numerical experiments to evaluate MH-MT. In this section, due to space limitations, we present the setup (Sec. IV-A) and results (Sec. IV-B) for a single dataset and fog topology. The full set of results can be found in Appendix I.

A. Experimental Setup

Referring to Fig. 3, we consider a fog network consisting of a main server and three subsequent layers. There are 125 edge devices in the bottom layer (\mathcal{L}^3), clustered into groups of 5 nodes. Each of these clusters communicates with one of 25 parent nodes in layer \mathcal{L}^2 . The nodes at this layer are in turn clustered into groups of 5, with 5 parent nodes at layer \mathcal{L}^1 that communicate with the main server. We consider the cases where (i) all clusters are configured to operate in LUT mode and (ii) all are EUT, which allows us to evaluate the performance differences in terms of model convergence, energy consumption, and parameters transferred. In the LUT case, connectivity within clusters follows a random geometric graph (see Appendix I).

For the ML model, we consider a 10-class image classification task on the standard MNIST dataset of 70K handwritten digits (<http://yann.lecun.com/exdb/mnist/>). We evaluate with both regularized SVM and fully-connected neural network (NN) classifiers as loss functions; SVM satisfies Assumption 1 while NN does not. Unless stated otherwise, the results are presented using SVM. Samples are distributed across devices in either an i.i.d. or non-i.i.d. manner; for i.i.d., each device has samples from each class, while for non-i.i.d., each device has samples from only one class, allowing us to evaluate the robustness of our method to different distributions. More details on the dataset, classifiers, and hyperparameter tuning procedure are available in Appendix I: there, we also provide additional results on the Fashion MNIST (F-MNIST) dataset and for a network of 625 edge devices; the results are qualitatively similar.

B. Results and Discussion

1) *MH-MT with fixed rounds of consensus*: We first consider a scenario in which the number of consensus rounds is set to be constant value θ over all clusters. In Fig. 5, we compare the performance of MH-MT over global aggregations k when all the clusters work in LUT mode and have fixed rounds of consensus with the case where the network consists of all EUT clusters (referred to as “EUT baseline”). The EUT case is identical (in terms of convergence) to carrying out centralized gradient descent over the entire dataset. We see that increasing the number of consensus at different layers increases the accuracy and stability of the model training for MH-MT. Though convergence is not achieved in all cases (in particular, when θ is 1 and 2), if the number of consensus rounds chosen is larger than 15, comparable performance to EUT is achieved. This performance is characterized by linear convergence, as can be seen in Fig. 5(c).

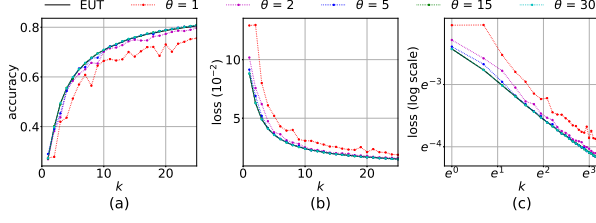


Fig. 5: Performance comparison between baseline EUT and MH-MT when a fixed number of consensus rounds θ is used at every cluster of the network, for non-i.i.d. As the number of consensus rounds increases, MH-MT performs more similar to the EUT baseline and the learning is more stable.

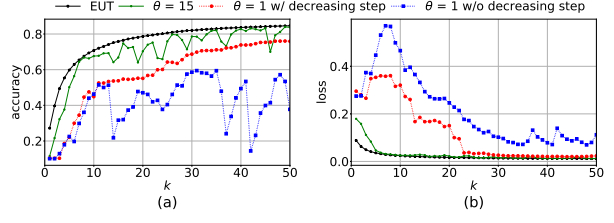


Fig. 6: Performance comparison between baseline EUT, and MH-MT with and without (w/o) decreasing the gradient descent step size. Decreasing the step size can provide convergence to the optimal solution in cases where a fixed step size is not capable, but also has a slower convergence speed.

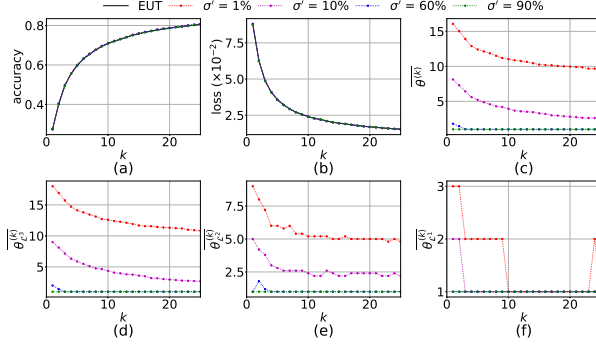


Fig. 7: Performance comparison between baseline EUT and MH-MT for i.i.d. when a finite optimality gap is tolerable. σ_i at \mathcal{L}^i is fixed as $\sigma_i = \sigma' \max_{\mathcal{L}^j \in \mathcal{L}^i} \Upsilon_{\mathcal{L}^j}^{(1)}$. Tapering of consensus rounds though time and space (layers) can be observed.

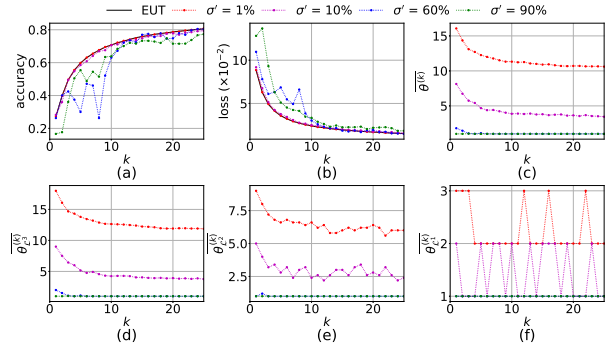


Fig. 8: Performance comparison between baseline EUT and MH-MT for non-i.i.d. when a finite optimality gap is tolerable. σ_i is set as in Fig. 7. Smaller loss and higher accuracy are achieved with smaller σ' , implying more rounds of consensus.

2) *MH-MT with decaying gradient descent step size*: The effect of decreasing the gradient descent step size according to Proposition 3 is depicted in Fig. 6. This verifies that the decay can suppress the finite optimality bound and converge to the optimal model. At the same time, the convergence occurs at a slower pace compared with the EUT baseline, which is also inline with our theoretical results (convergence rate of $O(1/k)$). Fig. 6 also reveals the inherent trade-off between conducting a higher number of consensus rounds with a constant learning rate (higher power consumption with a fast convergence speed) and performing a fewer number of consensus rounds with a decaying learning rate (lower power consumption with a slower convergence).

3) *MH-MT with adaptive rounds of consensus*: We now study the case when our distributed consensus tuning scheme is utilized. The results are depicted for both convergence criteria cases, i.e., where a finite gap of convergence is tolerable (Figs. 7, 8) and when the linear convergence to the optimal solution is desired (Figs. 9, 10). Recall that Propositions 1&2 obtain the sufficient number of consensus based on an upper bound; for this experiment, we observed that $\log(\sigma_j)$, $\log(\sigma_j^{(k)})$ in (15) and (17) can be scaled and used as $\log(\chi\sigma_j^{(k)})$, $\log(\chi\sigma_j^{(k)})$, where $\chi \in [1, 15]$, $\forall j$ to obtain fewer rounds of consensus while satisfying the desired convergence characteristics.

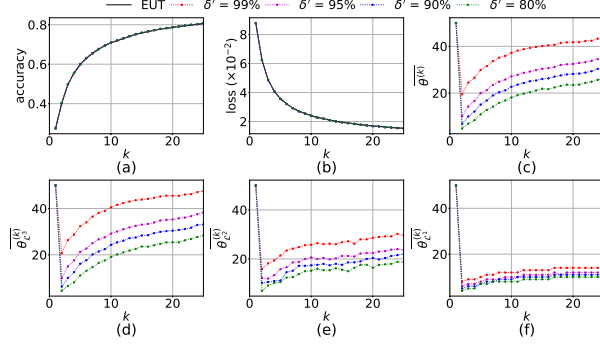


Fig. 9: Performance comparison between baseline EUT and MH-MT for i.i.d. when linear convergence to the optimal is desired. The value of δ is set at $\delta = \delta' \frac{\mu}{\eta}$. Boosting of the consensus rounds though time can be observed. Also, tapering through space can be observed by comparing the consensus rounds in the bottom subplots.

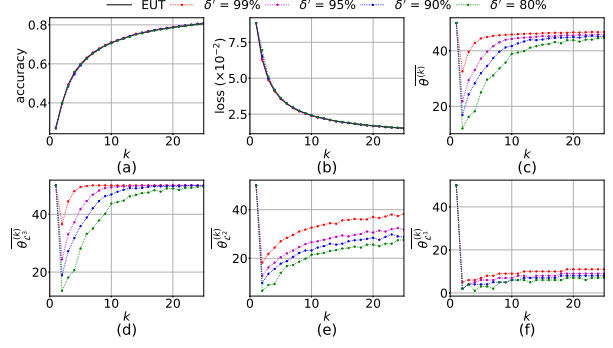


Fig. 10: Performance comparison between baseline EUT and MH-MT for non-i.i.d. when linear convergence to the optimal is desired. The value of δ is set as in Fig. 9. Smaller values of loss and higher accuracy are both associated with larger value of δ , which results in lower error tolerance and more rounds of consensus.

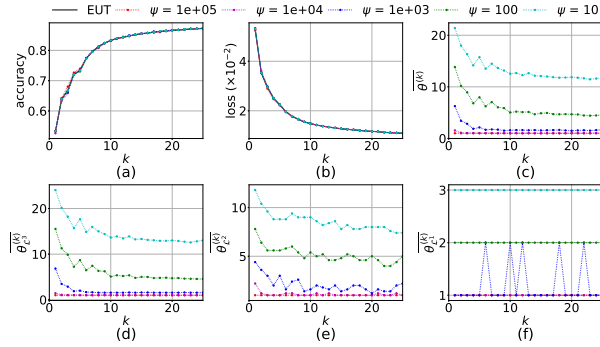


Fig. 11: Performance comparison between baseline EUT and MH-MT under i.i.d. using NNs with different values of ψ . Tapering the consensus rounds though time can be observed. Also, tapering through space can be observed by comparing the consensus rounds in the bottom subplots.

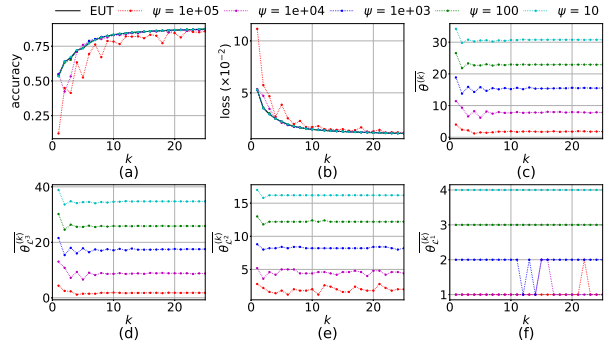


Fig. 12: Performance comparison between baseline EUT and MH-MT under non-i.i.d. using NNs with different values of ψ . Lower loss and higher accuracy are associate with smaller values of ψ , which result in lower error tolerance and larger values of consensus rounds.

Fig. 7 depicts the result for the case where local datasets are i.i.d., with the values of $\{\sigma_j\}_{j=1}^{|\mathcal{L}|}$ depicted. In the figures, $\overline{\theta^{(k)}}$ denotes the average number of consensus rounds over all the network layers at global iteration k , and $\overline{\theta_{\mathcal{L}^j}^{(k)}}$ denotes the average number of consensus rounds at iteration k in layer \mathcal{L}^j . We observe that: (i) the number of consensus performed at the network is tapered through time (subplot c), and (ii) the number of consensus performed at different network layers is tapered through space, where higher layers of the network perform lower numbers of consensus (subplots d, e, and f). We perform the same experiment with non-i.i.d. datasets across the nodes in Fig. 8. Comparing Fig. 8 to 7, it can be observed that non-i.i.d. introduces oscillations to the number of consensus performed at different network layers, and the smaller values of error control parameters result in larger number of consensus rounds which leads to more stable training.

The same experiment is repeated in Figs. 9, 10 for the linear convergence case. We see that

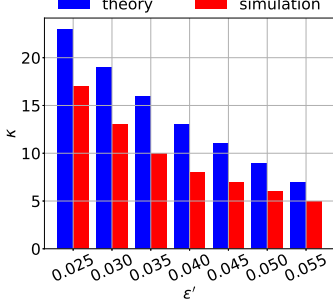


Fig. 13: Comparison between the theoretical and simulation results regarding the number of global iterations to achieve an accuracy of $\epsilon'(F(w^{(0)}) - F(w^*))$ for different ϵ' . Convergence in practice is faster than the derived upper bound.

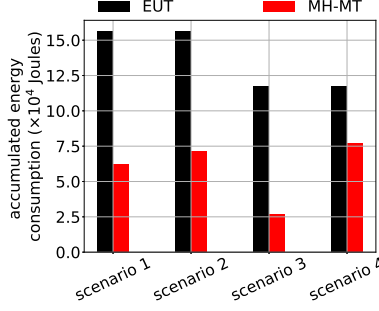


Fig. 14: Comparison of accumulated energy consumption between EUT and MH-MT over scenario 1: $\sigma' = 0.1$ from Fig. 7, scenario 2: $\sigma' = 0.1$ from Fig. 8, scenario 3: $\psi = 10^4$ from Fig. 11, and scenario 4: $\psi = 10^4$ from Fig. 12.

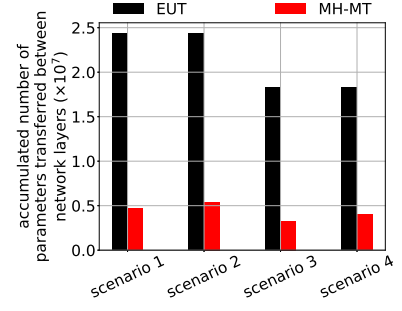


Fig. 15: Comparison of parameters transferred among layers in EUT vs MH-MT over scenario 1: $\sigma' = 0.1$ from Fig. 7, scenario 2: $\sigma' = 0.1$ from Fig. 8, scenario 3: $\psi = 10^4$ from Fig. 11, and scenario 4: $\psi = 10^4$ from Fig. 12.

the number of consensus rounds is tapered through space (subplots d, e, and f) and boosts by increasing the number of iterations in different network layers. This is due to the decrease in the norm of gradient in the right hand side of (29) over time, which calls for an increment in the number of consensus rounds for more precision as the gradient becomes smaller. Comparing Figs. 9 and 10 with Figs. 7 and 8, it can be concluded that guaranteeing the linear convergence comes with the price of performing higher rounds of consensus over time. In Figs. 7, 8, a small optimality gap is achieved while the number of consensus is tapered over time.

4) *MH-MT with adaptive rounds of consensus for non-convex models:* Figs. 11 and 12 depict experimental results with NNs for different values of tolerable error of aggregations ψ , under i.i.d and non-i.i.d data distributions, respectively. These figures show the effect of tolerable error of aggregations on the performance of NNs; by decreasing the tolerable error, the number of consensus rounds is increased, and the performance is enhanced. These figures also reveal a tapering of the number of consensus through time and space in the i.i.d case.

5) *Analytical vs. experimental bound comparison:* In Fig. 13, we investigate the number of global iterations required to obtain a certain accuracy under the linear convergence in Corollary 1. We compare the result obtained from Policy B implementing (29) in Sec. III-D to that observed in the experiment. The results indicate that the theoretical results are indeed an upper bound.

6) *Network resource utilization of MH-MT:* We have seen that MH-MT can achieve comparable performance to the EUT baseline in terms of model convergence. We now consider the difference in network resource utilization. In particular, we consider the following two metrics: (i) the amount of data transferred between the network layers, and (ii) the accumulated energy

consumption of the edge devices. In both cases, EUT and MH-MT are trained up to reaching 98% of the final accuracy of achieved after 50 iterations of centralized gradient descent. We consider four scenarios, corresponding to those used in the experiments of Figs. 7, 8, 11, 12. To obtain the accumulated energy, we consider the typical transmission power of edge devices to be 10dbm in D2D mode and 24dbm in uplink mode [50], [51], and assume that transmission of parameters at each round takes 0.25 sec with a data rate of 1Mbit/s at 32 bits quantization. The accumulated energy consumption of the edge devices through the training phase is depicted in Fig. 14, which reveals around 50% energy saving in average as compared to EUT baseline. The accumulated number of parameters transferred over the network layers are shown in Fig. 15 revealing 80% reduction in the number of parameters transferred over the layers as compared to the EUT.

V. CONCLUSION AND FUTURE WORK

In this paper, we developed multi-stage hybrid model training (MH-MT) for large-scale wireless fog networks, a novel methodology which migrates the start topology of federated learning to a multi-layer distributed architecture using D2D communications. We theoretically obtained the convergence bound of MH-MT explicitly considering the time varying network topology, time varying number of consensus at different network clusters, and inherent ML model characteristics. We proposed a set of policies under which convergence either to a finite optimality gap or the global optimum can be achieved, and used them to develop a set of adaptive distributed control algorithms that tune the number of consensus rounds at different clusters of the network. Our experimental results validated the improvement in network resource utilization MH-MT achieves.

This paper motivates several directions for future work. Investigating more specific system characteristics that have been considered for federated learning – such as communication imperfections, mitigation of stragglers, and device scheduling – for the multi-stage hybrid structure of FogL is promising. Also, the proposed hybrid learning introduces the network dimension, which motivates follow-up works on network (re-)formation and topology design.

REFERENCES

- [1] G. D. Maayan. The IoT rundown for 2020: Stats, risks, and solutions. [Online]. Available: <https://securitytoday.com/Articles/2020/01/13/The-IoT-Rundown-for-2020.aspx?Page=2>
- [2] M. Chiang and T. Zhang, “Fog and IoT: An overview of research opportunities,” *IEEE Internet Things J.*, vol. 3, no. 6, pp. 854–864, 2016.

- [3] D. Ciregan, U. Meier, and J. Schmidhuber, "Multi-column deep neural networks for image classification," in *Proc. IEEE Conf. Comput. Vision Pattern Recog. (CVPR)*, 2012, pp. 3642–3649.
- [4] R. Collobert and J. Weston, "A unified architecture for natural language processing: Deep neural networks with multitask learning," in *Proc. Int. Conf. Mach. Learn.*, 2008, pp. 160–167.
- [5] B. McMahan, E. Moore, D. Ramage, S. Hampson, and B. A. y Arcas, "Communication-efficient learning of deep networks from decentralized data," in *Proc. Artif. Intell. Stat.*, 2017, pp. 1273–1282.
- [6] J. Konečný, H. B. McMahan, F. X. Yu, P. Richtárik, A. T. Suresh, and D. Bacon, "Federated learning: Strategies for improving communication efficiency," *arXiv preprint arXiv:1610.05492*, 2016.
- [7] Y. Tu, Y. Ruan, S. Wang, S. Wagle, C. G. Brinton, and C. Joe-Wang, "Network-aware optimization of distributed learning for fog computing," in *Proc. IEEE Int. Conf. Comput. Commun. (INFOCOM)*, 2020.
- [8] S. Hosseinalipour, C. G. Brinton, V. Aggarwal, H. Dai, and M. Chiang, "From federated learning to fog learning: Towards large-scale distributed machine learning in heterogeneous wireless networks," *arXiv preprint arXiv:2006.03594*, 2020.
- [9] M. N. Tehrani, M. Uysal, and H. Yanikomeroglu, "Device-to-device communication in 5G cellular networks: challenges, solutions, and future directions," *IEEE Commun. Mag.*, vol. 52, no. 5, pp. 86–92, 2014.
- [10] M. Abolhasan, T. Wysocki, and E. Dutkiewicz, "A review of routing protocols for mobile ad hoc networks," *Ad hoc Netw.*, vol. 2, no. 1, pp. 1–22, 2004.
- [11] S. Zeadally, R. Hunt, Y.-S. Chen, A. Irwin, and A. Hassan, "Vehicular ad hoc networks (VANETS): status, results, and challenges," *Telecommun. Syst.*, vol. 50, no. 4, pp. 217–241, 2012.
- [12] I. Bekmezci, O. K. Sahingoz, and Ş. Temel, "Flying ad-hoc networks (FANETs): A survey," *Ad hoc Netw.*, vol. 11, no. 3, pp. 1254–1270, 2013.
- [13] K. Akkaya and M. Younis, "A survey on routing protocols for wireless sensor networks," *Ad hoc Netw.*, vol. 3, no. 3, pp. 325–349, 2005.
- [14] S. Maheshwari, D. Raychaudhuri, I. Seskar, and F. Bronzino, "Scalability and performance evaluation of edge cloud systems for latency constrained applications," in *Proc. IEEE/ACM Symp. Edge Comput. (SEC)*, 2018, pp. 286–299.
- [15] M. Chen, Z. Yang, W. Saad, C. Yin, H. V. Poor, and S. Cui, "A joint learning and communications framework for federated learning over wireless networks," *arXiv preprint arXiv:1909.07972*, 2019.
- [16] N. H. Tran, W. Bao, A. Zomaya, M. N. H. Nguyen, and C. S. Hong, "Federated learning over wireless networks: Optimization model design and analysis," in *Proc. IEEE Int. Conf. Comput. Commun. (INFOCOM)*, 2019, pp. 1387–1395.
- [17] G. Zhu, Y. Wang, and K. Huang, "Broadband analog aggregation for low-latency federated edge learning," *IEEE Trans. Wireless Commun.*, vol. 19, no. 1, pp. 491–506, 2020.
- [18] M. M. Amiri and D. Gündüz, "Federated learning over wireless fading channels," *IEEE Trans. Wireless Commun.*, vol. 19, no. 5, pp. 3546–3557, 2020.
- [19] N. Shlezinger, M. Chen, Y. C. Eldar, H. V. Poor, and S. Cui, "Federated learning with quantization constraints," in *Proc. IEEE Int. Conf. Acoustics, Speech, Signal Process. (ICASSP)*, 2020, pp. 8851–8855.
- [20] C. Renggli, S. Ashkboos, M. Aghagolzadeh, D. Alistarh, and T. Hoefer, "SparCML: High-performance sparse communication for machine learning," in *Proc. Int. Conf. High Perform. Comput., Netw., Storage Anal.*, 2019, pp. 1–15.
- [21] S. Wang, T. Tuor, T. Salonidis, K. K. Leung, C. Makaya, T. He, and K. Chan, "Adaptive federated learning in resource constrained edge computing systems," *IEEE J. Sel. Areas Commun. (JSAC)*, vol. 37, no. 6, pp. 1205–1221, 2019.
- [22] D. Ye, R. Yu, M. Pan, and Z. Han, "Federated learning in vehicular edge computing: A selective model aggregation approach," *IEEE Access*, vol. 8, pp. 23 920–23 935, 2020.

- [23] S. Dhakal, S. Prakash, Y. Yona, S. Talwar, and N. Himayat, "Coded federated learning," in *IEEE Glob. Commun. Conf. Workshop (GLOBECOM Workshop)*, 2019, pp. 1–6.
- [24] S. Ji, W. Jiang, A. Walid, and X. Li, "Dynamic sampling and selective masking for communication-efficient federated learning," *arXiv preprint arXiv:2003.09603*, 2020.
- [25] W. Wang, Y. Sun, B. Eriksson, W. Wang, and V. Aggarwal, "Wide compression: Tensor ring nets," in *Proc. IEEE Conf. Comput. Vision Pattern Recog. (CVPR)*, 2018, pp. 9329–9338.
- [26] R. C. Geyer, T. Klein, and M. Nabi, "Differentially private federated learning: A client level perspective," *arXiv preprint arXiv:1712.07557*, 2017.
- [27] S. Hardy, W. Henecka, H. Ivey-Law, R. Nock, G. Patrini, G. Smith, and B. Thorne, "Private federated learning on vertically partitioned data via entity resolution and additively homomorphic encryption," *arXiv preprint arXiv:1711.10677*, 2017.
- [28] A. Elgabli, J. Park, A. S. Bedi, M. Bennis, and V. Aggarwal, "GADMM: Fast and communication efficient framework for distributed machine learning," *arXiv preprint arXiv:1909.00047*, 2019.
- [29] V. Smith, S. Forte, C. Ma, M. Takáč, M. I. Jordan, and M. Jaggi, "CoCoA: A general framework for communication-efficient distributed optimization," *J. Mach. Learn. Res.*, vol. 18, no. 1, pp. 8590–8638, 2017.
- [30] P. Richtárik and M. Takáč, "Distributed coordinate descent method for learning with big data," *J. Mach. Learn. Res.*, vol. 17, no. 1, pp. 2657–2681, 2016.
- [31] S. Niknam, H. S. Dhillon, and J. H. Reed, "Federated learning for wireless communications: Motivation, opportunities and challenges," *arXiv preprint arXiv:1908.06847*, 2019.
- [32] G. Zhu, D. Liu, Y. Du, C. You, J. Zhang, and K. Huang, "Toward an intelligent edge: Wireless communication meets machine learning," *IEEE Commun. Mag.*, vol. 58, no. 1, pp. 19–25, 2020.
- [33] C. L. P. Chen, G. Wen, Y. Liu, and F. Wang, "Adaptive consensus control for a class of nonlinear multiagent time-delay systems using neural networks," *IEEE Trans. Neural Netw. Learning Syst.*, vol. 25, no. 6, pp. 1217–1226, 2014.
- [34] T. Li and J.-F. Zhang, "Consensus conditions of multi-agent systems with time-varying topologies and stochastic communication noises," *IEEE Trans. Autom. Control*, vol. 55, no. 9, pp. 2043–2057, 2010.
- [35] S. Kar and J. M. F. Moura, "Distributed consensus algorithms in sensor networks with imperfect communication: Link failures and channel noise," *IEEE Trans. Signal Process.*, vol. 57, no. 1, pp. 355–369, 2009.
- [36] S. Manfredi, "Design of a multi-hop dynamic consensus algorithm over wireless sensor networks," *Control Eng. Practice*, vol. 21, no. 4, pp. 381–394, 2013.
- [37] T. Chang, M. Hong, and X. Wang, "Multi-agent distributed optimization via inexact consensus ADMM," *IEEE Trans. Signal Process.*, vol. 63, no. 2, pp. 482–497, 2015.
- [38] T. Chang, A. Nedić, and A. Scaglione, "Distributed constrained optimization by consensus-based primal-dual perturbation method," *IEEE Trans. Autom. Control*, vol. 59, no. 6, pp. 1524–1538, 2014.
- [39] B. Johansson, T. Keviczky, M. Johansson, and K. H. Johansson, "Subgradient methods and consensus algorithms for solving convex optimization problems," in *Proc. IEEE Conf. Decis. Control*, 2008, pp. 4185–4190.
- [40] R. N. Clarke, "Expanding mobile wireless capacity: The challenges presented by technology and economics," *Telecommun. Policy*, vol. 38, no. 8-9, pp. 693–708, 2014.
- [41] U. N. Kar and D. K. Sanyal, "An overview of device-to-device communication in cellular networks," *ICT Express*, vol. 4, no. 4, pp. 203–208, 2018.
- [42] C. Hu, J. Jiang, and Z. Wang, "Decentralized federated learning: A segmented gossip approach," *arXiv preprint arXiv:1908.07782*, 2019.
- [43] S. Savazzi, M. Nicoli, and V. Rampa, "Federated learning with cooperating devices: A consensus approach for massive IoT networks," *IEEE Internet Things J.*, vol. 7, no. 5, pp. 4641–4654, 2020.

- [44] T. Zeng, O. Semiari, M. Mozaffari, M. Chen, W. Saad, and M. Bennis, "Federated learning in the sky: Joint power allocation and scheduling with UAV swarms," *arXiv preprint arXiv:2002.08196*, 2020.
- [45] L. Xiao and S. Boyd, "Fast linear iterations for distributed averaging," *Syst. & Control Lett.*, vol. 53, no. 1, pp. 65–78, 2004.
- [46] A. Reisizadeh, A. Mokhtari, H. Hassani, A. Jadbabaie, and R. Pedarsani, "Fedpaq: A communication-efficient federated learning method with periodic averaging and quantization," *arXiv preprint arXiv:1909.13014*, 2019.
- [47] C. Dinh, N. H. Tran, M. N. Nguyen, C. S. Hong, W. Bao, A. Zomaya, and V. Gramoli, "Federated learning over wireless networks: Convergence analysis and resource allocation," *arXiv preprint arXiv:1910.13067*, 2019.
- [48] M. P. Friedlander and M. Schmidt, "Hybrid deterministic-stochastic methods for data fitting," *SIAM J. Sci. Comput.*, vol. 34, no. 3, pp. A1380–A1405, 2012.
- [49] L. Xiao, S. Boyd, and S.-J. Kim, "Distributed average consensus with least-mean-square deviation," *J. Parallel Distrib. Comput.*, vol. 67, no. 1, pp. 33–46, 2007.
- [50] M. Hmila, M. Fernández-Veiga, M. Rodríguez-Pérez, and S. Herrería-Alonso, "Energy efficient power and channel allocation in underlay device to multi device communications," *IEEE Trans. Commun.*, vol. 67, no. 8, pp. 5817–5832, 2019.
- [51] S. Dominic and L. Jacob, "Joint resource block and power allocation through distributed learning for energy efficient underlay D2D communication with rate guarantee," *Comput. Commun.*, 2020.
- [52] B. T. Polyak, "Gradient methods for minimizing functionals," *Zh. Vychisl. Mat. Mat. Fiz.*, vol. 3, no. 4, pp. 643–653, 1963.
- [53] D. P. Bertsekas and J. N. Tsitsiklis, *Neuro-dynamic programming*. Athena Scientific, 1996.

APPENDIX A

PROOF OF THEOREM 1

Proof. We first aim to bound the per-iteration decrease of the gap between the function $F(\mathbf{w}^{(k)})$ and $F(\mathbf{w}^*)$. Using Taylor expansion and the η -smoothness of function F , the following quadratic upper-bound can be obtained:

$$F(\mathbf{w}^{(k+1)}) \leq F(\mathbf{w}^{(k)}) + (\mathbf{w}^{(k+1)} - \mathbf{w}^{(k)})^\top \nabla F(\mathbf{w}^{(k)}) + \frac{\eta}{2} \|\mathbf{w}^{(k+1)} - \mathbf{w}^{(k)}\|^2, \quad \forall k. \quad (31)$$

To find the relationship between $\mathbf{w}^{(k)}$ and $\mathbf{w}^{(k+1)}$, we follow the procedure described in the main text. For parent node a_p , let a'_{p+1} denote the corresponding sampled node, $\forall p$. This corresponds to one realization of the sampling at different parent nodes. We later demonstrate that the result of the theorem holds regardless of the sampling distributions. It can be verified that the parameter of the sampled node a'_1 by the main server (considered as a_0 for tractability) is given by:

$$\begin{aligned} \hat{\mathbf{w}}_{L^1_{a'_1}}^{(k+1)} &= \frac{\sum_{a_1 \in \mathcal{L}_1^1} \sum_{a_2 \in \mathcal{Q}(a_1)} \sum_{a_3 \in \mathcal{Q}(a_2)} \cdots \sum_{a_{|\mathcal{L}|} \in \mathcal{Q}(a_{|\mathcal{L}|-1})} |\mathcal{D}_{a_{|\mathcal{L}|}}| \mathbf{w}_{a_{|\mathcal{L}|}}^{(k)}}{|\mathcal{L}_1^1|} \\ &\quad - \frac{\sum_{a_1 \in \mathcal{L}_1^1} \sum_{a_2 \in \mathcal{Q}(a_1)} \sum_{a_3 \in \mathcal{Q}(a_2)} \cdots \sum_{a_{|\mathcal{L}|} \in \mathcal{Q}(a_{|\mathcal{L}|-1})} \beta |\mathcal{D}_{a_{|\mathcal{L}|}}| \nabla f_{a_{|\mathcal{L}|}}(\mathbf{w}_{a_{|\mathcal{L}|}}^{(k)})}{|\mathcal{L}_1^1|} \\ &\quad + \sum_{a_1 \in \mathcal{L}_1^1} \sum_{a_2 \in \mathcal{Q}(a_1)} \sum_{a_3 \in \mathcal{Q}(a_2)} \cdots \sum_{a_{|\mathcal{L}|-1} \in \mathcal{Q}(a_{|\mathcal{L}|-2})} \frac{\mathbb{1}_{\{\mathcal{Q}(a_{|\mathcal{L}|-1})\}}^{(k+1)} |\mathcal{Q}(a_{|\mathcal{L}|-1})| \mathbf{c}_{a'_{|\mathcal{L}|}}^{(k+1)}}{|\mathcal{L}_1^1|} \\ &\quad + \sum_{a_1 \in \mathcal{L}_1^1} \sum_{a_2 \in \mathcal{Q}(a_1)} \sum_{a_3 \in \mathcal{Q}(a_2)} \cdots \sum_{a_{|\mathcal{L}|-2} \in \mathcal{Q}(a_{|\mathcal{L}|-3})} \frac{\mathbb{1}_{\{\mathcal{Q}(a_{|\mathcal{L}|-2})\}}^{(k+1)} |\mathcal{Q}(a_{|\mathcal{L}|-2})| \mathbf{c}_{a'_{|\mathcal{L}|-1}}^{(k+1)}}{|\mathcal{L}_1^1|} + \\ &\quad \vdots \\ &\quad + \sum_{a_1 \in \mathcal{L}_1^1} \frac{\mathbb{1}_{\{\mathcal{Q}(a_1)\}}^{(k+1)} |\mathcal{Q}(a_1)| \mathbf{c}_{a'_2}^{(k+1)}}{|\mathcal{L}_1^1|} + \mathbb{1}_{\{\mathcal{L}_1^1\}}^{(k+1)} \mathbf{c}_{a'_1}^{(k+1)}, \end{aligned} \quad (32)$$

which the main server uses to obtain the next global parameter as follows (due to the existence of the indicator function in the last term of the above expression, the following expression holds regardless of the operating mode of the cluster at layer \mathcal{L}^1):

$$\mathbf{w}^{(k+1)} = \frac{|\mathcal{L}_1^1| \mathbf{w}_{L^1_{a'_1}}^{(k+1)}}{D}. \quad (33)$$

It can be verified that:

$$\sum_{a_1 \in \mathcal{L}_1^1} \sum_{a_2 \in \mathcal{Q}(a_1)} \sum_{a_3 \in \mathcal{Q}(a_2)} \cdots \sum_{a_{|\mathcal{L}|} \in \mathcal{Q}(a_{|\mathcal{L}|-1})} |\mathcal{D}_{a_{|\mathcal{L}|}}| \mathbf{w}_{a_{|\mathcal{L}|}}^{(k)} = D \mathbf{w}^{(k)}. \quad (34)$$

Also, using (1), we have:

$$\sum_{a_1 \in \mathcal{L}_1^1} \sum_{a_2 \in \mathcal{Q}(a_1)} \sum_{a_3 \in \mathcal{Q}(a_2)} \cdots \sum_{a_{|\mathcal{L}|} \in \mathcal{Q}(a_{|\mathcal{L}|-1})} \beta |\mathcal{D}_{a_{|\mathcal{L}|}}| \nabla f_{a_{|\mathcal{L}|}}(\mathbf{w}_{a_{|\mathcal{L}|}}^{(k)}) = \beta D \nabla F(\mathbf{w}^{(k)}). \quad (35)$$

Replacing the above two equation in (32) and performing the update given by (33), we get:

$$\begin{aligned} \mathbf{w}^{(k+1)} &= \mathbf{w}^{(k)} - \beta \nabla F(\mathbf{w}^{(k)}) \\ &+ \frac{1}{D} \left(\sum_{a_1 \in \mathcal{L}_1^1} \sum_{a_2 \in \mathcal{Q}(a_1)} \sum_{a_3 \in \mathcal{Q}(a_2)} \cdots \sum_{a_{|\mathcal{L}|-1} \in \mathcal{Q}(a_{|\mathcal{L}|-2})} \mathbb{1}_{\{\mathcal{Q}(a_{|\mathcal{L}|-1})\}} | \mathcal{Q}(a_{|\mathcal{L}|-1}) | \mathbf{c}_{a'_{|\mathcal{L}|}}^{(k+1)} \right. \\ &+ \sum_{a_1 \in \mathcal{L}_1^1} \sum_{a_2 \in \mathcal{Q}(a_1)} \sum_{a_3 \in \mathcal{Q}(a_2)} \cdots \sum_{a_{|\mathcal{L}|-2} \in \mathcal{Q}(a_{|\mathcal{L}|-3})} \mathbb{1}_{\{\mathcal{Q}(a_{|\mathcal{L}|-2})\}} | \mathcal{Q}(a_{|\mathcal{L}|-2}) | \mathbf{c}_{a'_{|\mathcal{L}|-1}}^{(k+1)} + \\ &\vdots \\ &\left. + \sum_{a_1 \in \mathcal{L}_1^1} \mathbb{1}_{\{\mathcal{Q}(a_1)\}} | \mathcal{Q}(a_1) | \mathbf{c}_{a'_2}^{(k+1)} + \mathbb{1}_{\{\mathcal{L}_1^1\}} | \mathcal{L}_1^1 | \mathbf{c}_{a'_1}^{(k+1)} \right), \end{aligned} \quad (36)$$

Calculating $\mathbf{w}^{(k+1)} - \mathbf{w}^{(k)}$ using the above equation and replacing the result in (31) yields:

$$\begin{aligned} F(\mathbf{w}^{(k+1)}) - F(\mathbf{w}^{(k)}) &\leq \left(\frac{\eta \beta^2}{2} - \beta \right) \left\| \nabla F(\mathbf{w}^{(k)}) \right\|^2 \\ &+ \left(\frac{1 - \beta \eta}{D} \right) \left(\sum_{a_1 \in \mathcal{L}_1^1} \sum_{a_2 \in \mathcal{Q}(a_1)} \sum_{a_3 \in \mathcal{Q}(a_2)} \cdots \sum_{a_{|\mathcal{L}|-1} \in \mathcal{Q}(a_{|\mathcal{L}|-2})} \mathbb{1}_{\{\mathcal{Q}(a_{|\mathcal{L}|-1})\}} | \mathcal{Q}(a_{|\mathcal{L}|-1}) | \mathbf{c}_{a'_{|\mathcal{L}|}}^{(k+1)} \right. \\ &+ \sum_{a_1 \in \mathcal{L}_1^1} \sum_{a_2 \in \mathcal{Q}(a_1)} \sum_{a_3 \in \mathcal{Q}(a_2)} \cdots \sum_{a_{|\mathcal{L}|-2} \in \mathcal{Q}(a_{|\mathcal{L}|-3})} \mathbb{1}_{\{\mathcal{Q}(a_{|\mathcal{L}|-2})\}} | \mathcal{Q}(a_{|\mathcal{L}|-2}) | \mathbf{c}_{a'_{|\mathcal{L}|-1}}^{(k+1)} + \cdots \\ &\left. + \sum_{a_1 \in \mathcal{L}_1^1} \mathbb{1}_{\{\mathcal{Q}(a_1)\}} | \mathcal{Q}(a_1) | \mathbf{c}_{a'_2}^{(k+1)} + \mathbb{1}_{\{\mathcal{L}_1^1\}} | \mathcal{L}_1^1 | \mathbf{c}_{a'_1}^{(k+1)} \right)^\top \nabla F(\mathbf{w}^{(k)}) \\ &+ \frac{\eta}{2D^2} \left\| \sum_{a_1 \in \mathcal{L}_1^1} \sum_{a_2 \in \mathcal{Q}(a_1)} \sum_{a_3 \in \mathcal{Q}(a_2)} \cdots \sum_{a_{|\mathcal{L}|-1} \in \mathcal{Q}(a_{|\mathcal{L}|-2})} \mathbb{1}_{\{\mathcal{Q}(a_{|\mathcal{L}|-1})\}} | \mathcal{Q}(a_{|\mathcal{L}|-1}) | \mathbf{c}_{a'_{|\mathcal{L}|}}^{(k+1)} \right. \\ &+ \sum_{a_1 \in \mathcal{L}_1^1} \sum_{a_2 \in \mathcal{Q}(a_1)} \sum_{a_3 \in \mathcal{Q}(a_2)} \cdots \sum_{a_{|\mathcal{L}|-2} \in \mathcal{Q}(a_{|\mathcal{L}|-3})} \mathbb{1}_{\{\mathcal{Q}(a_{|\mathcal{L}|-2})\}} | \mathcal{Q}(a_{|\mathcal{L}|-2}) | \mathbf{c}_{a'_{|\mathcal{L}|-1}}^{(k+1)} + \cdots \\ &\left. + \sum_{a_1 \in \mathcal{L}_1^1} \mathbb{1}_{\{\mathcal{Q}(a_1)\}} | \mathcal{Q}(a_1) | \mathbf{c}_{a'_2}^{(k+1)} + \mathbb{1}_{\{\mathcal{L}_1^1\}} | \mathcal{L}_1^1 | \mathbf{c}_{a'_1}^{(k+1)} \right\|^2. \end{aligned} \quad (37)$$

Tuning the learning rate as $\beta = \frac{1}{\eta}$, we obtain:

$$\begin{aligned}
F(\mathbf{w}^{(k+1)}) - F(\mathbf{w}^{(k)}) &\leq \frac{-1}{2\eta} \|\nabla F(\mathbf{w}^{(k)})\|^2 + \\
&\frac{\eta}{2D^2} \left\| \sum_{a_1 \in \mathcal{L}_1^1} \sum_{a_2 \in \mathcal{Q}(a_1)} \sum_{a_3 \in \mathcal{Q}(a_2)} \cdots \sum_{a_{|\mathcal{L}|-1} \in \mathcal{Q}(a_{|\mathcal{L}|-2})} \mathbb{1}_{\{\mathcal{Q}(a_{|\mathcal{L}|-1})\}} | \mathcal{Q}(a_{|\mathcal{L}|-1}) | \mathbf{c}_{a'_{|\mathcal{L}|}}^{(k+1)} \right. \\
&+ \sum_{a_1 \in \mathcal{L}_1^1} \sum_{a_2 \in \mathcal{Q}(a_1)} \sum_{a_3 \in \mathcal{Q}(a_2)} \cdots \sum_{a_{|\mathcal{L}|-2} \in \mathcal{Q}(a_{|\mathcal{L}|-3})} \mathbb{1}_{\{\mathcal{Q}(a_{|\mathcal{L}|-2})\}} | \mathcal{Q}(a_{|\mathcal{L}|-2}) | \mathbf{c}_{a'_{|\mathcal{L}|-1}}^{(k+1)} + \\
&\vdots \\
&+ \left. \sum_{a_1 \in \mathcal{L}_1^1} \mathbb{1}_{\{\mathcal{Q}(a_1)\}} | \mathcal{Q}(a_1) | \mathbf{c}_{a'_2}^{(k+1)} + \mathbb{1}_{\{\mathcal{L}_1^1\}} | \mathcal{L}_1^1 | \mathbf{c}_{a'_1}^{(k+1)} \right\|^2.
\end{aligned} \tag{38}$$

Considering the right hand side of the above inequality, to bound $\|\nabla F(\mathbf{w}^{(k)})\|^2$, we use the strong convexity property of F . Considering the strong convexity criterion in Assumption 1 with x replaced by $\mathbf{w}^{(k)}$ and minimizing the both hand sides, the minimum of the left hand side occurs at $y = \mathbf{w}^*$ and the minimum of the right hand side occurs at $y = \mathbf{w}^{(k)} - \frac{1}{\mu} \nabla F(\mathbf{w}^{(k)})$. Replacing these values in the strong convexity criterion in Assumption 1 results in Polyak-Lojasiewicz inequality [52] in the following form:

$$\|\nabla F(\mathbf{w}^{(k)})\|^2 \geq (F(\mathbf{w}^{(k)}) - F(\mathbf{w}^*))2\mu. \tag{39}$$

Also, to bound the second term on the right hand side of (38), we first take the expectation from both hand sides with respect to the error of consensus at different clusters that yields:

$$\begin{aligned}
F(\mathbf{w}^{(k+1)}) - F(\mathbf{w}^{(k)}) &\leq \frac{-\mu}{\eta} (F(\mathbf{w}^{(k)}) - F(\mathbf{w}^*)) + \\
&\frac{\eta}{2D^2} \left[\left\| \sum_{a_1 \in \mathcal{L}_1^1} \sum_{a_2 \in \mathcal{Q}(a_1)} \sum_{a_3 \in \mathcal{Q}(a_2)} \cdots \sum_{a_{|\mathcal{L}|-1} \in \mathcal{Q}(a_{|\mathcal{L}|-2})} \mathbb{1}_{\{\mathcal{Q}(a_{|\mathcal{L}|-1})\}} | \mathcal{Q}(a_{|\mathcal{L}|-1}) | \mathbf{c}_{a'_{|\mathcal{L}|}}^{(k+1)} \right. \right. \\
&+ \sum_{a_1 \in \mathcal{L}_1^1} \sum_{a_2 \in \mathcal{Q}(a_1)} \sum_{a_3 \in \mathcal{Q}(a_2)} \cdots \sum_{a_{|\mathcal{L}|-2} \in \mathcal{Q}(a_{|\mathcal{L}|-3})} \mathbb{1}_{\{\mathcal{Q}(a_{|\mathcal{L}|-2})\}} | \mathcal{Q}(a_{|\mathcal{L}|-2}) | \mathbf{c}_{a'_{|\mathcal{L}|-1}}^{(k+1)} + \\
&\vdots \\
&+ \left. \left. \sum_{a_1 \in \mathcal{L}_1^1} \mathbb{1}_{\{\mathcal{Q}(a_1)\}} | \mathcal{Q}(a_1) | \mathbf{c}_{a'_2}^{(k+1)} + \mathbb{1}_{\{\mathcal{L}_1^1\}} | \mathcal{L}_1^1 | \mathbf{c}_{a'_1}^{(k+1)} \right\|^2 \right].
\end{aligned} \tag{40}$$

Then, we perform the following algebraic steps to bound the second term on the right hand side of the above inequality as follows:

$$\begin{aligned}
& \left\| \sum_{a_1 \in \mathcal{L}_1^1} \sum_{a_2 \in \mathcal{Q}(a_1)} \sum_{a_3 \in \mathcal{Q}(a_2)} \cdots \sum_{a_{|\mathcal{L}|-1} \in \mathcal{Q}(a_{|\mathcal{L}|-2})} \mathbb{1}_{\{\mathcal{Q}(a_{|\mathcal{L}|-1})\}}^{(k+1)} |\mathcal{Q}(a_{|\mathcal{L}|-1})| \mathbf{c}_{a'_{|\mathcal{L}|}}^{(k+1)} \right. \\
& + \sum_{a_1 \in \mathcal{L}_1^1} \sum_{a_2 \in \mathcal{Q}(a_1)} \sum_{a_3 \in \mathcal{Q}(a_2)} \cdots \sum_{a_{|\mathcal{L}|-2} \in \mathcal{Q}(a_{|\mathcal{L}|-3})} \mathbb{1}_{\{\mathcal{Q}(a_{|\mathcal{L}|-2})\}}^{(k+1)} |\mathcal{Q}(a_{|\mathcal{L}|-2})| \mathbf{c}_{a'_{|\mathcal{L}|-1}}^{(k+1)} + \cdots \\
& + \sum_{a_1 \in \mathcal{L}_1^1} \mathbb{1}_{\{\mathcal{Q}(a_1)\}}^{(k+1)} |\mathcal{Q}(a_1)| \mathbf{c}_{a'_2}^{(k+1)} + \mathbb{1}_{\{\mathcal{L}_1^1\}}^{(k+1)} |\mathcal{L}_1^1| \mathbf{c}_{a'_1}^{(k+1)} \left. \right\|^2 \\
& \leq \left(\left\| \sum_{a_1 \in \mathcal{L}_1^1} \sum_{a_2 \in \mathcal{Q}(a_1)} \sum_{a_3 \in \mathcal{Q}(a_2)} \cdots \sum_{a_{|\mathcal{L}|-1} \in \mathcal{Q}(a_{|\mathcal{L}|-2})} \mathbb{1}_{\{\mathcal{Q}(a_{|\mathcal{L}|-1})\}}^{(k+1)} |\mathcal{Q}(a_{|\mathcal{L}|-1})| \mathbf{c}_{a'_{|\mathcal{L}|}}^{(k+1)} \right\| \right. \\
& + \left\| \sum_{a_1 \in \mathcal{L}_1^1} \sum_{a_2 \in \mathcal{Q}(a_1)} \sum_{a_3 \in \mathcal{Q}(a_2)} \cdots \sum_{a_{|\mathcal{L}|-2} \in \mathcal{Q}(a_{|\mathcal{L}|-3})} \mathbb{1}_{\{\mathcal{Q}(a_{|\mathcal{L}|-2})\}}^{(k+1)} |\mathcal{Q}(a_{|\mathcal{L}|-2})| \mathbf{c}_{a'_{|\mathcal{L}|-1}}^{(k+1)} \right\| \\
& + \cdots \\
& + \left. \left\| \sum_{a_1 \in \mathcal{L}_1^1} \mathbb{1}_{\{\mathcal{Q}(a_1)\}}^{(k+1)} |\mathcal{Q}(a_1)| \mathbf{c}_{a'_2}^{(k+1)} \right\| + \left\| \mathbb{1}_{\{\mathcal{L}_1^1\}}^{(k+1)} |\mathcal{L}_1^1| \mathbf{c}_{a'_1}^{(k+1)} \right\| \right)^2 \\
& \leq \left(\sum_{a_1 \in \mathcal{L}_1^1} \sum_{a_2 \in \mathcal{Q}(a_1)} \sum_{a_3 \in \mathcal{Q}(a_2)} \cdots \sum_{a_{|\mathcal{L}|-1} \in \mathcal{Q}(a_{|\mathcal{L}|-2})} \mathbb{1}_{\{\mathcal{Q}(a_{|\mathcal{L}|-1})\}}^{(k+1)} |\mathcal{Q}(a_{|\mathcal{L}|-1})| \left\| \mathbf{c}_{a'_{|\mathcal{L}|}}^{(k+1)} \right\| \right. \\
& + \sum_{a_1 \in \mathcal{L}_1^1} \sum_{a_2 \in \mathcal{Q}(a_1)} \sum_{a_3 \in \mathcal{Q}(a_2)} \cdots \sum_{a_{|\mathcal{L}|-2} \in \mathcal{Q}(a_{|\mathcal{L}|-3})} \mathbb{1}_{\{\mathcal{Q}(a_{|\mathcal{L}|-2})\}}^{(k+1)} |\mathcal{Q}(a_{|\mathcal{L}|-2})| \left\| \mathbf{c}_{a'_{|\mathcal{L}|-1}}^{(k+1)} \right\| \\
& + \cdots \\
& + \left. \sum_{a_1 \in \mathcal{L}_1^1} \mathbb{1}_{\{\mathcal{Q}(a_1)\}}^{(k+1)} |\mathcal{Q}(a_1)|^2 \left\| \mathbf{c}_{a'_2}^{(k+1)} \right\| + \mathbb{1}_{\{\mathcal{L}_1^1\}}^{(k+1)} |\mathcal{L}_1^1|^2 \left\| \mathbf{c}_{a'_1}^{(k+1)} \right\| \right)^2 \\
& \stackrel{(a)}{\leq} \\
& \Phi \left[\sum_{a_1 \in \mathcal{L}_1^1} \sum_{a_2 \in \mathcal{Q}(a_1)} \sum_{a_3 \in \mathcal{Q}(a_2)} \cdots \sum_{a_{|\mathcal{L}|-1} \in \mathcal{Q}(a_{|\mathcal{L}|-2})} \mathbb{1}_{\{\mathcal{Q}(a_{|\mathcal{L}|-1})\}}^{(k+1)} |\mathcal{Q}(a_{|\mathcal{L}|-1})|^2 \left\| \mathbf{c}_{a'_{|\mathcal{L}|}}^{(k+1)} \right\|^2 \right. \\
& + \sum_{a_1 \in \mathcal{L}_1^1} \sum_{a_2 \in \mathcal{Q}(a_1)} \sum_{a_3 \in \mathcal{Q}(a_2)} \cdots \sum_{a_{|\mathcal{L}|-2} \in \mathcal{Q}(a_{|\mathcal{L}|-3})} \mathbb{1}_{\{\mathcal{Q}(a_{|\mathcal{L}|-2})\}}^{(k+1)} |\mathcal{Q}(a_{|\mathcal{L}|-2})|^2 \left\| \mathbf{c}_{a'_{|\mathcal{L}|-1}}^{(k+1)} \right\|^2 \\
& + \cdots \\
& + \left. \sum_{a_1 \in \mathcal{L}_1^1} \mathbb{1}_{\{\mathcal{Q}(a_1)\}}^{(k+1)} |\mathcal{Q}(a_1)|^2 \left\| \mathbf{c}_{a'_2}^{(k+1)} \right\|^2 + \mathbb{1}_{\{\mathcal{L}_1^1\}}^{(k+1)} |\mathcal{L}_1^1|^2 \left\| \mathbf{c}_{a'_1}^{(k+1)} \right\|^2 \right],
\end{aligned} \tag{41}$$

where the triangle inequality, e.g, for vectors \mathbf{a}_i , $1 \leq i \leq n$: $\|\sum_{i=1}^n \mathbf{a}_i\| \leq \sum_{i=1}^n \|\mathbf{a}_i\|$, is applied sequentially and

$$\Phi = N_{|\mathcal{L}|-1} + N_{|\mathcal{L}|-2} + \cdots + N_1 + 1. \quad (42)$$

Also, inequality (a) in (41) is obtained by exploiting the Cauchy–Schwarz inequality, $\langle \mathbf{a}, \mathbf{a}' \rangle \leq \|\mathbf{a}\| \cdot \|\mathbf{a}'\|$, which results in the following bound, where $\mathbf{q} = [q_1, \cdots, q_b]$:

$$\left(\sum_{a=1}^b q_i \right)^2 = (\langle \mathbf{1}, \mathbf{q} \rangle)^2 \leq b \sum_{a=1}^b q_i^2. \quad (43)$$

To further find each of the error terms in the right hand side of (41), we need to bound $\left\| \mathbf{c}_{a'_p}^{(k+1)} \right\|^2$, $1 \leq p \leq |\mathcal{L}|$. For notations simplicity we consider bounding $\left\| \mathbf{c}_{a'_{|\mathcal{L}|}}^{(k)} \right\|^2$ for the case where sampling is conducted from the nodes of the cluster \mathcal{C} located in the bottom-most layer $a'_{|\mathcal{L}|} \in \mathcal{C}$, $\mathcal{C} \in \mathcal{L}^{|\mathcal{L}|}$. Let $c_1, \cdots, c_{|\mathcal{C}|}$ denote the nodes belonging to cluster \mathcal{C} , where $a'_{|\mathcal{L}|}$ is among them. The evolution of nodes parameters in this cluster can be described by (12) as:

$$\left[\widehat{\mathbf{W}}_{\mathcal{C}}^{(k)} \right]_m = \left(\mathbf{V}_{\mathcal{C}}^{(k)} \right)^{\theta_{\mathcal{C}}^{(k)}} \left[\mathbf{W}_{\mathcal{C}}^{(k)} \right]_m, \quad (44)$$

where

$$\left[\mathbf{W}_{\mathcal{C}}^{(k)} \right]_m = \left[\left(\widetilde{\mathbf{w}}_{c_1}^{(k)} \right)_m, \cdots, \left(\widetilde{\mathbf{w}}_{c_{|\mathcal{C}|}}^{(k)} \right)_m \right]^\top, \quad (45)$$

and

$$\left[\widehat{\mathbf{W}}_{\mathcal{C}}^{(k)} \right]_m = \left[\left(\widehat{\mathbf{w}}_{c_1}^{(k)} \right)_m, \cdots, \left(\widehat{\mathbf{w}}_{c_{|\mathcal{C}|}}^{(k)} \right)_m \right]^\top, \quad (46)$$

where $(\cdot)_m$ denotes the m -th element of the vector. Also, the average of the vector of parameters in LUT cluster \mathcal{C} can be written as:

$$\overline{\left[\mathbf{W}_{\mathcal{C}}^{(k)} \right]_m} = \frac{\mathbf{1}_{|\mathcal{C}|} \mathbf{1}_{|\mathcal{C}|}^\top \left[\mathbf{W}_{\mathcal{C}}^{(k)} \right]_m}{|\mathcal{C}|}, \forall m. \quad (47)$$

It is straightforward to verify that:

$$\left\| \left(\widehat{\mathbf{w}}_{c_u}^{(k)} \right)_m - \frac{\left(\sum_{b=1}^{|\mathcal{C}|} \widetilde{\mathbf{w}}_{c_b}^{(k)} \right)_m}{|\mathcal{C}|} \right\| \leq \left\| \left[\widehat{\mathbf{W}}_{\mathcal{C}}^{(k)} \right]_m - \overline{\left[\mathbf{W}_{\mathcal{C}}^{(k)} \right]_m} \right\|, \quad 1 \leq u \leq |\mathcal{C}|. \quad (48)$$

Also, considering the definition of the average vector in (47), the following equality is immediate:

$$\left[\mathbf{W}_c^{(k)}\right]_m = \overline{\left[\mathbf{W}_c^{(k)}\right]}_m + \mathbf{r}, \quad (49)$$

where for vector \mathbf{r} , we have: $\langle \mathbf{1}_{|C|}, \mathbf{r} \rangle = 0$. Based on this and the properties of the consensus matrix given in Assumption 2, we bound the right hand side of (48) as follows:

$$\begin{aligned} \left\| \left[\widehat{\mathbf{W}}_c^{(k)}\right]_m - \overline{\left[\mathbf{W}_c^{(k)}\right]}_m \right\| &= \left\| \left(\mathbf{V}_c^{(k)}\right)^{\theta_c^{(k)}} \left[\mathbf{W}_c^{(k)}\right]_m - \overline{\left[\mathbf{W}_c^{(k)}\right]}_m \right\| = \\ &= \left\| \left(\mathbf{V}_c^{(k)}\right)^{\theta_c^{(k)}} \left(\overline{\left[\mathbf{W}_c^{(k)}\right]}_m + \mathbf{r} \right) - \overline{\left[\mathbf{W}_c^{(k)}\right]}_m \right\| = \left\| \left(\mathbf{V}_c^{(k)}\right)^{\theta_c^{(k)}} \mathbf{r} \right\| = \\ &= \left\| \left(\left(\mathbf{V}_c^{(k)}\right)^{\theta_c^{(k)}} - \frac{\mathbf{1}_{|C|}\mathbf{1}_{|C|}^\top}{|C|} \right) \mathbf{r} \right\|. \end{aligned} \quad (50)$$

Note that $\left(\frac{\mathbf{1}_{|C|}\mathbf{1}_{|C|}^\top}{|C|}\right)$ is idempotent⁵. This immediately makes $\mathbf{I} - \frac{\mathbf{1}_{|C|}\mathbf{1}_{|C|}^\top}{|C|}$ idempotent, where \mathbf{I} is the identity matrix. Using the properties of the consensus matrix given in Assumption 2, this yields:

$$\begin{aligned} \left(\mathbf{V}_c^{(k)}\right)^{\theta_c^{(k)}} - \frac{\mathbf{1}_{|C|}\mathbf{1}_{|C|}^\top}{|C|} &= \left(\mathbf{V}_c^{(k)}\right)^{\theta_c^{(k)}} \left(\mathbf{I} - \frac{\mathbf{1}_{|C|}\mathbf{1}_{|C|}^\top}{|C|} \right) \\ &= \left(\mathbf{V}_c^{(k)}\right)^{\theta_c^{(k)}} \left(\mathbf{I} - \frac{\mathbf{1}_{|C|}\mathbf{1}_{|C|}^\top}{|C|} \right)^{\theta_c^{(k)}} = \left(\mathbf{V}_c^{(k)} \left(\mathbf{I} - \frac{\mathbf{1}_{|C|}\mathbf{1}_{|C|}^\top}{|C|} \right) \right)^{\theta_c^{(k)}} \\ &= \left(\mathbf{V}_c^{(k)} - \frac{\mathbf{1}_{|C|}\mathbf{1}_{|C|}^\top}{|C|} \right)^{\theta_c^{(k)}}. \end{aligned} \quad (51)$$

Using the above equality in (50) and the matrix norm characteristics gives us:

$$\begin{aligned} \left\| \left(\left(\mathbf{V}_c^{(k)}\right)^{\theta_c^{(k)}} - \frac{\mathbf{1}_{|C|}\mathbf{1}_{|C|}^\top}{|C|} \right) \mathbf{r} \right\| &\leq \left\| \left(\mathbf{V}_c^{(k)} - \left(\frac{\mathbf{1}_{|C|}\mathbf{1}_{|C|}^\top}{|C|} \right) \right)^{\theta_c^{(k)}} \right\| \|\mathbf{r}\| \leq \\ &= \left\| \left(\mathbf{V}_c^{(k)} - \left(\frac{\mathbf{1}_{|C|}\mathbf{1}_{|C|}^\top}{|C|} \right) \right)^{\theta_c^{(k)}} \right\| \|\mathbf{r}\| \leq (\lambda_c)^{\theta_c^{(k)}} \|\mathbf{r}\|. \end{aligned} \quad (52)$$

where the last inequality is due to the fact that for a symmetric matrix \mathbf{A} , we have $\|\mathbf{A}\| = \rho(\mathbf{A})$,

⁵A matrix \mathbf{x} is called idempotent if $\mathbf{x}^y = \mathbf{x}$, $y \in \mathbb{N}$.

where ρ is defined in Assumption 2. According to Definition 1, we have:

$$\|\tilde{\mathbf{w}}_{c_u}^{(k)} - \tilde{\mathbf{w}}_{c_{u'}}^{(k)}\| \leq \Upsilon_{\mathcal{C}}^{(k)}, \quad \forall c_u, c_{u'} \in \mathcal{C}, \quad (53)$$

which results in:

$$\left\| \left(\tilde{\mathbf{w}}_{c_u}^{(k)} \right)_m - \left(\tilde{\mathbf{w}}_{c_{u'}}^{(k)} \right)_m \right\| \leq \Upsilon_{\mathcal{C}}^{(k)}, \quad \forall c_u, c_{u'} \in \mathcal{C}. \quad (54)$$

As a result, considering (49), we have:

$$\begin{aligned} \|(\mathbf{r})_u\| &= \left\| \left(\tilde{\mathbf{w}}_{c_u}^{(k)} \right)_m - \frac{\left(\sum_{b=1}^{|\mathcal{C}|} \tilde{\mathbf{w}}_{c_b}^{(k)} \right)_m}{|\mathcal{C}|} \right\| = \frac{1}{|\mathcal{C}|} \left\| |\mathcal{C}| \left(\tilde{\mathbf{w}}_{c_u}^{(k)} \right)_m - \left(\sum_{b=1}^{|\mathcal{C}|} \tilde{\mathbf{w}}_{c_b}^{(k)} \right)_m \right\| \\ &= \frac{1}{|\mathcal{C}|} \left\| \left(\sum_{b=1}^{|\mathcal{C}|} [\tilde{\mathbf{w}}_{c_b}^{(k)} - \tilde{\mathbf{w}}_{c_u}^{(k)}] \right)_m \right\| \leq \frac{|\mathcal{C}| - 1}{|\mathcal{C}|} \Upsilon_{\mathcal{C}}^{(k)}, \quad 1 \leq u \leq |\mathcal{C}|. \end{aligned} \quad (55)$$

Thus, $\|\mathbf{r}\| \leq (|\mathcal{C}| - 1) \Upsilon_{\mathcal{C}}^{(k)} \leq |\mathcal{C}| \Upsilon_{\mathcal{C}}^{(k)}$.

Remark 1. In Definition 1, the divergence could have been defined per parameter dimension, i.e., different bounds on the right hand side of (54) for each dimension, which would have resulted in tighter upper bounds. However, in practice it is hard to obtain such quantity in large-scale networks when the size of parameter vector is large.

Replacing the above result in (52) and combining with (48), gives us:

$$\left\| \left(\hat{\mathbf{w}}_{c_u}^{(k)} \right)_m - \frac{\left(\sum_{b=1}^{|\mathcal{C}|} \tilde{\mathbf{w}}_{c_b}^{(k)} \right)_m}{|\mathcal{C}|} \right\| \leq (\lambda_{\mathcal{C}})^{\theta_{\mathcal{C}}^{(k)}} |\mathcal{C}| \Upsilon_{\mathcal{C}}^{(k)}, \quad 1 \leq u \leq |\mathcal{C}|. \quad (56)$$

Using the above inequality, we have:

$$\begin{aligned} \left\| \hat{\mathbf{w}}_{c_u}^{(k)} - \frac{\sum_{b=1}^{|\mathcal{C}|} \tilde{\mathbf{w}}_{c_b}^{(k)}}{|\mathcal{C}|} \right\| &\leq \sum_{m=1}^M \left\| \left(\hat{\mathbf{w}}_{c_u}^{(k)} \right)_m - \frac{\left(\sum_{b=1}^{|\mathcal{C}|} \tilde{\mathbf{w}}_{c_b}^{(k)} \right)_m}{|\mathcal{C}|} \right\| \\ &\leq (\lambda_{\mathcal{C}})^{\theta_{\mathcal{C}}^{(k)}} |\mathcal{C}| \Upsilon_{\mathcal{C}}^{(k)} M, \quad 1 \leq u \leq |\mathcal{C}|. \end{aligned} \quad (57)$$

Considering the fact that the above inequality bounds the error of consensus at every node with respect to the average value of the cluster, and the parent node samples one of the nodes of the

cluster, for any sampled node $a'_{|\mathcal{C}|} \in \mathcal{C}$, we get: $\|\mathbf{c}_{a'_{|\mathcal{C}|}}^{(k)}\|^2 \leq (\lambda_{\mathcal{C}})^{2\theta_{\mathcal{C}}^{(k)}} |\mathcal{C}|^2 \left(\Upsilon_{\mathcal{C}}^{(k)}\right)^2 M^2$. Changing the global iteration count yields:

$$\|\mathbf{c}_{a'_{|\mathcal{C}|}}^{(k+1)}\|^2 \leq (\lambda_{\mathcal{C}})^{2\theta_{\mathcal{C}}^{(k+1)}} |\mathcal{C}|^2 \left(\Upsilon_{\mathcal{C}}^{(k+1)}\right)^2 M^2, \quad a'_{|\mathcal{C}|} \in \mathcal{C}. \quad (58)$$

The above mentioned prove can be generalized to every cluster with slight modifications in parameter definition in (44), which results in:

$$\|\mathbf{c}_{a'_p}^{(k+1)}\|^2 \leq (\lambda_{\mathcal{C}})^{2\theta_{\mathcal{C}}^{(k+1)}} |\mathcal{C}|^2 \left(\Upsilon_{\mathcal{C}}^{(k+1)}\right)^2 M^2, \quad a'_p \in \mathcal{C}. \quad (59)$$

Replacing the above inequality in (41) combined with (40) gives us:

$$\begin{aligned} F(\mathbf{w}^{(k+1)}) - F(\mathbf{w}^{(k)}) &\leq \frac{-\mu}{\eta} F(\mathbf{w}^{(k)}) - F(\mathbf{w}^*) + \\ &\frac{\eta\Phi M^2}{2D^2} \left[\sum_{a_1 \in \mathcal{L}_1^1} \sum_{a_2 \in \mathcal{Q}(a_1)} \cdots \sum_{a_{|\mathcal{L}|-1} \in \mathcal{Q}(a_{|\mathcal{L}|-2})} \mathbb{I}_{\{\mathcal{Q}(a_{|\mathcal{L}|-1})\}}^{(k+1)} |\mathcal{Q}(a_{|\mathcal{L}|-1})|^4 \left(\lambda_{\mathcal{Q}(a_{|\mathcal{L}|-1})}^{(k+1)}\right)^{2\theta_{\mathcal{Q}(a_{|\mathcal{L}|-1})}^{(k+1)}} \left(\Upsilon_{\mathcal{Q}(a_{|\mathcal{L}|-1})}^{(k+1)}\right)^2 \right. \\ &+ \sum_{a_1 \in \mathcal{L}_1^1} \sum_{a_2 \in \mathcal{Q}(a_1)} \cdots \sum_{a_{|\mathcal{L}|-2} \in \mathcal{Q}(a_{|\mathcal{L}|-3})} \mathbb{I}_{\{\mathcal{Q}(a_{|\mathcal{L}|-2})\}}^{(k+1)} |\mathcal{Q}(a_{|\mathcal{L}|-2})|^4 \left(\lambda_{\mathcal{Q}(a_{|\mathcal{L}|-2})}^{(k+1)}\right)^{2\theta_{\mathcal{Q}(a_{|\mathcal{L}|-2})}^{(k+1)}} \left(\Upsilon_{\mathcal{Q}(a_{|\mathcal{L}|-2})}^{(k+1)}\right)^2 \\ &\left. + \cdots + \sum_{a_1 \in \mathcal{L}_1^1} \mathbb{I}_{\{\mathcal{Q}(a_1)\}}^{(k+1)} |\mathcal{Q}(a_1)|^4 \left(\lambda_{\mathcal{Q}(a_1)}^{(k+1)}\right)^{2\theta_{\mathcal{Q}(a_1)}^{(k+1)}} \left(\Upsilon_{\mathcal{Q}(a_1)}^{(k+1)}\right)^2 + \mathbb{I}_{\{\mathcal{L}_1^1\}}^{(k+1)} |\mathcal{L}_1^1|^4 \left(\lambda_{\mathcal{L}_1^1}^{(k+1)}\right)^{2\theta_{\mathcal{L}_1^1}^{(k+1)}} \left(\Upsilon_{\mathcal{L}_1^1}^{(k+1)}\right)^2 \right]. \quad (60) \end{aligned}$$

Adding $F(\mathbf{w}^{(k)})$ to both hands sides and subtracting $F(\mathbf{w}^*)$ from both hand sides, we get:

$$\begin{aligned} F(\mathbf{w}^{(k+1)}) - F(\mathbf{w}^*) &\leq \left(1 - \frac{\mu}{\eta}\right) F(\mathbf{w}^{(k)}) - F(\mathbf{w}^*) + \\ &\frac{\eta\Phi M^2}{2D^2} \left[\sum_{a_1 \in \mathcal{L}_1^1} \sum_{a_2 \in \mathcal{Q}(a_1)} \cdots \sum_{a_{|\mathcal{L}|-1} \in \mathcal{Q}(a_{|\mathcal{L}|-2})} \mathbb{I}_{\{\mathcal{Q}(a_{|\mathcal{L}|-1})\}}^{(k+1)} |\mathcal{Q}(a_{|\mathcal{L}|-1})|^4 \left(\lambda_{\mathcal{Q}(a_{|\mathcal{L}|-1})}^{(k+1)}\right)^{2\theta_{\mathcal{Q}(a_{|\mathcal{L}|-1})}^{(k+1)}} \left(\Upsilon_{\mathcal{Q}(a_{|\mathcal{L}|-1})}^{(k+1)}\right)^2 \right. \\ &+ \sum_{a_1 \in \mathcal{L}_1^1} \sum_{a_2 \in \mathcal{Q}(a_1)} \cdots \sum_{a_{|\mathcal{L}|-2} \in \mathcal{Q}(a_{|\mathcal{L}|-3})} \mathbb{I}_{\{\mathcal{Q}(a_{|\mathcal{L}|-2})\}}^{(k+1)} |\mathcal{Q}(a_{|\mathcal{L}|-2})|^4 \left(\lambda_{\mathcal{Q}(a_{|\mathcal{L}|-2})}^{(k+1)}\right)^{2\theta_{\mathcal{Q}(a_{|\mathcal{L}|-2})}^{(k+1)}} \left(\Upsilon_{\mathcal{Q}(a_{|\mathcal{L}|-2})}^{(k+1)}\right)^2 \\ &\left. + \cdots + \sum_{a_1 \in \mathcal{L}_1^1} \mathbb{I}_{\{\mathcal{Q}(a_1)\}}^{(k+1)} |\mathcal{Q}(a_1)|^4 \left(\lambda_{\mathcal{Q}(a_1)}^{(k+1)}\right)^{2\theta_{\mathcal{Q}(a_1)}^{(k+1)}} \left(\Upsilon_{\mathcal{Q}(a_1)}^{(k+1)}\right)^2 + \mathbb{I}_{\{\mathcal{L}_1^1\}}^{(k+1)} |\mathcal{L}_1^1|^4 \left(\lambda_{\mathcal{L}_1^1}^{(k+1)}\right)^{2\theta_{\mathcal{L}_1^1}^{(k+1)}} \left(\Upsilon_{\mathcal{L}_1^1}^{(k+1)}\right)^2 \right]. \quad (61) \end{aligned}$$

Expanding the first term on the right hand side of the inequality in a recursive manner, results the theorem. ■

APPENDIX B
PROOF OF PROPOSITION 1

Consider the bound on the number of consensus that is given in the proposition statement. For \mathcal{L}_i^j , if $\sigma_j \leq |\mathcal{L}_i^j|^4 \left(\Upsilon_{\mathcal{L}_i^j}^{(k)} \right)^2$, $\forall i$, the proposed number of consensus guarantees $\theta_{\mathcal{L}_i^j}^{(k)} \geq \frac{\log(\sigma_j) - 2 \log \left(|\mathcal{L}_i^j|^2 \Upsilon_{\mathcal{L}_i^j}^{(k)} \right)}{2 \log \left(\lambda_{\mathcal{L}_i^j}^{(k)} \right)}$,

which results in:

$$\begin{aligned} \theta_{\mathcal{L}_i^j}^{(k)} &\geq \frac{\log(\sigma_j) - 2 \log \left(|\mathcal{L}_i^j|^2 \Upsilon_{\mathcal{L}_i^j}^{(k)} \right)}{2 \log \left(\lambda_{\mathcal{L}_i^j}^{(k)} \right)} \\ &\Rightarrow \theta_{\mathcal{L}_i^j}^{(k)} \geq \frac{1}{2} \frac{\log \left(\frac{\sigma_j}{|\mathcal{L}_i^j|^4 \left(\Upsilon_{\mathcal{L}_i^j}^{(k)} \right)^2} \right)}{\log \left(\lambda_{\mathcal{L}_i^j}^{(k)} \right)} \\ &\Rightarrow \left(\lambda_{\mathcal{L}_i^j}^{(k)} \right)^{2\theta_{\mathcal{L}_i^j}^{(k)}} \leq \frac{\sigma_j}{|\mathcal{L}_i^j|^4 \left(\Upsilon_{\mathcal{L}_i^j}^{(k)} \right)^2}, \quad \forall k, \end{aligned} \tag{62}$$

where the last inequality is due to the facts that $\frac{\log a}{\log b} = \log_a^b$, $a^{\log_a^b} = b$, and $\lambda_{\mathcal{L}_i^j}^{(k)} < 1$. Also, for \mathcal{L}_i^j , if $\sigma_j \geq |\mathcal{L}_i^j|^4 \left(\Upsilon_{\mathcal{L}_i^j}^{(k)} \right)^2$, any $\theta_{\mathcal{L}_i^j}^{(k)} \geq 0$ ensures $\sigma_j \geq |\mathcal{L}_i^j|^4 \left(\Upsilon_{\mathcal{L}_i^j}^{(k)} \right)^2 \left(\lambda_{\mathcal{L}_i^j}^{(k)} \right)^{2\theta_{\mathcal{L}_i^j}^{(k)}}$, $\forall k$. Replacing the above result in (14), we get:

$$\begin{aligned} F(\mathbf{w}^{(k)}) - F(\mathbf{w}^*) &\leq \frac{\eta \Phi M^2}{2D^2} \sum_{t=0}^{k-1} \left(\frac{\eta - \mu}{\eta} \right)^t \left[\right. \\ &\quad \sum_{a_1 \in \mathcal{L}_1^1} \sum_{a_2 \in \mathcal{Q}(a_1)} \cdots \sum_{a_{|\mathcal{L}|-1} \in \mathcal{Q}(a_{|\mathcal{L}|-2})} \mathbb{1}_{\{\mathcal{Q}(a_{|\mathcal{L}|-1})\}}^{(k-t)} \sigma_{|\mathcal{L}|} + \\ &\quad \sum_{a_1 \in \mathcal{L}_1^1} \sum_{a_2 \in \mathcal{Q}(a_1)} \cdots \sum_{a_{|\mathcal{L}|-2} \in \mathcal{Q}(a_{|\mathcal{L}|-3})} \mathbb{1}_{\{\mathcal{Q}(a_{|\mathcal{L}|-2})\}}^{(k-t)} \sigma_{|\mathcal{L}|-1} + \cdots \\ &\quad \left. + \sum_{a_1 \in \mathcal{L}_1^1} \mathbb{1}_{\{\mathcal{Q}(a_1)\}}^{(k-t)} \sigma_2 + \mathbb{1}_{\{\mathcal{L}_1^1\}}^{(k-t)} \sigma_1 \right] + \left(\frac{\eta - \mu}{\eta} \right)^k (F(\mathbf{w}^{(0)}) - F(\mathbf{w}^*)) \\ &\leq \frac{\eta \Phi M^2}{2D^2} \sum_{t=0}^{k-1} \left(\frac{\eta - \mu}{\eta} \right)^t \left[N_{|\mathcal{L}|-1} \sigma_{|\mathcal{L}|} + N_{|\mathcal{L}|-2} \sigma_{|\mathcal{L}|-1} + \cdots \right. \\ &\quad \left. + N_1 \sigma_2 + N_0 \sigma_1 \right] + \left(\frac{\eta - \mu}{\eta} \right)^k (F(\mathbf{w}^{(0)}) - F(\mathbf{w}^*)). \end{aligned} \tag{63}$$

Taking the limit with respect to k , we get:

$$\lim_{k \rightarrow \infty} F(\mathbf{w}^{(k)}) - F(\mathbf{w}^*) \leq \frac{\eta \Phi M^2}{2D^2} \left(\sum_{j=0}^{|\mathcal{L}|-1} \sigma_{j+1} N_j \right) \frac{1}{1 - (\frac{\eta - \mu}{\eta})}, \quad (64)$$

which concludes the proof.

APPENDIX C

PROOF OF PROPOSITION 2

Consider the per-iteration decrease of the objective function given by (61). Following a similar procedure as Appendix B, given the proposed number of consensus rounds in the proposition statement, we get:

$$F(\mathbf{w}^{(k+1)}) - F(\mathbf{w}^*) \leq (1 - \frac{\mu}{\eta}) F(\mathbf{w}^{(k)}) - F(\mathbf{w}^*) + \frac{\eta \Phi M^2}{2D^2} \left[\sum_{j=0}^{|\mathcal{L}|-1} \sigma_{j+1}^{(k+1)} N_j \right]. \quad (65)$$

Using the fact that $\nabla F(\mathbf{w}^*) = 0$ combined with η -smoothness of F , we get:

$$\|\nabla F(\mathbf{w}^{(k)})\| = \|\nabla F(\mathbf{w}^{(k)}) - \nabla F(\mathbf{w}^*)\| \leq \eta \|\mathbf{w}^{(k)} - \mathbf{w}^*\|. \quad (66)$$

Also, it is straightforward to verify that strong convexity of F , expressed in Assumption 1, implies the following inequality:

$$\mu/2 \|\mathbf{w}^{(k)} - \mathbf{w}^*\|^2 \leq F(\mathbf{w}^{(k)}) - F(\mathbf{w}^*). \quad (67)$$

Combining the above results with the condition given in the proposition statement, i.e., (18), we get:

$$\begin{aligned} \sum_{j=0}^{|\mathcal{L}|-1} \sigma_{j+1}^{(k+1)} N_j &\leq \frac{D^2 \mu (\mu - \delta \eta)}{\eta^4 \Phi M^2} \|\nabla F(\mathbf{w}^{(k)})\|^2 \\ &\leq \frac{D^2 \mu (\mu - \delta \eta)}{\eta^2 \Phi M^2} \|\mathbf{w}^{(k)} - \mathbf{w}^*\|^2 \\ &\leq \frac{2D^2 (\mu - \delta \eta)}{\eta^2 \Phi M^2} (F(\mathbf{w}^{(k)}) - F(\mathbf{w}^*)) \end{aligned} \quad (68)$$

By replacing the above inequality in (65) we get:

$$F(\mathbf{w}^{(k+1)}) - F(\mathbf{w}^*) \leq (1 - \mu/\eta) (F(\mathbf{w}^{(k)}) - F(\mathbf{w}^*)) + (\mu/\eta - \delta) (F(\mathbf{w}^{(k)}) - F(\mathbf{w}^*)), \quad (69)$$

which readily leads to the proposition result.

APPENDIX D
PROOF OF COROLLARY 1

Regarding the first condition, at global iteration κ , using the number of consensus given in the corollary statement, according to (63), we have:

$$\begin{aligned} F(\mathbf{w}^{(\kappa)}) - F(\mathbf{w}^*) &\leq \frac{\eta\Phi M^2}{2D^2} \sum_{j=0}^{|\mathcal{L}|-1} \sigma_{j+1} N_j \frac{1 - \left(1 - \frac{\mu}{\eta}\right)^\kappa}{\mu/\eta} \left(\frac{\eta - \mu}{\eta}\right)^\kappa (F(\mathbf{w}^{(0)}) - F(\mathbf{w}^*)) \\ &= \left(1 - \frac{\mu}{\eta}\right)^\kappa \left(F(\mathbf{w}^{(0)}) - F(\mathbf{w}^*) - \frac{\eta^2\Phi M^2}{2\mu D^2} \sum_{j=0}^{|\mathcal{L}|-1} \sigma_{j+1} N_j \right) + \frac{\eta^2\Phi M^2}{2\mu D^2} \sum_{j=0}^{|\mathcal{L}|-1} \sigma_{j+1} N_j. \end{aligned} \quad (70)$$

Thus to satisfy the accuracy requirement, it is sufficient to have:

$$\left(1 - \frac{\mu}{\eta}\right)^\kappa \left(F(\mathbf{w}^{(0)}) - F(\mathbf{w}^*) - \frac{\eta^2\Phi M^2}{2\mu D^2} \sum_{j=0}^{|\mathcal{L}|-1} \sigma_{j+1} N_j \right) + \frac{\eta^2\Phi M^2}{2\mu D^2} \sum_{j=0}^{|\mathcal{L}|-1} \sigma_{j+1} N_j \leq \epsilon. \quad (71)$$

Performing some algebraic steps leads to (20).

Regarding the second condition, given the number of consensus rounds stated in the proposition statement, we first recursively expand the right hand side of (69) to get:

$$F(\mathbf{w}^{(\kappa)}) - F(\mathbf{w}^*) \leq (1 - \delta)^\kappa (F(\mathbf{w}^{(0)}) - F(\mathbf{w}^*)). \quad (72)$$

Thus, to satisfy the desired accuracy, it is sufficient to have:

$$(1 - \delta)^\kappa [F(\mathbf{w}^{(0)}) - F(\mathbf{w}^*)] \leq \epsilon, \quad (73)$$

which readily leads to (21). Note that the criterion given in the corollary statement for ϵ guarantees that: $0 < \delta \leq \mu/\eta$.

APPENDIX E
PROOF OF COROLLARY 2

Regarding the first condition, upon using the number of consensus rounds described in the corollary statement, we get (71), which can be written as:

$$\left(1 - \frac{\mu}{\eta}\right)^\kappa \leq \frac{\epsilon - \frac{\eta^2\Phi M^2}{2\mu D^2} \sum_{j=0}^{|\mathcal{L}|-1} \sigma_{j+1} N_j}{F(\mathbf{w}^{(0)}) - F(\mathbf{w}^*) - \frac{\eta^2\Phi M^2}{2\mu D^2} \sum_{j=0}^{|\mathcal{L}|-1} \sigma_{j+1} N_j}. \quad (74)$$

To obtain κ , we need to take the logarithm with base $1 - \mu/\eta$, where $0 < 1 - \mu/\eta < 1$. Using the characteristic of the logarithm upon having a positive base less than one, we get:

$$\kappa \geq \log_{1-\mu/\eta} \frac{\epsilon - \frac{\eta^2 \Phi M^2}{2\mu D^2} \sum_{j=0}^{|\mathcal{L}|-1} \sigma_{j+1} N_j}{F(\mathbf{w}^{(0)}) - F(\mathbf{w}^*) - \frac{\eta^2 \Phi M^2}{2\mu D^2} \sum_{j=0}^{|\mathcal{L}|-1} \sigma_{j+1} N_j}, \quad (75)$$

which can be written as (22).

Regarding the second condition, upon using the number of consensus rounds described in the corollary statement, we get (73). To obtain κ , we take the logarithm with base $1 - \delta$ from both hand sides of the equation, using the fact that $0 < 1 - \delta < 1$ and the characteristic of the logarithm upon having a positive base less than one, we get:

$$\kappa \geq \log_{1-\delta} \left(\epsilon / (F(\mathbf{w}^{(0)}) - F(\mathbf{w}^*)) \right), \quad (76)$$

which can be written as (23).

APPENDIX F

PROOF OF PROPOSITION 3

Upon sharing the gradients, the nodes in the bottom layer share their weighted gradients (multiplying their gradients by their number of data points), while the rest of the procedure, i.e., traversing of the parameters over the hierarchy, is the same as sharing the parameters. For parent node a_p , let a'_{p+1} denote the corresponding sampled node, $\forall p$. Let $\hat{g}_{a'_1}^{(k+1)}$ denote the sampled value by the root node (main server) at global iteration $k + 1$. It can be verified that we have:

$$\begin{aligned} \hat{\mathbf{g}}_{a'_1}^{(k+1)} &= \frac{\sum_{a_1 \in \mathcal{L}_1^1} \sum_{a_2 \in \mathcal{Q}(a_1)} \sum_{a_3 \in \mathcal{Q}(a_2)} \cdots \sum_{a_{|\mathcal{L}|-1} \in \mathcal{Q}(a_{|\mathcal{L}|-2})} |\mathcal{D}_{a_{|\mathcal{L}|}}| \nabla f_{a_{|\mathcal{L}|}}(\mathbf{w}_{a_{|\mathcal{L}|}}^{(k)})}{|\mathcal{L}_1^1|} \\ &+ \sum_{a_1 \in \mathcal{L}_1^1} \sum_{a_2 \in \mathcal{Q}(a_1)} \sum_{a_3 \in \mathcal{Q}(a_2)} \cdots \sum_{a_{|\mathcal{L}|-1} \in \mathcal{Q}(a_{|\mathcal{L}|-2})} \frac{\mathbb{1}_{\{\mathcal{Q}(a_{|\mathcal{L}|-1})\}} |\mathcal{Q}(a_{|\mathcal{L}|-1})| \mathbf{c}_{a'_{|\mathcal{L}|}}^{(k+1)}}{|\mathcal{L}_1^1|} \\ &+ \sum_{a_1 \in \mathcal{L}_1^1} \sum_{a_2 \in \mathcal{Q}(a_1)} \sum_{a_3 \in \mathcal{Q}(a_2)} \cdots \sum_{a_{|\mathcal{L}|-2} \in \mathcal{Q}(a_{|\mathcal{L}|-3})} \frac{\mathbb{1}_{\{\mathcal{Q}(a_{|\mathcal{L}|-2})\}} |\mathcal{Q}(a_{|\mathcal{L}|-2})| \mathbf{c}_{a'_{|\mathcal{L}|-1}}^{(k+1)}}{|\mathcal{L}_1^1|} + \\ &\vdots \\ &+ \sum_{a_1 \in \mathcal{L}_1^1} \frac{\mathbb{1}_{\{\mathcal{Q}(a_1)\}} |\mathcal{Q}(a_1)| \mathbf{c}_{a'_2}^{(k+1)}}{|\mathcal{L}_1^1|} + \mathbb{1}_{\{\mathcal{L}_1^1\}} \mathbf{c}_{a'_1}^{(k+1)}. \end{aligned} \quad (77)$$

The main server then uses this vector as the estimation of global gradient and builds the parameter vector for the next iteration as follows (note that although the root only receives the gradients, it has the knowledge of the previous parameters that it broadcasted, i.e., $\mathbf{w}^{(k)}$):

$$\begin{aligned}
\widehat{\mathbf{w}}_{L_1^0}^{(k+1)} &= D \frac{\mathbf{w}^{(k)}}{|\mathcal{L}_1^1|} - \\
&\beta \left[\frac{\sum_{a_1 \in \mathcal{L}_1^1} \sum_{a_2 \in \mathcal{Q}(a_1)} \sum_{a_3 \in \mathcal{Q}(a_2)} \cdots \sum_{a_{|\mathcal{L}|} \in \mathcal{Q}(a_{|\mathcal{L}|-1})} |\mathcal{D}_{a_{|\mathcal{L}|}}| \nabla f_{a_{|\mathcal{L}|}}(\mathbf{w}_{a_{|\mathcal{L}|}}^{(k)})}{|\mathcal{L}_1^1|} \right. \\
&+ \sum_{a_1 \in \mathcal{L}_1^1} \sum_{a_2 \in \mathcal{Q}(a_1)} \sum_{a_3 \in \mathcal{Q}(a_2)} \cdots \sum_{a_{|\mathcal{L}|-1} \in \mathcal{Q}(a_{|\mathcal{L}|-2})} \frac{\mathbb{1}_{\{\mathcal{Q}(a_{|\mathcal{L}|-1})\}}^{(k+1)} |\mathcal{Q}(a_{|\mathcal{L}|-1})| \mathbf{c}_{a'_{|\mathcal{L}|}}^{(k+1)}}{|\mathcal{L}_1^1|} \\
&+ \sum_{a_1 \in \mathcal{L}_1^1} \sum_{a_2 \in \mathcal{Q}(a_1)} \sum_{a_3 \in \mathcal{Q}(a_2)} \cdots \sum_{a_{|\mathcal{L}|-2} \in \mathcal{Q}(a_{|\mathcal{L}|-3})} \frac{\mathbb{1}_{\{\mathcal{Q}(a_{|\mathcal{L}|-2})\}}^{(k+1)} |\mathcal{Q}(a_{|\mathcal{L}|-2})| \mathbf{c}_{a'_{|\mathcal{L}|-1}}^{(k+1)}}{|\mathcal{L}_1^1|} + \\
&\vdots \\
&\left. + \sum_{a_1 \in \mathcal{L}_1^1} \frac{\mathbb{1}_{\{\mathcal{Q}(a_1)\}}^{(k+1)} |\mathcal{Q}(a_1)| \mathbf{c}_{a'_2}^{(k+1)}}{|\mathcal{L}_1^1|} + \mathbb{1}_{\{\mathcal{L}_1^1\}}^{(k+1)} \mathbf{c}_{a'_1}^{(k+1)} \right], \tag{78}
\end{aligned}$$

which is used to obtain the next global parameter (due to the existence of the indicator function in the last term of the above expression, the following expression holds regardless of the operating mode of the cluster at layer \mathcal{L}^1):

$$\mathbf{w}^{(k+1)} = \frac{|\mathcal{L}_1^1| \widehat{\mathbf{w}}_{L_1^0}^{(k+1)}}{D}. \tag{79}$$

According to (1), it can be verified that:

$$\sum_{a_1 \in \mathcal{L}_1^1} \sum_{a_2 \in \mathcal{Q}(a_1)} \sum_{a_3 \in \mathcal{Q}(a_2)} \cdots \sum_{a_{|\mathcal{L}|} \in \mathcal{Q}(a_{|\mathcal{L}|-1})} |\mathcal{D}_i| \nabla f_{a_{|\mathcal{L}|}}(\mathbf{w}_{a_{|\mathcal{L}|}}^{(k)}) = D \nabla F(\mathbf{w}^{(k)}). \tag{80}$$

Replacing the above equation in (78) and performing the update given by (79), we get:

$$\begin{aligned}
\mathbf{w}^{(k+1)} &= \mathbf{w}^{(k)} - \beta \left[\nabla F(\mathbf{w}^{(k)}) + \frac{1}{D} \left(\sum_{a_1 \in \mathcal{L}_1^1} \sum_{a_2 \in \mathcal{Q}(a_1)} \cdots \sum_{a_{|\mathcal{L}|-1} \in \mathcal{Q}(a_{|\mathcal{L}|-2})} \mathbb{1}_{\{\mathcal{Q}(a_{|\mathcal{L}|-1})\}} | \mathcal{Q}(a_{|\mathcal{L}|-1}) | \mathbf{c}_{a'_{|\mathcal{L}|}}^{(k+1)} \right. \right. \\
&+ \sum_{a_1 \in \mathcal{L}_1^1} \sum_{a_2 \in \mathcal{Q}(a_1)} \cdots \sum_{a_{|\mathcal{L}|-2} \in \mathcal{Q}(a_{|\mathcal{L}|-3})} \mathbb{1}_{\{\mathcal{Q}(a_{|\mathcal{L}|-2})\}} | \mathcal{Q}(a_{|\mathcal{L}|-2}) | \mathbf{c}_{a'_{|\mathcal{L}|-1}}^{(k+1)} + \\
&\vdots \\
&+ \left. \sum_{a_1 \in \mathcal{L}_1^1} \mathbb{1}_{\{\mathcal{Q}(a_1)\}} | \mathcal{Q}(a_1) | \mathbf{c}_{a'_2}^{(k+1)} + \mathbb{1}_{\{\mathcal{L}_1^1\}} | \mathcal{L}_1^1 | \mathbf{c}_{a'_1}^{(k+1)} \right) \Big].
\end{aligned} \tag{81}$$

Using the above equality in (31), we have:

$$\begin{aligned}
F(\mathbf{w}^{(k+1)}) &\leq F(\mathbf{w}^{(k)}) - \beta_k (\nabla F(\mathbf{w}^{(k)}) + \mathbf{c}^{(k+1)})^\top \nabla F(\mathbf{w}^{(k)}) + \frac{\eta}{2} \beta_k^2 \|\nabla F(\mathbf{w}^{(k)}) + \mathbf{c}^{(k+1)}\|^2 \\
&= F(\mathbf{w}^{(k)}) - \beta_k \|\nabla F(\mathbf{w}^{(k)})\|^2 - \beta_k (\mathbf{c}^{(k+1)})^\top \nabla F(\mathbf{w}^{(k)}) + \frac{\eta}{2} \beta_k^2 \|\nabla F(\mathbf{w}^{(k)}) + \mathbf{c}^{(k+1)}\|^2 \\
&= F(\mathbf{w}^{(k)}) - \beta_k \|\nabla F(\mathbf{w}^{(k)})\|^2 - \beta_k (\mathbf{c}^{(k+1)})^\top \nabla F(\mathbf{w}^{(k)}) + \frac{\eta \beta_k^2}{2} \|\nabla F(\mathbf{w}^{(k)})\|^2 \\
&+ \beta_k^2 \eta (\nabla F(\mathbf{w}^{(k)})^\top \mathbf{c}^{(k+1)}) + \frac{\eta \beta_k^2}{2} \|\mathbf{c}^{(k+1)}\|^2,
\end{aligned} \tag{82}$$

where

$$\begin{aligned}
\mathbf{c}^{(k+1)} &\triangleq \frac{1}{D} \left(\sum_{a_1 \in \mathcal{L}_1^1} \sum_{a_2 \in \mathcal{Q}(a_1)} \sum_{a_3 \in \mathcal{Q}(a_2)} \cdots \sum_{a_{|\mathcal{L}|-1} \in \mathcal{Q}(a_{|\mathcal{L}|-2})} \mathbb{1}_{\{\mathcal{Q}(a_{|\mathcal{L}|-1})\}} | \mathcal{Q}(a_{|\mathcal{L}|-1}) | \mathbf{c}_{a'_{|\mathcal{L}|}}^{(k+1)} \right. \\
&+ \sum_{a_1 \in \mathcal{L}_1^1} \sum_{a_2 \in \mathcal{Q}(a_1)} \sum_{a_3 \in \mathcal{Q}(a_2)} \cdots \sum_{a_{|\mathcal{L}|-2} \in \mathcal{Q}(a_{|\mathcal{L}|-3})} \mathbb{1}_{\{\mathcal{Q}(a_{|\mathcal{L}|-2})\}} | \mathcal{Q}(a_{|\mathcal{L}|-2}) | \mathbf{c}_{a'_{|\mathcal{L}|-1}}^{(k+1)} + \\
&\vdots \\
&+ \left. \sum_{a_1 \in \mathcal{L}_1^1} \mathbb{1}_{\{\mathcal{Q}(a_1)\}} | \mathcal{Q}(a_1) | \mathbf{c}_{a'_2}^{(k+1)} + \mathbb{1}_{\{\mathcal{L}_1^1\}} | \mathcal{L}_1^1 | \mathbf{c}_{a'_1}^{(k+1)} \right).
\end{aligned} \tag{83}$$

Taking the expectation from both hand sides (with respect to the consensus errors) and using the fact that upon using the consensus method, when one node is sampled uniformly at random we have:⁶ $\mathbb{E}[\mathbf{c}_{a'_p}^{(k+1)}] = \mathbf{0}, \forall p$. This implies $\mathbb{E}[\mathbf{c}^{(k+1)}] = \mathbf{0}, \forall k$, replacing which in (82) gives us:

$$\mathbb{E}[F(\mathbf{w}^{(k+1)})] \leq F(\mathbf{w}^{(k)}) - (1 - \frac{\eta \beta_k}{2}) \beta_k \|\nabla F(\mathbf{w}^{(k)})\|^2 + \frac{\eta \beta_k^2}{2} E[\|\mathbf{c}^{(k+1)}\|^2]. \tag{84}$$

⁶Assume a set of n numbers denoted by x_1, \dots, x_n with mean \bar{x} . Assume that X denotes a random variable with probability mass function $p(X = x_i) = \frac{1}{n}, 1 \leq i \leq n$. It is straightforward to verify that $E(X - \bar{x}) = 0$.

Using the fact that $\beta_0 \leq 1/\eta$, we get $\beta_k \leq 1/\eta$, and thus $1 - \eta\beta_k/2 \geq 1/2$. Using this in the above inequality gives us:

$$\mathbb{E}[F(\mathbf{w}^{(k+1)})] \leq F(\mathbf{w}^{(k)}) - \frac{\beta_k}{2} \|\nabla F(\mathbf{w}^{(k)})\|^2 + \frac{\eta\beta_k^2}{2} E[\|\mathbf{c}^{(k+1)}\|^2]. \quad (85)$$

Using the strong convexity, we get Polyak-Lojasiewicz inequality [52] in the following form: $\|\nabla F(\mathbf{w}^{(k)})\|^2 \geq 2\mu[F(\mathbf{w}^{(k)}) - F(\mathbf{w}^*)]$, using which in the above inequality yields:

$$\mathbb{E}[F(\mathbf{w}^{(k+1)})] \leq F(\mathbf{w}^{(k)}) - \beta_k\mu[F(\mathbf{w}^{(k)}) - F(\mathbf{w}^*)] + \frac{\eta\beta_k^2}{2} E[\|\mathbf{c}^{(k+1)}\|^2], \quad (86)$$

or, equivalently:

$$\mathbb{E}[F(\mathbf{w}^{(k+1)})] - F(\mathbf{w}^*) \leq (1 - \beta_k\mu)[F(\mathbf{w}^{(k)}) - F(\mathbf{w}^*)] + \frac{\eta\beta_k^2}{2} E[\|\mathbf{c}^{(k+1)}\|^2]. \quad (87)$$

Taking total expectation, with respect to all the consensus errors until iteration $k + 1$, from both hand sides results in:

$$\mathbb{E}[F(\mathbf{w}^{(k+1)}) - F(\mathbf{w}^*)] \leq (1 - \beta_k\mu)\mathbb{E}[F(\mathbf{w}^{(k)}) - F(\mathbf{w}^*)] + \frac{\eta\beta_k^2}{2} E[\|\mathbf{c}^{(k+1)}\|^2]. \quad (88)$$

The proposition result trivially holds for iteration 0. Assume that the result holds for iteration k , i.e., $\mathbb{E}[F(\mathbf{w}^{(k)}) - F(\mathbf{w}^*)] \leq \frac{\Gamma}{k+\lambda}$. We aim to show that the result also holds for iteration $k + 1$.

Using (88), we get:

$$\begin{aligned} \mathbb{E}[F(\mathbf{w}^{(k+1)}) - F(\mathbf{w}^*)] &\leq (1 - \frac{\alpha}{k+\lambda}\mu)\frac{\Gamma}{k+\lambda} + \frac{\eta\alpha^2}{2(k+\lambda)^2} \mathbb{E}[\|\mathbf{c}^{(k+1)}\|^2] \\ &= \left(\frac{k+\lambda-\alpha\mu}{(k+\lambda)^2} \right) \Gamma + \frac{\eta\alpha^2}{2(k+\lambda)^2} \mathbb{E}[\|\mathbf{c}^{(k+1)}\|^2] \\ &= \left(\frac{k+\lambda-1}{(k+\lambda)^2} \right) \Gamma - \frac{\alpha\mu-1}{(k+\lambda)^2} \Gamma + \frac{\eta\alpha^2}{2(k+\lambda)^2} \mathbb{E}[\|\mathbf{c}^{(k+1)}\|^2]. \end{aligned} \quad (89)$$

Note that using a similar method as Appendix A, we can get:⁷

$$\begin{aligned}
\mathbb{E} \left[\|\mathbf{c}^{(k+1)}\|^2 \right] &\leq \frac{\Phi M^2}{D^2} \left[\sum_{a_1 \in \mathcal{L}_1^1} \sum_{a_2 \in \mathcal{Q}(a_1)} \cdots \sum_{a_{|\mathcal{L}|-1} \in \mathcal{Q}(a_{|\mathcal{L}|-2})} \mathbb{I}_{\{\mathcal{Q}(a_{|\mathcal{L}|-1})\}}^{(k+1)} |\mathcal{Q}(a_{|\mathcal{L}|-1})|^4 \left(\lambda_{\mathcal{Q}(a_{|\mathcal{L}|-1})}^{(k+1)} \right)^{2\theta_{\mathcal{Q}(a_{|\mathcal{L}|-1})}^{(k+1)}} \left(\Upsilon_{\mathcal{Q}(a_{|\mathcal{L}|-1})}^{(k+1)} \right)^2 \right. \\
&+ \sum_{a_1 \in \mathcal{L}_1^1} \sum_{a_2 \in \mathcal{Q}(a_1)} \cdots \sum_{a_{|\mathcal{L}|-2} \in \mathcal{Q}(a_{|\mathcal{L}|-3})} \mathbb{I}_{\{\mathcal{Q}(a_{|\mathcal{L}|-2})\}}^{(k+1)} |\mathcal{Q}(a_{|\mathcal{L}|-2})|^4 \left(\lambda_{\mathcal{Q}(a_{|\mathcal{L}|-2})}^{(k+1)} \right)^{2\theta_{\mathcal{Q}(a_{|\mathcal{L}|-2})}^{(k+1)}} \left(\Upsilon_{\mathcal{Q}(a_{|\mathcal{L}|-2})}^{(k+1)} \right)^2 \\
&+ \cdots + \sum_{a_1 \in \mathcal{L}_1^1} \mathbb{I}_{\{\mathcal{Q}(a_1)\}}^{(k+1)} |\mathcal{Q}(a_1)|^4 \left(\lambda_{\mathcal{Q}(a_1)}^{(k+1)} \right)^{2\theta_{\mathcal{Q}(a_1)}^{(k+1)}} \left(\Upsilon_{\mathcal{Q}(a_1)}^{(k+1)} \right)^2 + \mathbb{I}_{\{\mathcal{L}_1^1\}}^{(k+1)} |\mathcal{L}_1^1|^4 \left(\lambda_{\mathcal{L}_1^1}^{(k+1)} \right)^{2\theta_{\mathcal{L}_1^1}^{(k+1)}} \left(\Upsilon_{\mathcal{L}_1^1}^{(k+1)} \right)^2 \left. \right]. \quad (90)
\end{aligned}$$

Using the number of consensus rounds given in the proposition, similar to the approach taken in Appendix B it can be verified that $E[\|\mathbf{c}^{(k+1)}\|^2] \leq C = \frac{\Phi M^2}{D^2} \sum_{j=0}^{|\mathcal{L}|-1} N_j \sigma_{j+1}$, $\forall k$. Using this and the definition of Γ in (25), we get: $\Gamma \geq \frac{\eta \alpha^2 C}{2(\alpha \mu - 1)}$, $\forall k$. Using this result in the last line of (89), we get:

$$\mathbb{E}[F(\mathbf{w}^{(k+1)}) - F(\mathbf{w}^*)] \leq \left(\frac{k + \lambda - 1}{(k + \lambda)^2} \right) \Gamma. \quad (91)$$

Note that since $k + \lambda > 1$, we have $(k + \lambda)^2 \geq (k + \lambda - 1)(k + \lambda + 1)$. Using this fact in (91), we get:

$$\mathbb{E}[F(\mathbf{w}^{(k+1)}) - F(\mathbf{w}^*)] \leq \left(\frac{1}{k + \lambda + 1} \right) \Gamma, \quad (92)$$

which completes the induction and thus the proof.

APPENDIX G

CLUSTER SAMPLING

In a system of million/billion users, one technique that a main server can use to reduce the network load is to engage a portion of the devices in each global iteration. We realize this in FogL via *cluster sampling* using which at each global iteration, a portion of the clusters of the bottom-most layer are engaged in model training, which we call *active clusters*. We assume that at each global iteration k , the main server engages a set of $|\mathcal{S}^{(k)}|$ clusters in the learning, where each element of the set $\mathcal{S}^{(k)}$ corresponds to one cluster in the bottom-most layer. Consequently, we partition the nodes in different layers into active nodes (those that are through the path

⁷Note that if for every realization of random variable X , inequality $\|X\|^2 < y$ holds, then we get: $\mathbb{E}[\|X\|^2] < y$.

$$\begin{aligned}
F(\mathbf{w}^{(k)}) - F(\mathbf{w}^*) &\leq \left[\prod_{l=1}^k \left(1 - \frac{\mu}{\eta} + 8 \frac{c_2}{D^2} (D - D_s^{(l)})^2 \right) \right] (F(\mathbf{w}^{(0)}) - F(\mathbf{w}^*)) + \left(\sum_{t=1}^k \left[\prod_{l=t+1}^k \left(1 - \frac{\mu}{\eta} + 8 \frac{c_2}{D^2} (D - D_s^{(l)})^2 \right) \right] \right. \\
&\quad \left(\frac{\eta \Phi M^2}{(D_s^{(t)})^2} \left[\sum_{a_1 \in \mathcal{L}_1^1} \sum_{a_2 \in \mathcal{Q}(a_1)} \cdots \sum_{a_{|\mathcal{L}|-1} \in \mathcal{Q}(a_{|\mathcal{L}|-2})} \mathbb{1}_{\{\mathcal{Q}(a_{|\mathcal{L}|-1})\}}^{(t)} |\mathcal{Q}(a_{|\mathcal{L}|-1})|^4 \left(\lambda_{\mathcal{Q}(a_{|\mathcal{L}|-1})}^{(t)} \right)^{2\theta_{\mathcal{Q}(a_{|\mathcal{L}|-1})}^{(t)}} \left(\Upsilon_{\mathcal{Q}(a_{|\mathcal{L}|-1})}^{(t)} \right)^2 \right. \right. \\
&\quad + \sum_{a_1 \in \mathcal{L}_1^1} \sum_{a_2 \in \mathcal{Q}(a_1)} \cdots \sum_{a_{|\mathcal{L}|-2} \in \mathcal{Q}(a_{|\mathcal{L}|-3})} \mathbb{1}_{\{\mathcal{Q}(a_{|\mathcal{L}|-2})\}}^{(t)} |\mathcal{Q}(a_{|\mathcal{L}|-2})|^4 \left(\lambda_{\mathcal{Q}(a_{|\mathcal{L}|-2})}^{(t)} \right)^{2\theta_{\mathcal{Q}(a_{|\mathcal{L}|-2})}^{(t)}} \left(\Upsilon_{\mathcal{Q}(a_{|\mathcal{L}|-2})}^{(t)} \right)^2 + \cdots \\
&\quad + \sum_{a_1 \in \mathcal{L}_1^1} \mathbb{1}_{\{\mathcal{Q}(a_1)\}}^{(t)} |\mathcal{Q}(a_1)|^4 \left(\lambda_{\mathcal{Q}(a_1)}^{(t)} \right)^{2\theta_{\mathcal{Q}(a_1)}^{(t)}} \left(\Upsilon_{\mathcal{Q}(a_1)}^{(t)} \right)^2 \\
&\quad \left. \left. + \mathbb{1}_{\{\mathcal{L}_1^1\}}^{(t)} |\mathcal{L}_1^1|^4 \left(\lambda_{\mathcal{L}_1^1}^{(t)} \right)^{2\theta_{\mathcal{L}_1^1}^{(t)}} \left(\Upsilon_{\mathcal{L}_1^1}^{(t)} \right)^2 \right] + \frac{4}{\eta} \left(\frac{D - D_s^{(t)}}{D} \right)^2 c_1 \right) \Bigg)
\end{aligned} \tag{94}$$

between an active cluster and the main server) and passive nodes. Similarly, for the clusters of the middle layers, if the cluster contains at least one active node, it is called an *active cluster*. To capture these dynamics, with some abuse of notation, let $\mathbb{1}_{\{\mathcal{C}\}}^{(k)}$ take the value of 1 if cluster \mathcal{C} is both in active mode and operates in LUT mode in global aggregation k , and 0 otherwise. To conduct analysis, in addition to our assumptions made in Assumptions 1 and 2, we also consider the following assumption that is common in stochastic optimization literature [53]:

$$\exists c_1 \geq 0, c_2 \geq 1 : \|\nabla f_i(x)\|^2 \leq c_1 + c_2 \|\nabla F(x)\|^2, \quad \forall i, x. \tag{93}$$

Proposition 4. *For global iteration k , the per-iteration decrease of the objective function can be written as (94), where $D_s^{(k)}$ denotes the total number of data points of the sampled devices at iteration k , i.e., $D_s^{(k+1)} = \sum_{n \in \mathcal{L}|\mathcal{C}|} \mathbb{1}_{\{\mathcal{B}(n)\}}^{(k+1)} |\mathcal{D}_n|$, with $\mathcal{B}(n)$ referring to the cluster that the node n belongs to.⁸*

Proof. To find the relationship between $\mathbf{w}^{(k)}$ and $\mathbf{w}^{(k+1)}$, we follow the procedure described in the main text. Let $\mathbb{1}_{\{S(\mathcal{C})\}}^{(k)}$ take the value of 1 when cluster \mathcal{C} is in active mode in global aggregation k , and 0 otherwise. Also, with some abuse of notation, let $\mathbb{1}_{\{\mathcal{C}\}}^{(k)}$ take the value of 1 if cluster \mathcal{C} is both in active mode and operates in LUT mode in global aggregation k , and 0 otherwise. It can be verified that, at global iteration $k+1$, the parameter of the sampled node

⁸It is assumed that $\prod_{j=k+1}^k c_j = 1, \forall c_j$.

$$\begin{aligned}
\widehat{\mathbf{w}}_{L_{a'_1}^1}^{(k+1)} &= \frac{\sum_{a_1 \in \mathcal{L}_1^1} \sum_{a_2 \in \mathcal{Q}(a_1)} \sum_{a_3 \in \mathcal{Q}(a_2)} \cdots \sum_{a_{|\mathcal{L}|} \in \mathcal{Q}(a_{|\mathcal{L}|-1})} \mathbb{1}_{\{S(\mathcal{Q}(a_{|\mathcal{L}|-1}))\}}^{(k+1)} |\mathcal{D}_{a_{|\mathcal{L}|}}| \mathbf{w}_{a_{|\mathcal{L}|}}^{(k)}}{|\mathcal{L}_1^1|} \\
&\quad - \frac{\sum_{a_1 \in \mathcal{L}_1^1} \sum_{a_2 \in \mathcal{Q}(a_1)} \sum_{a_3 \in \mathcal{Q}(a_2)} \cdots \sum_{a_{|\mathcal{L}|} \in \mathcal{Q}(a_{|\mathcal{L}|-1})} \mathbb{1}_{\{S(\mathcal{Q}(a_{|\mathcal{L}|-1}))\}}^{(k+1)} \beta |\mathcal{D}_{a_{|\mathcal{L}|}}| \nabla f_{a_{|\mathcal{L}|}}(\mathbf{w}_{a_{|\mathcal{L}|}}^{(k)})}{|\mathcal{L}_1^1|} \\
&\quad + \sum_{a_1 \in \mathcal{L}_1^1} \sum_{a_2 \in \mathcal{Q}(a_1)} \sum_{a_3 \in \mathcal{Q}(a_2)} \cdots \sum_{a_{|\mathcal{L}|-1} \in \mathcal{Q}(a_{|\mathcal{L}|-2})} \frac{\mathbb{1}_{\{\mathcal{Q}(a_{|\mathcal{L}|-1})\}}^{(k+1)} |\mathcal{Q}(a_{|\mathcal{L}|-1})| \mathbf{c}_{a'_{|\mathcal{L}|}}^{(k+1)}}{|\mathcal{L}_1^1|} \\
&\quad + \sum_{a_1 \in \mathcal{L}_1^1} \sum_{a_2 \in \mathcal{Q}(a_1)} \sum_{a_3 \in \mathcal{Q}(a_2)} \cdots \sum_{a_{|\mathcal{L}|-2} \in \mathcal{Q}(a_{|\mathcal{L}|-3})} \frac{\mathbb{1}_{\{\mathcal{Q}(a_{|\mathcal{L}|-2})\}}^{(k+1)} |\mathcal{Q}(a_{|\mathcal{L}|-2})| \mathbf{c}_{a'_{|\mathcal{L}|-1}}^{(k+1)}}{|\mathcal{L}_1^1|} + \\
&\quad \vdots \\
&\quad + \sum_{a_1 \in \mathcal{L}_1^1} \frac{\mathbb{1}_{\{\mathcal{Q}(a_1)\}}^{(k+1)} |\mathcal{Q}(a_1)| \mathbf{c}_{a'_2}^{(k+1)}}{|\mathcal{L}_1^1|} + \mathbb{1}_{\{\mathcal{L}_1^1\}}^{(k+1)} \mathbf{c}_{a'_1}^{(k+1)}
\end{aligned} \tag{95}$$

located in the \mathcal{L}^1 by the main server, $L_{a'_1}^1$, is given by (95), which is used by the root node to obtain the next global parameter as follows:

$$\mathbf{w}^{(k+1)} = \frac{|\mathcal{L}_1^1| \mathbf{w}_{L_{a'_1}^1}^{(k+1)}}{D_s^{(k+1)}}, \tag{96}$$

where $D_s^{(k+1)} = \sum_{n \in \mathcal{L}^1} \mathbb{1}_{\{\mathcal{B}(n)\}}^{(k+1)} |\mathcal{D}_n|$, with $\mathcal{B}(n)$ referring to the cluster that the node n belongs to, is the total number of data points available at the sampled devices at global aggregation $k+1$, which is assumed to be known to the server (in this case the server needs the knowledge of the number of data points available at the active clusters). Following a similar procedure described in Appendix A, we obtain (97). Let us define

$$\begin{aligned}
\varpi^{(k+1)} &\triangleq \frac{1}{D_s^{(k+1)}} \left[\sum_{a_1 \in \mathcal{L}_1^1} \sum_{a_2 \in \mathcal{Q}(a_1)} \sum_{a_3 \in \mathcal{Q}(a_2)} \cdots \sum_{a_{|\mathcal{L}|-1} \in \mathcal{Q}(a_{|\mathcal{L}|-2})} \mathbb{1}_{\{\mathcal{Q}(a_{|\mathcal{L}|-1})\}}^{(k+1)} |\mathcal{Q}(a_{|\mathcal{L}|-1})| \mathbf{c}_{a'_{|\mathcal{L}|}}^{(k+1)} \right. \\
&\quad + \sum_{a_1 \in \mathcal{L}_1^1} \sum_{a_2 \in \mathcal{Q}(a_1)} \sum_{a_3 \in \mathcal{Q}(a_2)} \cdots \sum_{a_{|\mathcal{L}|-2} \in \mathcal{Q}(a_{|\mathcal{L}|-3})} \mathbb{1}_{\{\mathcal{Q}(a_{|\mathcal{L}|-2})\}}^{(k+1)} |\mathcal{Q}(a_{|\mathcal{L}|-2})| \mathbf{c}_{a'_{|\mathcal{L}|-1}}^{(k+1)} + \\
&\quad \vdots \\
&\quad \left. + \sum_{a_1 \in \mathcal{L}_1^1} \mathbb{1}_{\{\mathcal{Q}(a_1)\}}^{(k+1)} |\mathcal{Q}(a_1)| \mathbf{c}_{a'_2}^{(k+1)} + \mathbb{1}_{\{\mathcal{L}_1^1\}}^{(k+1)} |\mathcal{L}_1^1| \mathbf{c}_{a'_1}^{(k+1)} \right].
\end{aligned} \tag{98}$$

$$\begin{aligned}
\mathbf{w}_{L^0}^{(k+1)} &= \mathbf{w}^{(k)} - \\
&\sum_{a_1 \in \mathcal{L}_1^1} \sum_{a_2 \in \mathcal{Q}(a_1)} \sum_{a_3 \in \mathcal{Q}(a_2)} \cdots \sum_{a_{|\mathcal{L}|} \in \mathcal{Q}(a_{|\mathcal{L}|-1})} \mathbb{1}_{\{S(\mathcal{Q}(a_{|\mathcal{L}|-1}))\}}^{(k+1)} \beta \frac{|\mathcal{D}_{a_{|\mathcal{L}|}}|}{D_s^{(k+1)}} \nabla f_{a_{|\mathcal{L}|}}(\mathbf{w}_{a_{|\mathcal{L}|}}^{(k)}) \\
&+ \frac{1}{D_s^{(k+1)}} \left[\sum_{a_1 \in \mathcal{L}_1^1} \sum_{a_2 \in \mathcal{Q}(a_1)} \sum_{a_3 \in \mathcal{Q}(a_2)} \cdots \sum_{a_{|\mathcal{L}|-1} \in \mathcal{Q}(a_{|\mathcal{L}|-2})} \mathbb{1}_{\{\mathcal{Q}(a_{|\mathcal{L}|-1})\}}^{(k+1)} |\mathcal{Q}(a_{|\mathcal{L}|-1})| \mathbf{c}_{a_{|\mathcal{L}|}}^{(k+1)} \right. \\
&+ \sum_{a_1 \in \mathcal{L}_1^1} \sum_{a_2 \in \mathcal{Q}(a_1)} \sum_{a_3 \in \mathcal{Q}(a_2)} \cdots \sum_{a_{|\mathcal{L}|-2} \in \mathcal{Q}(a_{|\mathcal{L}|-3})} \mathbb{1}_{\{\mathcal{Q}(a_{|\mathcal{L}|-2})\}}^{(k+1)} |\mathcal{Q}(a_{|\mathcal{L}|-2})| \mathbf{c}_{a_{|\mathcal{L}|-1}}^{(k+1)} + \\
&\vdots \\
&\left. + \sum_{a_1 \in \mathcal{L}_1^1} \mathbb{1}_{\{\mathcal{Q}(a_1)\}}^{(k+1)} |\mathcal{Q}(a_1)| \mathbf{c}_{a_2}^{(k+1)} + \mathbb{1}_{\{\mathcal{L}_1^1\}}^{(k+1)} |\mathcal{L}_1^1| \mathbf{c}_{a_1'}^{(k+1)} \right]
\end{aligned} \tag{97}$$

By adding and subtracting a term, we rewrite (97) as follows:

$$\begin{aligned}
\mathbf{w}^{(k+1)} &= \mathbf{w}^{(k)} - \sum_{a_1 \in \mathcal{L}_1^1} \sum_{a_2 \in \mathcal{Q}(a_1)} \sum_{a_3 \in \mathcal{Q}(a_2)} \cdots \sum_{a_{|\mathcal{L}|} \in \mathcal{Q}(a_{|\mathcal{L}|-1})} \mathbb{1}_{\{S(\mathcal{Q}(a_{|\mathcal{L}|-1}))\}}^{(k+1)} \beta \frac{|\mathcal{D}_{a_{|\mathcal{L}|}}|}{D_s^{(k+1)}} \nabla f_{a_{|\mathcal{L}|}}(\mathbf{w}_{a_{|\mathcal{L}|}}^{(k)}) \\
&+ \sum_{a_1 \in \mathcal{L}_1^1} \sum_{a_2 \in \mathcal{Q}(a_1)} \sum_{a_3 \in \mathcal{Q}(a_2)} \cdots \sum_{a_{|\mathcal{L}|} \in \mathcal{Q}(a_{|\mathcal{L}|-1})} \beta \frac{|\mathcal{D}_{a_{|\mathcal{L}|}}|}{D} \nabla f_{a_{|\mathcal{L}|}}(\mathbf{w}_{a_{|\mathcal{L}|}}^{(k)}) \\
&- \sum_{a_1 \in \mathcal{L}_1^1} \sum_{a_2 \in \mathcal{Q}(a_1)} \sum_{a_3 \in \mathcal{Q}(a_2)} \cdots \sum_{a_{|\mathcal{L}|} \in \mathcal{Q}(a_{|\mathcal{L}|-1})} \beta \frac{|\mathcal{D}_{a_{|\mathcal{L}|}}|}{D} \nabla f_{a_{|\mathcal{L}|}}(\mathbf{w}_{a_{|\mathcal{L}|}}^{(k)}) + \varpi^{(k+1)},
\end{aligned} \tag{99}$$

or equivalently

$$\begin{aligned}
\mathbf{w}^{(k+1)} &= \mathbf{w}^{(k)} - \beta \nabla F(\mathbf{w}^{(k)}) \\
&- \sum_{a_1 \in \mathcal{L}_1^1} \sum_{a_2 \in \mathcal{Q}(a_1)} \sum_{a_3 \in \mathcal{Q}(a_2)} \cdots \sum_{a_{|\mathcal{L}|} \in \mathcal{Q}(a_{|\mathcal{L}|-1})} \mathbb{1}_{\{S(\mathcal{Q}(a_{|\mathcal{L}|-1}))\}}^{(k+1)} \beta \frac{|\mathcal{D}_{a_{|\mathcal{L}|}}|}{D_s^{(k+1)}} \nabla f_{a_{|\mathcal{L}|}}(\mathbf{w}_{a_{|\mathcal{L}|}}^{(k)}) \\
&+ \sum_{a_1 \in \mathcal{L}_1^1} \sum_{a_2 \in \mathcal{Q}(a_1)} \sum_{a_3 \in \mathcal{Q}(a_2)} \cdots \sum_{a_{|\mathcal{L}|} \in \mathcal{Q}(a_{|\mathcal{L}|-1})} \beta \frac{|\mathcal{D}_{a_{|\mathcal{L}|}}|}{D} \nabla f_{a_{|\mathcal{L}|}}(\mathbf{w}_{a_{|\mathcal{L}|}}^{(k)}) + \varpi^{(k+1)}.
\end{aligned} \tag{100}$$

Define $\varrho^{(k+1)}$ as follows:

$$\begin{aligned}
\varrho^{(k+1)} &\triangleq \beta \left[- \sum_{a_1 \in \mathcal{L}_1^1} \sum_{a_2 \in \mathcal{Q}(a_1)} \sum_{a_3 \in \mathcal{Q}(a_2)} \cdots \sum_{a_{|\mathcal{L}|} \in \mathcal{Q}(a_{|\mathcal{L}|-1})} \mathbb{1}_{\{S(\mathcal{Q}(a_{|\mathcal{L}|-1}))\}}^{(k+1)} \frac{|\mathcal{D}_{a_{|\mathcal{L}|}}|}{D_s^{(k+1)}} \nabla f_{a_{|\mathcal{L}|}}(\mathbf{w}_{a_{|\mathcal{L}|}}^{(k)}) \right. \\
&\left. + \sum_{a_1 \in \mathcal{L}_1^1} \sum_{a_2 \in \mathcal{Q}(a_1)} \sum_{a_3 \in \mathcal{Q}(a_2)} \cdots \sum_{a_{|\mathcal{L}|} \in \mathcal{Q}(a_{|\mathcal{L}|-1})} \frac{|\mathcal{D}_{a_{|\mathcal{L}|}}|}{D} \nabla f_{a_{|\mathcal{L}|}}(\mathbf{w}_{a_{|\mathcal{L}|}}^{(k)}) + \frac{1}{\beta} \varpi^{(k+1)} \right].
\end{aligned} \tag{101}$$

For global iteration $k+1$, let $\bar{\mathcal{S}}^{(k+1)}$ denotes the set of passive clusters, which is the comple-

$$\begin{aligned}
E\|\varpi^{(k+1)}\|^2 &\leq \frac{\Phi M^2}{\left(D_s^{(k+1)}\right)^2} \left[\right. \\
&\sum_{a_1 \in \mathcal{L}_1^1} \sum_{a_2 \in \mathcal{Q}(a_1)} \cdots \sum_{a_{|\mathcal{L}|-1} \in \mathcal{Q}(a_{|\mathcal{L}|-2})} \mathbb{1}_{\{\mathcal{Q}(a_{|\mathcal{L}|-1})\}}^{(k+1)} |\mathcal{Q}(a_{|\mathcal{L}|-1})|^4 \left(\lambda_{\mathcal{Q}(a_{|\mathcal{L}|-1})}^{(k+1)} \right)^{2\theta_{\mathcal{Q}(a_{|\mathcal{L}|-1})}^{(k+1)}} \left(\Upsilon_{\mathcal{Q}(a_{|\mathcal{L}|-1})}^{(k+1)} \right)^2 \\
&+ \sum_{a_1 \in \mathcal{L}_1^1} \sum_{a_2 \in \mathcal{Q}(a_1)} \cdots \sum_{a_{|\mathcal{L}|-2} \in \mathcal{Q}(a_{|\mathcal{L}|-3})} \mathbb{1}_{\{\mathcal{Q}(a_{|\mathcal{L}|-2})\}}^{(k+1)} |\mathcal{Q}(a_{|\mathcal{L}|-2})|^4 \left(\lambda_{\mathcal{Q}(a_{|\mathcal{L}|-2})}^{(k+1)} \right)^{2\theta_{\mathcal{Q}(a_{|\mathcal{L}|-2})}^{(k+1)}} \left(\Upsilon_{\mathcal{Q}(a_{|\mathcal{L}|-2})}^{(k+1)} \right)^2 \\
&+ \cdots + \sum_{a_1 \in \mathcal{L}_1^1} \mathbb{1}_{\{\mathcal{Q}(a_1)\}}^{(k+1)} |\mathcal{Q}(a_1)|^4 \left(\lambda_{\mathcal{Q}(a_1)}^{(k+1)} \right)^{2\theta_{\mathcal{Q}(a_1)}^{(k+1)}} \left(\Upsilon_{\mathcal{Q}(a_1)}^{(k+1)} \right)^2 + \mathbb{1}_{\{\mathcal{L}_1^1\}}^{(k+1)} |\mathcal{L}_1^1|^4 \left(\lambda_{\mathcal{L}_1^1}^{(k+1)} \right)^{2\theta_{\mathcal{L}_1^1}^{(k+1)}} \left(\Upsilon_{\mathcal{L}_1^1}^{(k+1)} \right)^2 \left. \right] \quad (103)
\end{aligned}$$

mentary set of $\mathcal{S}^{(k+1)}$, $\bar{\mathcal{S}}^{(k+1)} \cup \mathcal{S}^{(k+1)} = \mathcal{L}|\mathcal{L}|$, $\bar{\mathcal{S}}^{(k+1)} \cap \mathcal{S}^{(k+1)} = \emptyset$. Let $\mathbb{1}_{\{\bar{\mathcal{S}}(\mathcal{C})\}}^{(k+1)}$ take the value of 1 when cluster \mathcal{C} is in passive mode in global aggregation $k+1$, and 0 otherwise. Following the procedure described in the proof of Appendix A, we first aim to bound $\mathbb{E}[\|\varrho^{(k+1)}\|^2]$. The procedure is described in (105). In that series of simplifications, the triangle inequality is applied repeatedly. In inequality (a), we have used the fact that $(\|\mathbf{a}\| + \|\mathbf{b}\|)^2 \leq 2(\|\mathbf{a}\|^2 + \|\mathbf{b}\|^2)$, in inequality (b) we have used the fact that $\frac{1}{D_s^{(k+1)}} = \frac{1}{D} - \frac{D_s^{(k+1)} - D}{(D)(D_s^{(k+1)})}$, and in inequality (c) we have used the smoothness definition in Assumption 1 that can also be written as:

$$F(\mathbf{y}) \leq F(\mathbf{x}) + (\mathbf{y} - \mathbf{x})^\top \nabla F(\mathbf{x}) + \frac{\eta}{2} \|\mathbf{y} - \mathbf{x}\|^2, \quad \forall \mathbf{x}, \mathbf{y}, \quad (102)$$

minimizing the both hand sides of which results in: $\|\nabla F(\mathbf{w})\|^2 \leq 2\eta(F(\mathbf{w}) - F(\mathbf{w}^*))$, $\forall \mathbf{w}$. Note that $\|\varpi^{(k+1)}\|^2$ can be obtained similar to Appendix A as (103). Replacing this with $\beta = \frac{1}{\eta}$ in the bound in (105), and following the procedure of proof in Appendix A, we get (104), which can be recursively expanded to get the bound in the proposition statement. ■

$$\begin{aligned}
F(\mathbf{w}^{(k+1)}) - F(\mathbf{w}^*) &\leq \left(1 - \frac{\mu}{\eta}\right) (F(\mathbf{w}^{(k)}) - F(\mathbf{w}^*)) + \frac{\eta}{2} \left[\right. \\
&\frac{2\Phi M^2}{\left(D_s^{(k+1)}\right)^2} \left[\sum_{a_1 \in \mathcal{L}_1^1} \sum_{a_2 \in \mathcal{Q}(a_1)} \cdots \sum_{a_{|\mathcal{L}|-1} \in \mathcal{Q}(a_{|\mathcal{L}|-2})} \mathbb{1}_{\{\mathcal{Q}(a_{|\mathcal{L}|-1})\}}^{(k+1)} |\mathcal{Q}(a_{|\mathcal{L}|-1})|^4 \left(\lambda_{\mathcal{Q}(a_{|\mathcal{L}|-1})}^{(k+1)}\right)^{2\theta_{\mathcal{Q}(a_{|\mathcal{L}|-1})}^{(k+1)}} \left(\Upsilon_{\mathcal{Q}(a_{|\mathcal{L}|-1})}^{(k+1)}\right)^2 \right. \\
&+ \sum_{a_1 \in \mathcal{L}_1^1} \sum_{a_2 \in \mathcal{Q}(a_1)} \cdots \sum_{a_{|\mathcal{L}|-2} \in \mathcal{Q}(a_{|\mathcal{L}|-3})} \mathbb{1}_{\{\mathcal{Q}(a_{|\mathcal{L}|-2})\}}^{(k+1)} |\mathcal{Q}(a_{|\mathcal{L}|-2})|^4 \left(\lambda_{\mathcal{Q}(a_{|\mathcal{L}|-2})}^{(k+1)}\right)^{2\theta_{\mathcal{Q}(a_{|\mathcal{L}|-2})}^{(k+1)}} \left(\Upsilon_{\mathcal{Q}(a_{|\mathcal{L}|-2})}^{(k+1)}\right)^2 \quad (104) \\
&+ \cdots + \sum_{a_1 \in \mathcal{L}_1^1} \mathbb{1}_{\{\mathcal{Q}(a_1)\}}^{(k+1)} |\mathcal{Q}(a_1)|^4 \left(\lambda_{\mathcal{Q}(a_1)}^{(k+1)}\right)^{2\theta_{\mathcal{Q}(a_1)}^{(k+1)}} \left(\Upsilon_{\mathcal{Q}(a_1)}^{(k+1)}\right)^2 + \mathbb{1}_{\{\mathcal{L}_1^1\}}^{(k+1)} |\mathcal{L}_1^1|^4 \left(\lambda_{\mathcal{L}_1^1}^{(k+1)}\right)^{2\theta_{\mathcal{L}_1^1}^{(k+1)}} \left(\Upsilon_{\mathcal{L}_1^1}^{(k+1)}\right)^2 \left. \right] \\
&+ \frac{8}{\eta^2} \left(\frac{D - D_s^{(k+1)}}{D} \right)^2 (c_1 + 2c_2\eta(F(\mathbf{w}^{(k)}) - F(\mathbf{w}^*))) \left. \right]
\end{aligned}$$

The methodology used to derive all the previous results regarding the convergence and the number of consensus can be studied for this case, which we leave as future work. One key observation from (94) is that upon increasing the number of active clusters, often resulting in increasing $D_s^{(k)}$, $\forall k$, the right hand side of (94) starts to decrease, which implies a higher training accuracy, and the similarity between the bounds (14) and (94) increases. In the limiting case $D_s^{(k)} = D$, $\forall k$, bound (94) can be written similarly to (94), where $\frac{\eta\Phi M^2}{2D^2}$ in (14) would be replaced by a larger value $\frac{\eta\Phi M^2}{D^2}$.

APPENDIX H

AGGREGATION ERROR UPON USING ALGORITHM 3

According to (32), the aggregation error at the $k + 1$ -th global aggregation is given by:

$$\begin{aligned}
\mathbf{e}^{(k+1)} = & \frac{1}{D} \left(\sum_{a_1 \in \mathcal{L}_1^1} \sum_{a_2 \in \mathcal{Q}(a_1)} \sum_{a_3 \in \mathcal{Q}(a_2)} \cdots \sum_{a_{|\mathcal{L}|-1} \in \mathcal{Q}(a_{|\mathcal{L}|-2})} \mathbb{1}_{\{\mathcal{Q}(a_{|\mathcal{L}|-1})\}}^{(k+1)} |\mathcal{Q}(a_{|\mathcal{L}|-1})| \mathbf{c}_{a'_{|\mathcal{L}|}}^{(k+1)} \right. \\
& + \sum_{a_1 \in \mathcal{L}_1^1} \sum_{a_2 \in \mathcal{Q}(a_1)} \sum_{a_3 \in \mathcal{Q}(a_2)} \cdots \sum_{a_{|\mathcal{L}|-2} \in \mathcal{Q}(a_{|\mathcal{L}|-3})} \mathbb{1}_{\{\mathcal{Q}(a_{|\mathcal{L}|-2})\}}^{(k+1)} |\mathcal{Q}(a_{|\mathcal{L}|-2})| \mathbf{c}_{a'_{|\mathcal{L}|-1}}^{(k+1)} + \\
& \vdots \\
& \left. + \sum_{a_1 \in \mathcal{L}_1^1} \mathbb{1}_{\{\mathcal{Q}(a_1)\}}^{(k+1)} |\mathcal{Q}(a_1)| \mathbf{c}_{a'_2}^{(k+1)} + \mathbb{1}_{\{\mathcal{L}_1^1\}}^{(k+1)} |\mathcal{L}_1^1| \mathbf{c}_{a'_1}^{(k+1)} \right). \tag{106}
\end{aligned}$$

Following a similar procedure described in Appendix A, we get:

$$\begin{aligned}
\|\mathbf{e}^{(k+1)}\|^2 \leq & \frac{\Phi M^2}{D^2} \left[\sum_{a_1 \in \mathcal{L}_1^1} \sum_{a_2 \in \mathcal{Q}(a_1)} \cdots \sum_{a_{|\mathcal{L}|-1} \in \mathcal{Q}(a_{|\mathcal{L}|-2})} \mathbb{1}_{\{\mathcal{Q}(a_{|\mathcal{L}|-1})\}}^{(k+1)} |\mathcal{Q}(a_{|\mathcal{L}|-1})|^4 \left(\lambda_{\mathcal{Q}(a_{|\mathcal{L}|-1})}^{(k+1)} \right)^{2\theta_{\mathcal{Q}(a_{|\mathcal{L}|-1})}^{(k+1)}} \left(\Upsilon_{\mathcal{Q}(a_{|\mathcal{L}|-1})}^{(k+1)} \right)^2 \right. \\
& + \sum_{a_1 \in \mathcal{L}_1^1} \sum_{a_2 \in \mathcal{Q}(a_1)} \cdots \sum_{a_{|\mathcal{L}|-2} \in \mathcal{Q}(a_{|\mathcal{L}|-3})} \mathbb{1}_{\{\mathcal{Q}(a_{|\mathcal{L}|-2})\}}^{(k+1)} |\mathcal{Q}(a_{|\mathcal{L}|-2})|^4 \left(\lambda_{\mathcal{Q}(a_{|\mathcal{L}|-2})}^{(k+1)} \right)^{2\theta_{\mathcal{Q}(a_{|\mathcal{L}|-2})}^{(k+1)}} \left(\Upsilon_{\mathcal{Q}(a_{|\mathcal{L}|-2})}^{(k+1)} \right)^2 \\
& + \cdots + \sum_{a_1 \in \mathcal{L}_1^1} \mathbb{1}_{\{\mathcal{Q}(a_1)\}}^{(k+1)} |\mathcal{Q}(a_1)|^4 \left(\lambda_{\mathcal{Q}(a_1)}^{(k+1)} \right)^{2\theta_{\mathcal{Q}(a_1)}^{(k+1)}} \left(\Upsilon_{\mathcal{Q}(a_1)}^{(k+1)} \right)^2 + \mathbb{1}_{\{\mathcal{L}_1^1\}}^{(k+1)} |\mathcal{L}_1^1|^4 \left(\lambda_{\mathcal{L}_1^1}^{(k+1)} \right)^{2\theta_{\mathcal{L}_1^1}^{(k+1)}} \left(\Upsilon_{\mathcal{L}_1^1}^{(k+1)} \right)^2 \Big], \tag{107}
\end{aligned}$$

where $\Phi = N_{|\mathcal{L}|-1} + N_{|\mathcal{L}|-2} + \cdots + N_1 + 1$. By tuning the number of consensus according to (30), following a similar procedure as Appendix B, we get:

$$\begin{aligned}
\|\mathbf{e}^{(k+1)}\|^2 &\leq \frac{\Phi M^2}{D^2} \left[\sum_{a_1 \in \mathcal{L}_1^1} \sum_{a_2 \in \mathcal{Q}(a_1)} \cdots \sum_{a_{|\mathcal{L}|-1} \in \mathcal{Q}(a_{|\mathcal{L}|-2})} \mathbb{1}_{\{\mathcal{Q}(a_{|\mathcal{L}|-1})\}}^{(k+1)} \frac{\psi}{\frac{\Phi M^2}{D^2} N_{|\mathcal{L}|-1} |\mathcal{L}|} \right. \\
&+ \sum_{a_1 \in \mathcal{L}_1^1} \sum_{a_2 \in \mathcal{Q}(a_1)} \cdots \sum_{a_{|\mathcal{L}|-2} \in \mathcal{Q}(a_{|\mathcal{L}|-3})} \mathbb{1}_{\{\mathcal{Q}(a_{|\mathcal{L}|-2})\}}^{(k+1)} \frac{\psi}{\frac{\Phi M^2}{D^2} N_{|\mathcal{L}|-2} |\mathcal{L}|} + \cdots \\
&+ \left. \sum_{a_1 \in \mathcal{L}_1^1} \mathbb{1}_{\{\mathcal{Q}(a_1)\}}^{(k+1)} \frac{\psi}{\frac{\Phi M^2}{D^2} N_1 |\mathcal{L}|} + \mathbb{1}_{\{\mathcal{L}_1^1\}}^{(k+1)} \frac{\psi}{\frac{\Phi M^2}{D^2} N_0 |\mathcal{L}|} \right] \\
&\leq \frac{\Phi M^2}{D^2} \left[\sum_{a_1 \in \mathcal{L}_1^1} \sum_{a_2 \in \mathcal{Q}(a_1)} \cdots \sum_{a_{|\mathcal{L}|-1} \in \mathcal{Q}(a_{|\mathcal{L}|-2})} \frac{\psi}{\frac{\Phi M^2}{D^2} N_{|\mathcal{L}|-1} |\mathcal{L}|} \right. \\
&+ \sum_{a_1 \in \mathcal{L}_1^1} \sum_{a_2 \in \mathcal{Q}(a_1)} \cdots \sum_{a_{|\mathcal{L}|-2} \in \mathcal{Q}(a_{|\mathcal{L}|-3})} \mathbb{1}_{\{\mathcal{Q}(a_{|\mathcal{L}|-2})\}}^{(k+1)} \frac{\psi}{\frac{\Phi M^2}{D^2} N_{|\mathcal{L}|-2} |\mathcal{L}|} + \cdots \\
&+ \left. \sum_{a_1 \in \mathcal{L}_1^1} \frac{\psi}{\frac{\Phi M^2}{D^2} N_1 |\mathcal{L}|} + \frac{\psi}{\frac{\Phi M^2}{D^2} N_0 |\mathcal{L}|} \right] \\
&= \frac{\Phi M^2}{D^2} \left[\underbrace{\frac{\psi}{\frac{\Phi M^2}{D^2} |\mathcal{L}|} + \frac{\psi}{\frac{\Phi M^2}{D^2} |\mathcal{L}|} \cdots + \frac{\psi}{\frac{\Phi M^2}{D^2} |\mathcal{L}|} + \frac{\psi}{\frac{\Phi M^2}{D^2} |\mathcal{L}|}}_{|\mathcal{L}| \text{ terms}} \right].
\end{aligned} \tag{108}$$

Thus, we have:

$$\|\mathbf{e}^{(k+1)}\|^2 \leq \psi. \tag{109}$$

APPENDIX I

DETAILS OF THE SIMULATIONS SETTING AND FURTHER SIMULATIONS

In this section, we first present some details regarding simulations settings and parameter tuning and then present a series of simulation results regarding the choice of different datasets and larger network size as compared to the main text. The exact set of hyperparameters used on each network can be found at our implementation repository: <https://github.com/shams-sam/Federated2Fog>.

A. Simulation Setting

1) *Setup*: All simulations are performed on a single machine with 64GB RAM and 8GB GPU memory, which emulates the learning through a distributed learning framework *PySyft* that helps spin off virtually disjoint nodes with mutually exclusive model parameters and datasets, working on top of *PyTorch* machine learning library.

2) *Classifiers*: We consider two different classifiers - regularized Support Vector Machine (SVM) and fully-connected Neural Network (NN), initialized with a copy of global model before the learning process begins on each node participating in the learning process.

The regularized SVM is tuned to satisfy the strong convexity with $\mu = 0.1$. We also use the estimated value of $\eta = 10$ (similar values are observed in [21]). The NN classifier is a simple fully connected network with a single hidden layer and no convolutional units. *Softmax* activation at the output layer gives the class *logits* and the overall training optimizes negative log-likelihood loss function with L2 regularization.

Input size for both the models, SVM and NN is $28 \times 28 = 784$, with output size 10. The number of parameters optimized by the networks M is given by $M = (784 + 1) \times 10 = 7850$.

3) *Datasets and Data Distribution among the Nodes*: We consider two datasets MNIST and F-MNIST (Fashion MNIST)⁹, each of which contain 60000 training samples and 10000 testing samples. MNIST consists of handwritten digits 0 – 9, while F-MNIST consists of images associated with 10 classes in clothing domain. Each dataset consists of 28×28 grayscale images.

The datasets are distributed over nodes such that all nodes have approximately equal number of training samples. However the training samples, maybe either be i.i.d or non-i.i.d distributed. For i.i.d distribution, each node participating in the learning process has samples from each

⁹<https://github.com/zalandoresearch/fashion-mnist>

class of the dataset, while under non-i.i.d distribution, each node has access to only one of the classes. These are the extreme ends of possible split of data among nodes in terms of class distribution, helping us evaluate the overall robustness as well as differences in characteristics of our technique under different settings.

4) *Network Formation:* We consider two network configurations: (i) the network consists of 125 edge devices; (ii) the network consists of 625 edge devices. For the former case, we consider a fog network consisting of a main server and three sub-layers, to build our fog network we start with the 125 worker nodes in the bottom-most layer (\mathcal{L}^3) and dedicated local datasets sampled as explained above. The worker nodes update the local models with a copy of parameters from latest global model at the start of each iteration. The worker nodes are then clustered in groups of 5 to communicate with one of the 25 aggregators in their upper layer (i.e., \mathcal{L}^2), such that there is a 1-to-1 mapping between the clusters and the aggregators. Similarly the nodes in layer (\mathcal{L}^2) are clustered and communicate with the 5 aggregators in the layer \mathcal{L}^1 , followed by clustering and communicating the 5 nodes with the main server.

For the latter case, we consider a fog network consisting of a main server and four sub-layers, to build our fog network we start with the 625 worker nodes in the bottom-most layer (i.e., \mathcal{L}^4) and dedicated local datasets sampled as explained above. The worker nodes update the local models with a copy of parameters from latest global model at the start of each iteration. The worker nodes are then clustered in groups of 5 to communicate with one of the 125 aggregators in their upper layer (i.e., \mathcal{L}^3), such that there is a 1-to-1 mapping between the clusters and aggregators. Similarly nodes in \mathcal{L}^3 are again clustered and communicate to the 25 aggregators in the upper layer (i.e., \mathcal{L}^2). This is followed by clustering of these nodes in groups of 5 and communicating with 5 aggregators in layer \mathcal{L}^1 , which then communicate with the main server.

The connectivity among the nodes within a cluster is simulated using random geometric graphs with increasing connectivity as we traverse from the bottom-most layer to the main server. For the case with 125 edge device, layer \mathcal{L}^3 has average degree of the nodes around 2, followed by layer \mathcal{L}^2 with average degree around 3 and layer \mathcal{L}^1 with average degree around 4. For the case with 625 edge device, in layer \mathcal{L}^3 and \mathcal{L}^4 we have average degree of the nodes around 2, followed by layer \mathcal{L}^2 with average degree around 3 and layer \mathcal{L}^1 with average degree around 4. We use *NetworkX*¹⁰ library of *Python* for generating the graph. We adjust the radius parameter

¹⁰<https://networkx.github.io>

of the graph generator such that the average degree of the graph is within tolerance region of 0.2 from the desired degree of the graph.

For the D2D communications, we consider the common choice of the weights [45] that gives $\mathbf{z}_n^{(t+1)} = \mathbf{z}_n^{(t)} + d_C^{(k)} \sum_{m \in \mathcal{Q}^{(k)}(n)} (\mathbf{z}_m^{(t)} - \mathbf{z}_n^{(t)})$, $0 < d_C^{(k)} < 1/D_C^{(k)}$, for any node n in arbitrary cluster \mathcal{C} , where $D_C^{(k)}$ is the maximum degree of the nodes in $G_C^{(k)}$. Using this implementation, the nodes inside LUT cluster \mathcal{C} only need to have the knowledge of the parameter $d_C^{(k)}$, which is broadcasted by the respective parent node.

B. Further Simulation Results

This section presents the plots from complimentary experiments from Section IV. In the following, we explain the relationship between the figures presented in this appendix and the simulation results presented in the main text.

Fig. 5 from main text is repeated in Fig. 16 for MNIST dataset distributed over 625 edge devices, Fig. 27 for FMNIST dataset distributed over 125 edge devices and Fig. 38 for FMNIST dataset distributed over 625 edge devices.

Fig. 6 from main text is repeated in Fig. 17 for MNIST dataset distributed over 625 edge devices, Fig. 28 for FMNIST dataset distributed over 125 edge devices and Fig. 39 for FMNIST dataset distributed over 625 edge devices.

Fig. 7 from main text is repeated in Fig. 18 for MNIST dataset distributed over 625 edge devices, Fig. 29 for FMNIST dataset distributed over 125 edge devices and Fig. 40 for FMNIST dataset distributed over 625 edge devices.

Fig. 8 from main text is repeated in Fig. 19 for MNIST dataset distributed over 625 edge devices, Fig. 30 for FMNIST dataset distributed over 125 edge devices and Fig. 41 for FMNIST dataset distributed over 625 edge devices.

Fig. 9 from main text is repeated in Fig. 20 for MNIST dataset distributed over 625 edge devices, Fig. 31 for FMNIST dataset distributed over 125 edge devices and Fig. 42 for FMNIST dataset distributed over 625 edge devices.

Fig. 10 from main text is repeated in Fig. 21 for MNIST dataset distributed over 625 edge devices, Fig. 32 for FMNIST dataset distributed over 125 edge devices and Fig. 43 for FMNIST dataset distributed over 625 edge devices.

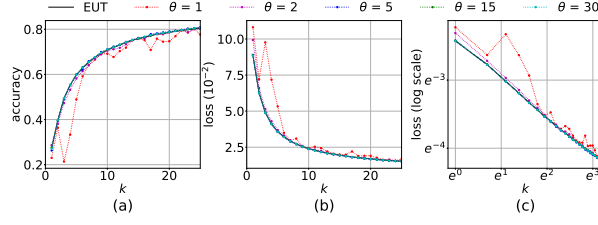


Fig. 16: Performance comparison between baseline EUT and MH-MT when a fixed number of consensus rounds θ is used at every cluster of the network, for non-i.i.d. As the number of consensus rounds increases, MH-MT performs more similar to the EUT baseline and the learning is more stable. (MNIST, 625 Edge Devices)

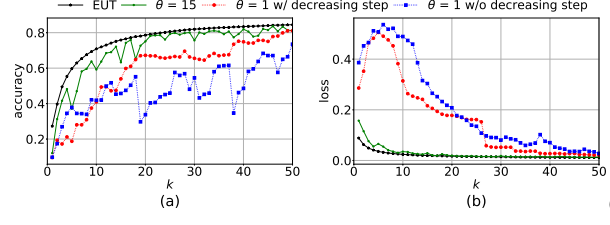


Fig. 17: Performance comparison between baseline EUT, and MH-MT with and without (w/o) decreasing the gradient descent step size. Decreasing the step size can provide convergence to the optimal solution in cases where a fixed step size is not capable, but also has a slower convergence speed. (MNIST, 625 Edge Devices)

Fig. 11 from main text is repeated in Fig. 22 for MNIST dataset distributed over 625 edge devices, Fig. 33 for FMNIST dataset distributed over 125 edge devices and Fig. 44 for FMNIST dataset distributed over 625 edge devices.

Fig. 12 from main text is repeated in Fig. 23 for MNIST dataset distributed over 625 edge devices, Fig. 34 for FMNIST dataset distributed over 125 edge devices and Fig. 45 for FMNIST dataset distributed over 625 edge devices.

Fig. 13 from main text is repeated in Fig. 24 for MNIST dataset distributed over 625 edge devices, Fig. 35 for FMNIST dataset distributed over 125 edge devices and Fig. 46 for FMNIST dataset distributed over 625 edge devices.

Fig. 14 from main text is repeated in Fig. 25 for MNIST dataset distributed over 625 edge devices, Fig. 36 for FMNIST dataset distributed over 125 edge devices and Fig. 47 for FMNIST dataset distributed over 625 edge devices.

Fig. 15 from main text is repeated in Fig. 26 for MNIST dataset distributed over 625 edge devices, Fig. 37 for FMNIST dataset distributed over 125 edge devices and Fig. 48 for FMNIST dataset distributed over 625 edge devices.

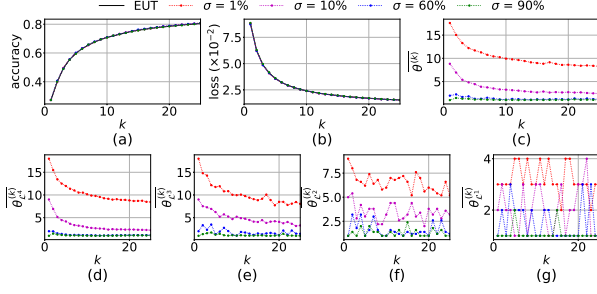


Fig. 18: Performance comparison between baseline EUT and MH-MT for i.i.d when a finite optimality gap is tolerable. σ_i at \mathcal{L}^i is fixed as $\sigma_i = \sigma' \max_{\mathcal{L}^j \in \mathcal{L}^i} \Upsilon_{\mathcal{L}^j}^{(1)}$. Tapering of consensus rounds though time and space (layers) can be observed. (MNIST, 625 Edge Devices)

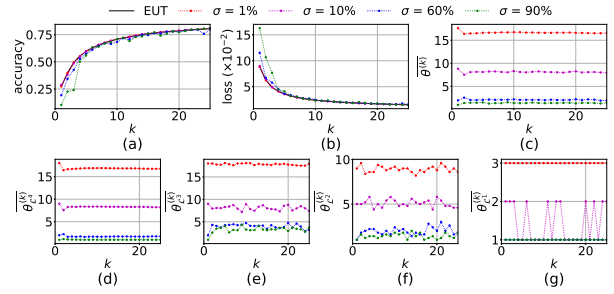


Fig. 19: Performance comparison between baseline EUT and MH-MT for non-i.i.d when a finite optimality gap is tolerable. σ_i is set as in Fig. 18. Smaller loss and higher accuracy are achieved with smaller σ' , implying more rounds of consensus. (MNIST, 625 Edge Devices)

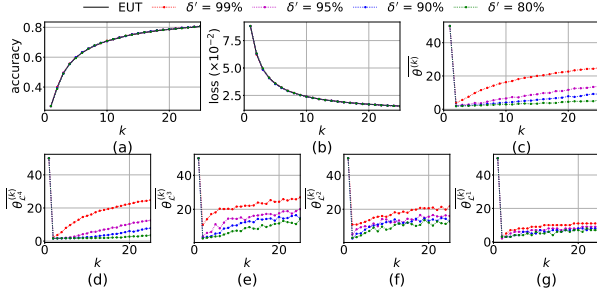


Fig. 20: Performance comparison between baseline EUT and MH-MT for i.i.d. when linear convergence to the optimal is desired. The value of δ is set at $\delta = \delta' \frac{\mu}{\eta}$. Boosting of the consensus rounds though time can be observed. Also, tapering through space can be observed by comparing the consensus rounds in the bottom subplots. (MNIST, 625 Edge Devices)

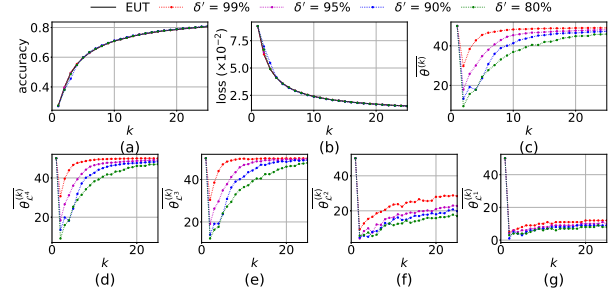


Fig. 21: Performance comparison between baseline EUT and MH-MT for non-i.i.d when linear convergence to the optimal is desired. The value of δ is set as in Fig. 20. Smaller values of loss and higher accuracy are both associated with larger value of δ , which results in lower error tolerance and more rounds of consensus. (MNIST, 625 Edge Devices)

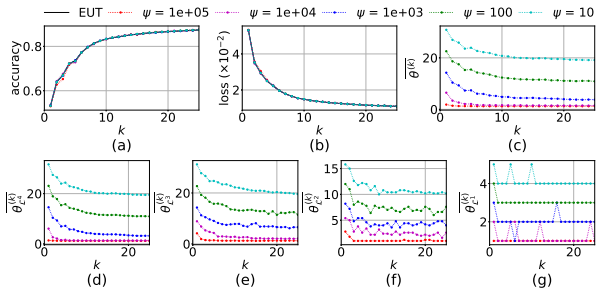


Fig. 22: Performance comparison between baseline EUT and MH-MT under i.i.d using NNs with different values of ψ . Tapering the consensus rounds though time can be observed. Also, tapering through space can be observed by comparing the consensus rounds in the bottom subplots. (MNIST, 625 Edge Devices)

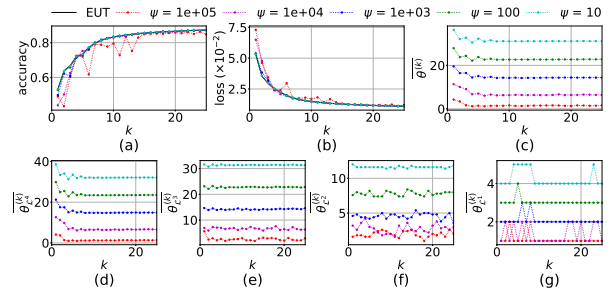


Fig. 23: Performance comparison between baseline EUT and MH-MT under non-i.i.d. using NNs with different values of ψ . Lower loss and higher accuracy are associate with smaller values of ψ , which result in lower error tolerance and larger values of consensus rounds over time. (MNIST, 625 Edge Devices)

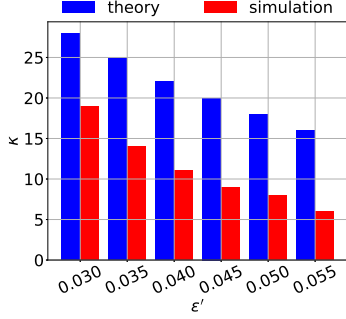


Fig. 24: Comparison between the theoretical and simulation results regarding the number of global iterations to achieve an accuracy of $\epsilon'(F(w^{(0)}) - F(w^*))$ for different ϵ' . Convergence in practice is faster than the derived upper bound. (MNIST, 625 Edge Devices)

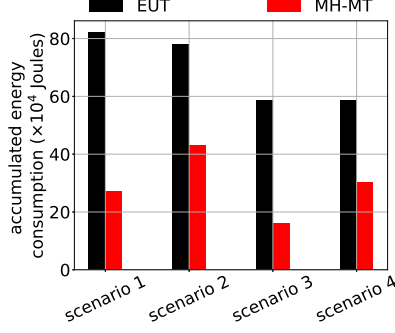


Fig. 25: Comparison of accumulated energy consumption between EUT and MH-MT over scenario 1: $\sigma' = 0.1$ from Fig. 18, scenario 2: $\sigma' = 0.1$ from Fig. 19, scenario 3: $\psi = 10^4$ from Fig. 22, and scenario 4: $\psi = 10^4$ from Fig. 23. (MNIST, 625 Edge Devices)

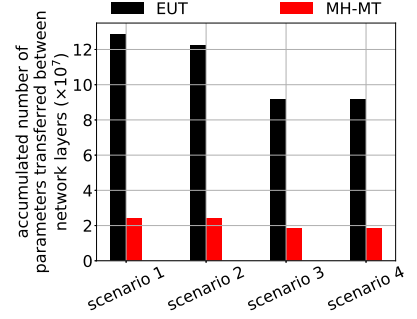


Fig. 26: Comparison of parameters transferred among layers in EUT vs MH-MT over scenario 1: $\sigma' = 0.1$ from Fig. 18, scenario 2: $\sigma' = 0.1$ from Fig. 19, scenario 3: $\psi = 10^4$ from Fig. 22, and scenario 4: $\psi = 10^4$ from Fig. 23. (MNIST, 625 Edge Devices)

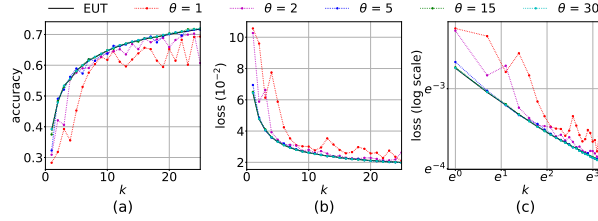


Fig. 27: Performance comparison between baseline EUT and MH-MT when a fixed number of consensus rounds θ is used at every cluster of the network, for non-i.i.d. As the number of consensus rounds increases, MH-MT performs more similar to the EUT baseline and the learning is more stable. (FMNIST, 125 Edge Devices)

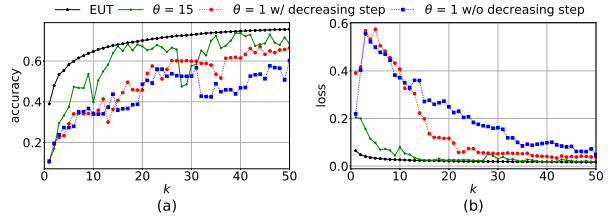


Fig. 28: Performance comparison between baseline EUT, and MH-MT with and without (w/o) decreasing the gradient descent step size. Decreasing the step size can provide convergence to the optimal solution in cases where a fixed step size is not capable, but also has a slower convergence speed. (FMNIST, 125 Edge Devices)

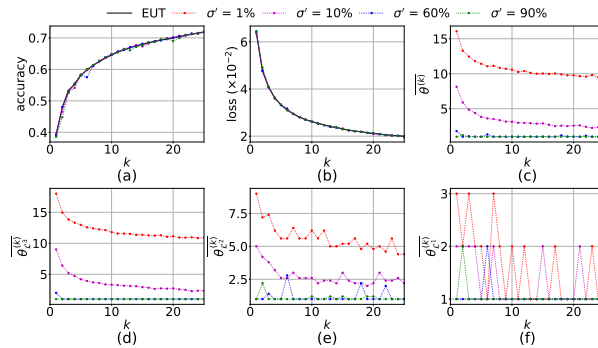


Fig. 29: Performance comparison between baseline EUT and MH-MT for i.i.d when a finite optimality gap is tolerable. σ_i at \mathcal{L}^i is fixed as $\sigma_i = \sigma' \max_{\mathcal{L}^j \in \mathcal{L}^i} \Upsilon_{\mathcal{L}^j}^{(1)}$. Tapering of consensus rounds though time and space (layers) can be observed. (FMNIST, 125 Edge Devices)

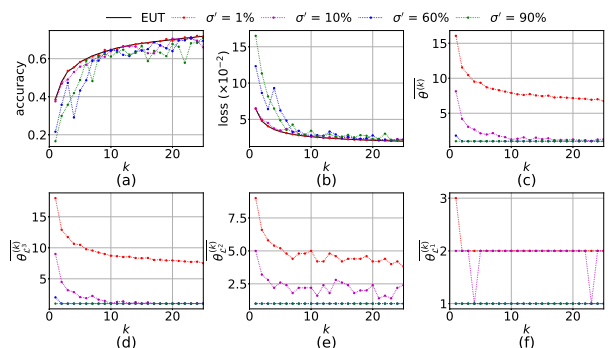


Fig. 30: Performance comparison between baseline EUT and MH-MT for non-i.i.d when a finite optimality gap is tolerable. σ_i is set as in Fig. 29. Smaller loss and higher accuracy are achieved with smaller σ' , implying more rounds of consensus. (FMNIST, 125 Edge Devices)

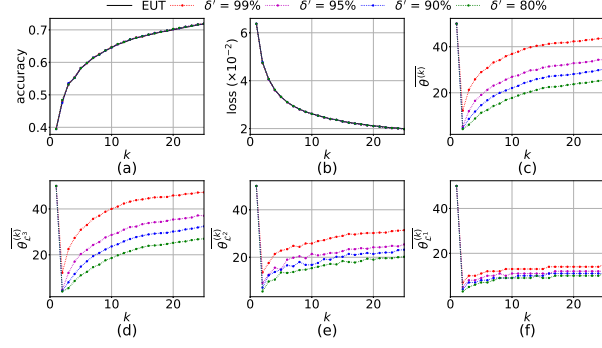


Fig. 31: Performance comparison between baseline EUT and MH-MT for i.i.d. when linear convergence to the optimal is desired. The value of δ is set at $\delta = \delta' \frac{\mu}{\eta}$. Boosting of the consensus rounds though time can be observed. Also, tapering through space can be observed by comparing the consensus rounds in the bottom subplots. (FMNIST, 125 Edge Devices)

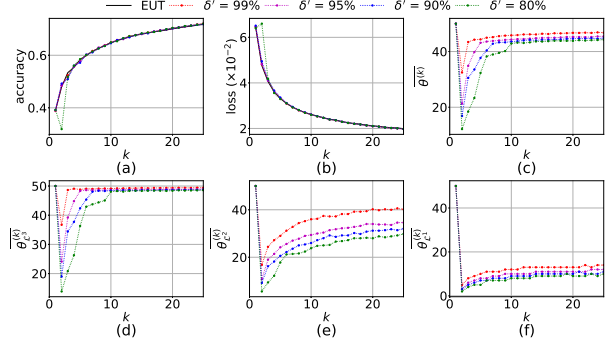


Fig. 32: Performance comparison between baseline EUT and MH-MT for non-i.i.d. when linear convergence to the optimal is desired. The value of δ is set as in Fig. 31. Smaller values of loss and higher accuracy are both associated with larger value of δ , which results in lower error tolerance and more rounds of consensus. (FMNIST, 125 Edge Devices)

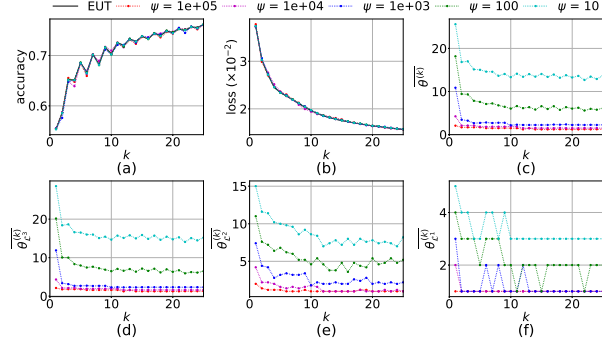


Fig. 33: Performance comparison between baseline EUT and MH-MT under i.i.d. using NNs with different values of ψ . Tapering the consensus rounds though time can be observed. Also, tapering through space can be observed by comparing the consensus rounds in the bottom subplots. (FMNIST, 125 Edge Devices)

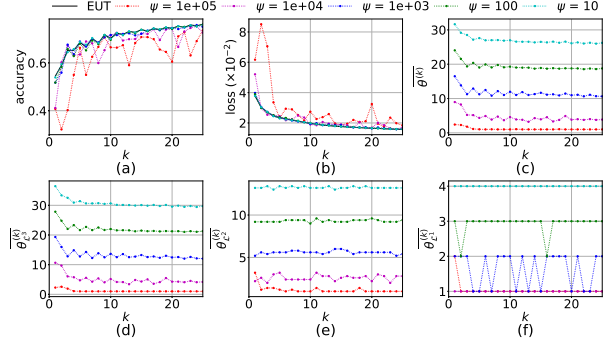


Fig. 34: Performance comparison between baseline EUT and MH-MT under non-i.i.d. using NNs with different values of ψ . Lower loss and higher accuracy are associate with smaller values of ψ , which result in lower error tolerance and larger values of consensus rounds over time. (FMNIST, 125 Edge Devices)

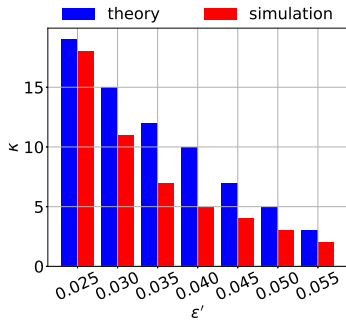


Fig. 35: Comparison between the theoretical and simulation results regarding the number of global iterations to achieve an accuracy of $\epsilon'(F(w^{(0)}) - F(w^*))$ for different ϵ' . Convergence in practice is faster than the derived upper bound. (FMNIST, 125 Edge Devices)

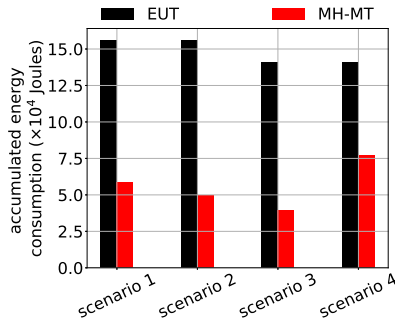


Fig. 36: Comparison of accumulated energy consumption between EUT and MH-MT over scenario 1: $\sigma' = 0.1$ from Fig. 29, scenario 2: $\sigma' = 0.1$ from Fig. 30, scenario 3: $\psi = 10^4$ from Fig. 33, and scenario 4: $\psi = 10^4$ from Fig. 34. (FMNIST, 125 Edge Devices)

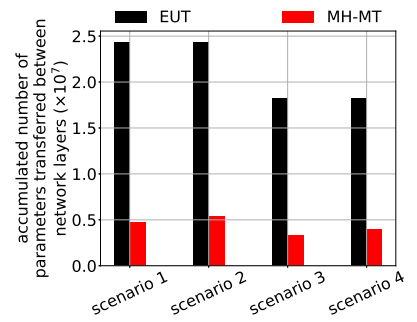


Fig. 37: Comparison of parameters transferred among layers in EUT vs MH-MT over scenario 1: $\sigma' = 0.1$ from Fig. 29, scenario 2: $\sigma' = 0.1$ from Fig. 30, scenario 3: $\psi = 10^4$ from Fig. 33, and scenario 4: $\psi = 10^4$ from Fig. 34. (FMNIST, 125 Edge Devices)

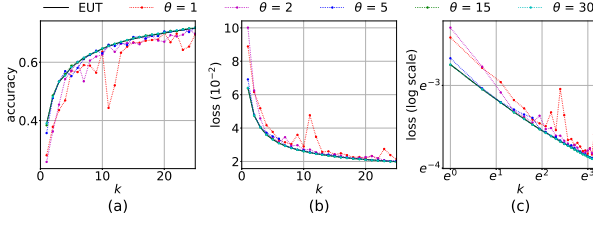


Fig. 38: Performance comparison between baseline EUT and MH-MT when a fixed number of consensus rounds θ is used at every cluster of the network, for non-i.i.d. As the number of consensus rounds increases, MH-MT performs more similar to the EUT baseline and the learning is more stable. (FMNIST, 625 Edge Devices)

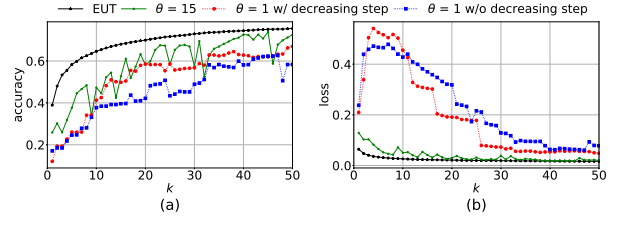


Fig. 39: Performance comparison between baseline EUT, and MH-MT with and without (w/o) decreasing the gradient descent step size. Decreasing the step size can provide convergence to the optimal solution in cases where a fixed step size is not capable, but also has a slower convergence speed. (FMNIST, 625 Edge Devices)

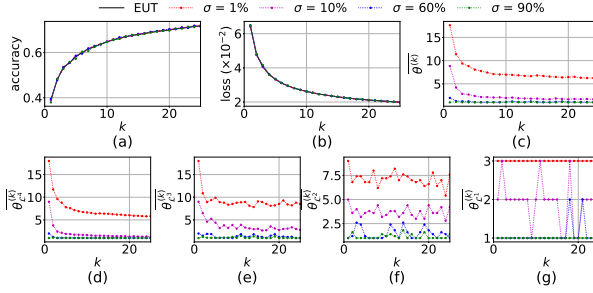


Fig. 40: Performance comparison between baseline EUT and MH-MT for i.i.d. when a finite optimality gap is tolerable. σ_i at \mathcal{L}^i is fixed as $\sigma_i = \sigma' \max_{\mathcal{L}^j \in \mathcal{L}^i} \Upsilon_{\mathcal{L}^j}^{(1)}$. Tapering of consensus rounds though time and space (layers) can be observed. (FMNIST, 625 Edge Devices)

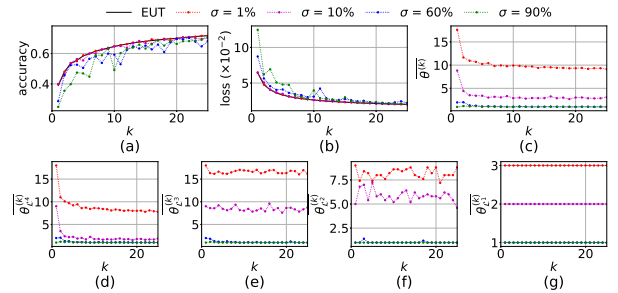


Fig. 41: Performance comparison between baseline EUT and MH-MT for non-i.i.d. when a finite optimality gap is tolerable. σ_i is set as in Fig. 40. Smaller loss and higher accuracy are achieved with smaller σ' , implying more rounds of consensus. (FMNIST, 625 Edge Devices)

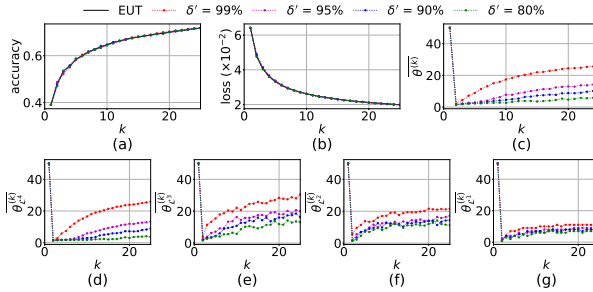


Fig. 42: Performance comparison between baseline EUT and MH-MT for i.i.d. when linear convergence to the optimal is desired. The value of δ is set at $\delta = \delta' \frac{\mu}{\eta}$. Boosting of the consensus rounds though time can be observed. Also, tapering through space can be observed by comparing the consensus rounds in the bottom subplots. (FMNIST, 625 Edge Devices)

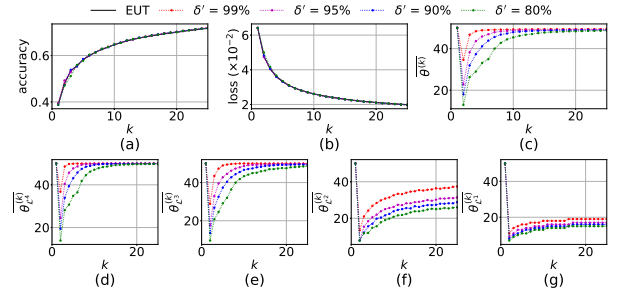


Fig. 43: Performance comparison between baseline EUT and MH-MT for non-i.i.d. when linear convergence to the optimal is desired. The value of δ is set as in Fig. 42. Smaller values of loss and higher accuracy are both associated with larger value of δ , which results in lower error tolerance and more rounds of consensus. (FMNIST, 625 Edge Devices)

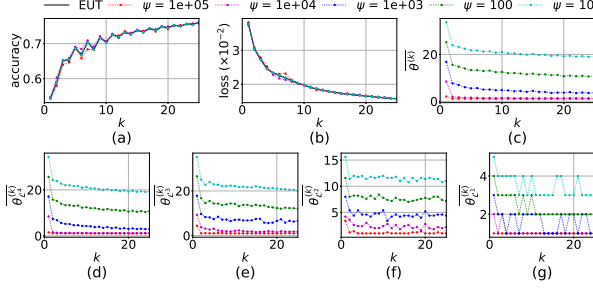


Fig. 44: Performance comparison between baseline EUT and MH-MT under i.i.d using NNs with different values of ψ . Tapering the consensus rounds though time can be observed. Also, tapering through space can be observed by comparing the consensus rounds in the bottom subplots. (FMNIST, 625 Edge Devices)

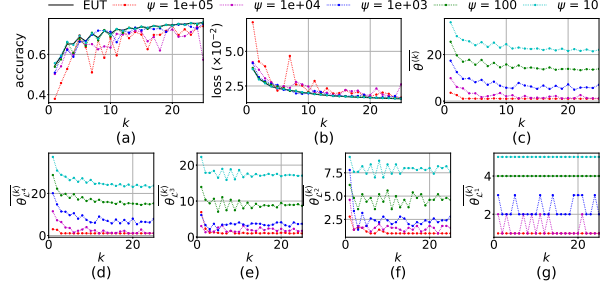


Fig. 45: Performance comparison between baseline EUT and MH-MT under non-i.i.d. using NNs with different values of ψ . Lower loss and higher accuracy are associate with smaller values of ψ , which result in lower error tolerance and larger values of consensus rounds over time. (FMNIST, 625 Edge Devices)

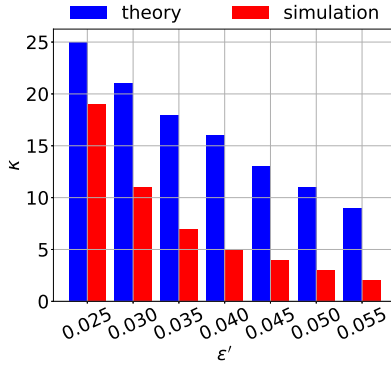


Fig. 46: Comparison between the theoretical and simulation results regarding the number of global iterations to achieve an accuracy of $\epsilon'(F(w^{(0)}) - F(w^*))$ for different ϵ' . Convergence in practice is faster than the derived upper bound. (FMNIST, 625 Edge Devices)

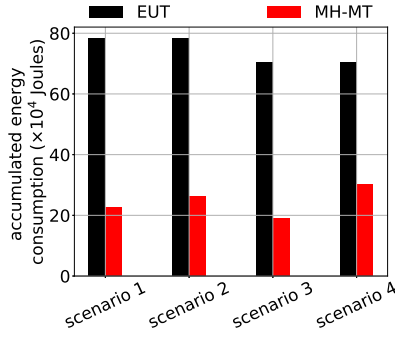


Fig. 47: Comparison of accumulated energy consumption between EUT and MH-MT over scenario 1: $\sigma' = 0.1$ from Fig. 40, scenario 2: $\sigma' = 0.1$ from Fig. 41, scenario 3: $\psi = 10^4$ from Fig. 44, and scenario 4: $\psi = 10^4$ from Fig. 45. (FMNIST, 625 Edge Devices)

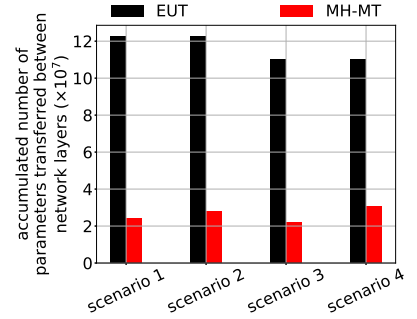


Fig. 48: Comparison of parameters transferred among layers in EUT vs MH-MT over scenario 1: $\sigma' = 0.1$ from Fig. 40, scenario 2: $\sigma' = 0.1$ from Fig. 41, scenario 3: $\psi = 10^4$ from Fig. 44, and scenario 4: $\psi = 10^4$ from Fig. 45. (FMNIST, 625 Edge Devices)